



DEVELOPMENT AND TESTING OF A
MULTIPLE FILTER APPROACH FOR PRECISE DGPS
POSITIONING AND CARRIER-PHASE AMBIGUITY RESOLUTION

THESIS

Paul E. Henderson, Captain, USAF
AFIT/GE/ENG/01M-15

DEPARTMENT OF THE AIR FORCE
AIR UNIVERSITY

AIR FORCE INSTITUTE OF TECHNOLOGY

Wright-Patterson Air Force Base, Ohio

APPROVED FOR PUBLIC RELEASE, DISTRIBUTION UNLIMITED

20010706 163

The views expressed in this document are those of the author and do not reflect the official policy or position of the United States Air Force, Department of Defense, or the U.S. Government.

DEVELOPMENT AND TESTING OF A
MULTIPLE FILTER APPROACH FOR PRECISE DGPS
POSITIONING AND CARRIER-PHASE AMBIGUITY RESOLUTION

THESIS

Presented to the Faculty

Department of Electrical Engineering

Graduate School of Engineering and Management

Air Force Institute of Technology

Air University

Air Education and Training Command

In Partial Fulfillment of the Requirements for the
Degree of Master of Science in Electrical Engineering

Paul E. Henderson, B.S.

Captain, USAF

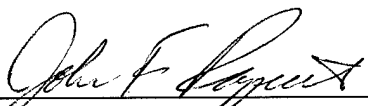
March 2001

APPROVED FOR PUBLIC RELEASE, DISTRIBUTION UNLIMITED

DEVELOPMENT AND TESTING OF A
MULTIPLE FILTER APPROACH FOR PRECISE DGPS
POSITIONING AND CARRIER-PHASE AMBIGUITY RESOLUTION

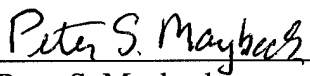
Paul E. Henderson, B.S.
Captain, USAF

Approved:



Major John F. Raquet, Ph.D.
Assistant Professor, Committee Chairman

7 MAR 01
Date



Dr. Peter S. Maybeck
Professor, Committee Member

7 MAR 01
Date



Lieutenant Colonel Mikel M. Miller, Ph.D.
Assistant Professor, Committee Member

7 Mar 01
Date

Acknowledgments

My thesis advisor, Major John Raquet deserves much of the credit for this work. He was always there, even late at night and on weekends, to give me encouragement and help on the more demanding parts of this thesis. His optimistic attitude, knowledge of GPS and MATLAB were invaluable, and at times sorely needed. Thank you for your support, help and dedication.

In addition, Dr. Peter Maybeck deserves credit for helping with this thesis. His knowledge of Kalman filtering is truly outstanding and his ability to explain the complex aspects of advanced Kalman filtering is second to none.

Thanks to my classmates in the guidance and control department: Captains Brian Bracy, Todd Broaddus and Mike Presnar. Late nights in the lab, and the unyielding AFIT workload have a way of making friends out of even the most unlikely individuals.

Finally, I need to thank the USAF/TPS who sponsored both my AFIT degree and graduation from USAF/TPS as a Flight Test Engineer. Special thanks to the “Dogs” of 00A and specifically to my flight test team: Major Jim “Crush” Duricy, Capt Lee “Rico” Davis, Capt Lee “SIEEpy” Olyniec, and Capt (CAF) Ryan “Chubby” Palmer. It was an honor to serve with all of you.

Table of Contents

	Page
Acknowledgments	iv
Table of Contents	v
List of Figures	ix
List of Tables	xii
Notation	xiv
Acronym List	xvi
Abstract	xviii
 1 Introduction	 1-1
1.1 Background	1-1
1.2 Problem Definition	1-6
1.3 Scope	1-6
1.4 Related Research	1-7
1.4.1 Kalman Filtering	1-7
1.4.1.1 Multiple Model Adaptive Estimation	1-8
1.4.2 Global Positioning System	1-9
1.4.2.1 Carrier-Phase Ambiguity Resolution	1-10
1.5 Methodology	1-12
1.6 Thesis Overview	1-13
 2 Theory	 2-1
2.1 Overview	2-1
2.2 Kalman Filters	2-1
2.2.1 State and Measurement Model Equations	2-2
2.2.2 Kalman Filter Equations	2-3
2.3 Extended Kalman Filters	2-5

2.3.1	State and Measurement Model Equations	2-5
2.3.2	State and Measurement Model Linearization	2-7
2.3.3	Extended Kalman Filter Equations	2-9
2.4	Multiple Model Adaptive Estimation.....	2-11
2.4.1	Elemental Filters	2-12
2.4.2	Conditional Probability Generation	2-13
2.4.2.1	Lower Probability Bounds	2-14
2.4.3	Overall MMAE State Estimate	2-15
2.4.4	MMAE Convergence	2-15
2.5	Global Positioning System.....	2-16
2.5.1	The GPS Signal	2-16
2.5.2	GPS Measurements	2-18
2.5.2.1	Code Measurements.....	2-18
2.5.2.2	GPS Carrier-Phase Measurements	2-19
2.5.2.3	Single Differencing	2-20
2.5.2.4	Differential Corrections	2-23
2.5.2.5	Double Differencing	2-24
2.5.2.6	Widelane Measurements	2-26
2.5.3	Carrier-phase Ambiguity Resolution	2-27
2.5.3.1	Ambiguity Set Generation	2-27
2.5.3.2	Ambiguity Set Determination	2-31
2.6	Summary	2-32
3	Methodology and Algorithm Development	3-1
3.1	Overview	3-1
3.2	Overall Algorithm Structure.....	3-1
3.3	Floating-Point Differential GPS Kalman Filter	3-2
3.3.1	Differential GPS Model Equations	3-4
3.3.2	Differential GPS Measurement Model.....	3-10
3.3.3	Discrete-Time Models.....	3-17
3.4	Carrier-phase Ambiguity Set Generation	3-19

3.5	Multiple Model Adaptive Estimator Design	3-20
3.5.1	Elemental Filter Design.....	3-21
3.5.1.1	Elemental Filter Model Equations	3-21
3.5.1.2	Elemental Filter Measurement Model	3-24
3.5.1.3	Discrete-Time Models	3-29
3.5.2	Conditional Probability Calculations	3-30
3.5.2.1	Lower Probability Bounds	3-32
3.5.3	Filter Pruning	3-33
3.6	Summary	3-35
4	Results and Analysis	4-1
4.1	Overview	4-1
4.2	Ground Tests	4-1
4.2.1	Case Definitions	4-2
4.2.2	Case 1: 250 m Baseline, Widelane Measurements	4-3
4.2.3	Case 2: 250 m Baseline, L1 Measurements	4-6
4.2.4	Case 3: 28.1 km Baseline, Widelane Measurements	4-11
4.2.5	Case 4: 100 km Baseline, Widelane Measurements	4-17
4.3	Flight Tests	4-22
4.3.1	Case Definitions	4-22
4.3.1.1	Ambiguity Set Generation	4-25
4.3.2	Case 5: 16.1 km Baseline, 10,000 ft Altitude, Widelane Measurements ..	4-26
4.3.3	Case 6: 16.1 km Baseline, 10,000 ft Altitude, Widelane Measurements ..	4-32
4.3.4	Case 7: 32.2 km Baseline, 10,000 ft Altitude, Widelane Measurements ..	4-39
4.4	Summary	4-43
5	Conclusions and Recommendations.....	5-1
5.1	Overview	5-1
5.2	Conclusions	5-2
5.3	Recommendations	5-5
Appendix A.	Flight Test Profiles	A-1

Bibliography.....	Bib-1
Vita	Vit-1

List of Figures

	Page
Figure 1-1. Typical GPS/DGPS Solution Time Histories	1-2
Figure 2-1. Multiple Model Filtering Algorithm	2-11
Figure 2-2. Single Differencing	2-20
Figure 2-3. Double Differencing	2-24
Figure 3-1. Overall Algorithm Description	3-2
Figure 4-1. Case 1 - Floating-Point Filter Position Errors	4-4
Figure 4-2. Case 1 - MMAE Position Errors	4-4
Figure 4-3. Case 1 - Sample Elemental Filter Conditional Probability Time Histories, First Minute	4-6
Figure 4-4. Case 2 - Floating-Point Filter Position Errors	4-7
Figure 4-5. Case 2 - MMAE Position Errors	4-8
Figure 4-6. Case 2 - Elemental Filter 21 Probability and Residual Time History (Correct Ambiguities)	4-9
Figure 4-7. Case 2 - Elemental Filter 24 Probability and Residual Time History (Incorrect Ambiguities)	4-9
Figure 4-8. Case 3 - Floating-Point Position Errors	4-12
Figure 4-9. Case 3 - MMAE Position Errors	4-12
Figure 4-10. Case 3 - Sample Elemental Filter Conditional Probability Time Histories	4-14

Figure 4-11. Case 3 - Elemental Filter 5 Probability and Residual Time History (Incorrect Ambiguities), First Six Minutes	4-15
Figure 4-12. Case 3 - Elemental Filter 68 Probability and Residual Time History (Correct Ambiguities), First Six Minutes	4-16
Figure 4-13. Case 4 - Floating-Point Filter Position Errors	4-18
Figure 4-14. Case 4 - MMAE Position Errors	4-18
Figure 4-15. Case 4 - Sample Elemental Filter Conditional Probability Time Histories	4-19
Figure 4-16. Case 5 – Floating-Point Filter Position Errors	4-27
Figure 4-17. Case 5 - MMAE Position Errors	4-27
Figure 4-18. Case 5 - Sample Elemental Filter Conditional Probability Time Histories	4-28
Figure 4-19. Case 5 - Elemental Filter 1 Probability and Residual Time History (Correct Ambiguities)	4-29
Figure 4-20. Case 5 - Elemental Filter 14 Probability and Residual Time History (Incorrect Ambiguities)	4-30
Figure 4-21. Case 6 – Floating-Point Filter Position Errors	4-32
Figure 4-22. Case 6 - MMAE Position Errors	4-33
Figure 4-23. Case 6 - Conditional Probability Time Histories	4-34
Figure 4-24. Case 6 - Elemental Filter 1 Probability and Residual Time Histories (Correct Ambiguities)	4-36
Figure 4-25. Case 6 - Elemental Filter 38 Probability and Residual Time Histories (Incorrect Ambiguities)	4-36

Figure 4-26. Case 6 - Elemental Filter 45 Probability and Residual Time Histories	
(Incorrect Ambiguities)	4-37
Figure 4-27. Case 7 – Floating-Point Filter Position Errors	4-40
Figure 4-28. Case 7 - MMAE Position Errors	4-40
Figure 4-29. Case 7 - Elemental Filter 1 Probability and Residual Time Histories	
(Correct Ambiguities)	4-42
Figure 4-30. Case 7 - Elemental Filter 2 Probability and Residual Time Histories	
(Incorrect Ambiguities)	4-42
Figure A-1. Primary Flight Test Point Profile.....	A-3

List of Tables

	Page
Table 1-1. Typical GPS/DGPS Accuracies	1-3
Table 2-1. GPS Signal Summary	2-17
Table 2-2. Phase Measurement Combinations	2-26
Table 3-1. Floating-Point Filter Dynamics Driving Noise Values.....	3-8
Table 3-2. Floating-Point Filter Initial Covariance Values.....	3-10
Table 3-3. Floating-Point Filter Measurement Covariance Error Values	3-16
Table 3-4. Elemental Filter Dynamics Driving Noise Values	3-23
Table 3-5. Elemental Filter Measurement Covariance Error Values	3-28
Table 4-1. Ground Test Case Parameter Description.....	4-2
Table 4-2. Case 1 - Position Solution Error Comparison.....	4-5
Table 4-3. Case 2 - Position Solution Error Comparison.....	4-8
Table 4-4. Case 3 - Position Solution Error Comparison.....	4-13
Table 4-5. Case 4 - True Ambiguities vs. Elemental Filter Ambiguities	4-20
Table 4-6. Case 4 - Position Solution Error Comparison.....	4-20
Table 4-7. Flight Test Case Parameter Description	4-23
Table 4-8. Case 5 - True Ambiguities vs. Elemental Filter Ambiguities.....	4-29
Table 4-9. Case 6 - True Ambiguities vs. Elemental Filter Ambiguities.....	4-35
Table 4-10. Case 7 - True Ambiguities vs. Elemental Filter Ambiguities.....	4-39
Table A-1. Primary Flight Test Data Points.....	A-2
Table A-2. Primary Flight Test Data Point Tolerances.....	A-2

Table A-3. Secondary Flight Test Data Points.....	A-4
Table A-4. Secondary Flight Test Data Point Tolerances.....	A-4

Notation

Scalars, Vectors, Matrices

Scalars are denoted by upper or lower case letters in italic type, as in the scalar x .

Vectors are denoted by lower case letters in boldface type, as in the vector \mathbf{x} made up of components x_i (always expressed as column vectors).

Matrices are denoted by upper case letters in boldface type, as in the matrix \mathbf{A} made up of elements A_{ij} (i th row, j th column).

Prefixes

- $E\{\cdot\}$ - Expected Value of $\{\cdot\}$
- $\Delta(\cdot)$ - Incremental change in (\cdot) over a period of time
- $\delta(\cdot)$ - Error in the estimated, computed, or measured (\cdot) w.r.t. the true (\cdot)

Overscores

- $\hat{\cdot}$ - Estimated, Computed, or Measured Value (not true value)
- $\dot{\cdot}$ - Time Derivative

Right Subscripts

- 0 - Initial, as in initial conditions
- $1,2$ - Counting indices (usually used as sub-subscripts)
- amb - Ambiguity as in carrier-phase ambiguity
- clk - Clock, as in user's GPS clock
- d - Discrete-Time
- f - Filter Model
- i,j - Sampling Time Index
- k - Elemental Filter index
- L - Lower Diagonal (as in Matrix)
- $L1$ - GPS L1 Frequency
- $L2$ - GPS L2 Frequency
- n - Nominal (as in trajectory), or GPS Satellite number n
- U - Upper Diagonal (as in Matrix)
- sv - Satellite Vehicle
- u - User GPS Receiver
- x,y - Generic GPS Receiver index (Receiver x , Receiver y)

Right Superscripts

- -1 - Matrix Inverse
- a,b - Generic GPS Satellite index (Satellite a , Satellite b)
- T - Vector or Matrix Transpose

Acronym List

<u>Abbreviation</u>	<u>Acronym</u>
AFIT	Air Force Institute of Technology
AFFTC	Air Force Flight Test Center
AFM	Ambiguity Function Method
C/A	Coarse/Acquisition, as in Code
CPDGPS	Carrier-Phase Differential Global Positioning System (GPS)
DGPS	Differential GPS
ECEF	Earth Centered Earth Fixed Coordinate Reference Frame
EF	Elemental Filter
EKF	Extended Kalman Filter
ENU	East, North, and Up Coordinate Reference Frame
FASF	Fast Ambiguity Search Filter
FOGMA	First Order Gauss Markov Acceleration
GDOP	Geometric Dilution of Precision
GPS	Global Positioning System
<i>h.o.t.</i>	Higher Order Terms
INS	Inertial Navigation System
INU	Inertial Navigation Unit
KF	Kalman Filter
KIAS	Knots Indicated Airspeed
L1	First GPS Carrier Frequency, 1575.42 MHz
L2	Second GPS Carrier Frequency, 1227.60 MHz
LAMBDA	Least-squares AMBIGUITY Decorrelation Adjustment method
LLA	Geodetic Latitude, Longitude, and Altitude
LLH	Geodetic Latitude, Longitude, and Height above the Ellipsoid
LLW	Geodetic Latitude, Longitude, and Wander Angle
LOS	Line-of-Sight
LSAST	Least Squares Ambiguity Search Technique
LTI	Linear Time-Invariant
NED	North, East, and Down Coordinate Reference Frame
nm	Nautical Mile
P	Precision, as in Code
PA	Pressure Altitude
PPS	Precise Positioning Service
PR	Pseudorange
PRN	Pseudo-Random Noise
PVA	Position, Velocity, Acceleration
PVT	Position, Velocity, Time
RF	Radio Frequency
RMS	Root-Mean-Square
SA	Selective Availability

SPS	Standard Positioning Service
SV	Satellite Vehicle
TPS	Test Pilot School
UERE	User-Equivalent Range Error
USAF	United States Air Force
WGN	White Gaussian Noise
WGS-84	1984 World Geodetic System ellipsoid model
WPAFB	Wright-Patterson Air Force Base

Abstract

The most precise relative positioning obtained using differential GPS depends on accurately determining carrier-phase integer ambiguities. In order to achieve high precision, many current static and kinematic surveying algorithms use a floating-point solution until enough information becomes available to fix the carrier-phase ambiguities accurately. However, in dynamic environments where many brief measurement outages or cycle slips are possible, these algorithms may never gain enough information to fix the ambiguities with the confidence required for a fixed-integer solution.

A new method is presented that uses a multiple model Kalman filter to resolve the carrier-phase integer ambiguities. This method starts with the floating-point results, yet smoothly and rapidly attains the precision of the correct fixed-integer solution, eliminating the need to decide when to switch from the floating to the fixed-integer solution. This method is based on a theoretically correct blending of solutions from multiple filters, each of which hypothesizes a different ambiguity set. This new technique is computationally efficient, providing a robust navigation solution useful in demanding applications such as precision landing and autonomous navigation.

The new method was evaluated during static ground and flight tests. Initial results indicate that the new method is capable of quickly resolving the carrier-phase ambiguities, transitioning smoothly to the true-fixed integer solution, and providing a highly accurate (centimeter-level) navigation solution. However, the performance of the new method depends on the correct carrier-phase ambiguity set being hypothesized by one of the multiple filters. Recommendations for further research are included.

DEVELOPMENT AND TESTING OF A
MULTIPLE FILTER APPROACH FOR PRECISE DGPS
POSITIONING AND CARRIER-PHASE AMBIGUITY RESOLUTION

1 Introduction

1.1 Background

The Global Positioning System (GPS), a satellite based radio navigation system, has become the accepted, if not the standard, navigation system for much of the world. GPS is used for many navigation applications: marine, airborne, and land navigation, as well as in many surveying applications. This increasing dependence on GPS has also caused a desire for an increased accuracy of the GPS solution.

GPS-determined position and velocity can be very accurate, but the accuracy depends on the type of receiver and the type of processing. Today's stand-alone civilian receivers (using only Coarse/Acquisition (C/A) code; see Section 1.4.2) have an accuracy of approximately 8-10 meters root-mean square (RMS) while military signal (P(Y); see Section 1.4.2) capable receivers have a slightly better accuracy of approximately 6-8 meters RMS.

For many applications, the accuracy provided by stand-alone GPS is not sufficient. To attain better accuracy, many types of Differential GPS (DGPS) systems have been developed. These DGPS techniques do not perform absolute positioning, but instead perform relative positioning between GPS receivers. Differential GPS techniques are based on the principle that many of the errors in the GPS signal are spatially correlated between receivers. Relative positioning removes the majority of the correlated errors, providing a significant performance increase over stand-alone GPS. Differential GPS techniques can be categorized into two main types based on the types of measurements used: code-based and carrier-based. Representative position solutions and the approximate accuracy of various types of GPS and DGPS systems are presented in Figure 1-1 and Table 1-1. For more detail the reader is referred to references [20, 34, 35].

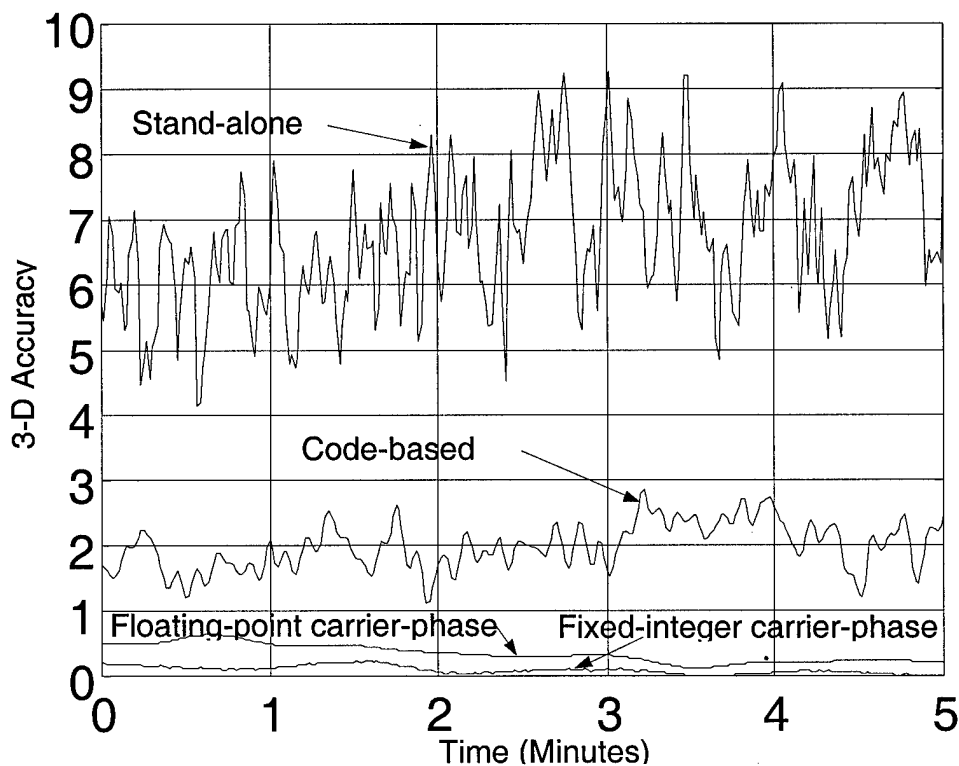


Figure 1-1. Typical GPS/DGPS Solution Time Histories

Table 1-1. Typical GPS/DGPS Accuracies

	Stand-alone GPS	Code based DGPS	Floating-Point CPDGPS	Fixed-Integer CPDGPS
Accuracy	6-10 m	1-3 m	0.2-0.5 m	0.01-0.03 m

Code-based DGPS techniques use the GPS “pseudorange” measurement. Code-based DGPS removes certain errors from the pseudorange measurements to provide an accurate position solution. The pseudorange measurement is obtained by the GPS receiver locking onto a GPS satellite’s pseudorandom code. The GPS pseudorange measurement is essentially the difference between the time of transmission of the GPS signal from the satellite and the time of reception by the GPS receiver. The pseudorange measurement is an absolute range measurement between the receiver and the satellite, and therefore DGPS systems are relatively easy to implement. Code-based DGPS systems are widely in use today and have a relative positioning accuracy of approximately of 1-3 meters RMS, as shown in Figure 1-1. The United States Coast Guard operates a code-based DGPS system for precision marine navigation on most of the country’s major waterways and harbors. Companies are also developing code-based DGPS system to monitor vehicles for a variety of applications such as mining, farming and cross-country trucking. Although widely in use today, code-based DGPS techniques are not the focus of this thesis.

Although code-based DGPS system provide a significant increase in accuracy over stand-alone GPS, carrier-phase based DGPS techniques must be employed to achieve the highest level of accuracy (on the order of centimeters) demanded by some applications.

Carrier-phase based DGPS techniques are based on the phase, or carrier cycles, of the GPS carrier frequency. A GPS carrier-phase measurement is the difference between the receiver's internally generated carrier signal, and the carrier signal received from a satellite. Unfortunately, a GPS receiver cannot tell the difference between one carrier cycle and the next. The receiver only counts the *change* in cycles between itself and the satellite. This means the initial number of cycles, which is by nature an integer value, between the receiver and satellite is unknown, or ambiguous. Because the initial number of cycles is unknown, carrier-phase measurements are not absolute range measurements. In order to use carrier-phase measurements for positioning, the carrier-phase integer ambiguities must be somehow estimated or resolved.

Floating-point carrier-phase DGPS techniques do not resolve carrier-phase ambiguities to their integer values, but simply estimate the carrier-phase ambiguities, generally using pseudorange measurements. The carrier-phase floating-point ambiguity estimates (which are not integer values) are then used to correct the carrier-phase measurements into absolute range measurements. Floating-point carrier-phase DGPS techniques use both pseudorange and carrier-phase measurement to generate an accurate relative position solution. Floating-point carrier-phase DGPS systems have a positioning accuracy of approximately 0.2 - 0.5 meters RMS. In addition, carrier-phase solutions tend to be "smoother" than code-based solutions, as shown in Figure 1-1.

To obtain the highest level of accuracy available with GPS measurements, the carrier-phase integer ambiguities must be correctly resolved. Once resolved these "fixed-integer" based carrier-phase DGPS systems have a positioning accuracy of approximately 0.01 - 0.03 meters RMS, as shown in Figure 1-1. Carrier-phase DGPS systems are

widely in use today with surveying companies. In addition, these types of systems are being developed for precision navigation, control, and autonomous landing of commercial and military aircraft.

Carrier-phase ambiguity resolution generally consists of two main functions, identifying possible ambiguity sets and determining which among these sets is correct. Numerous efficient methods have been developed to address the first part of the ambiguity resolution problem, and it is not the focus of this research. Additionally, many methods are currently available to determine the correct ambiguity set. Most current methods simply wait until enough information is obtained, by statistically comparing possible solutions, until the correct ambiguity set becomes evident. The disadvantage of this approach is it ignores the possibility of attaining a better position solution until the ambiguities are declared fixed. Some new efforts have explored the possibility of simply using the *best* set, namely the rounded floating-point ambiguity estimate, at each time step to obtain the optimal solution [8]. The disadvantage of this approach is that it relies only on a floating filter and ignores information available from other ambiguity set solutions and the information available from the time history of candidate ambiguity sets.

The disadvantages of both these approaches lend themselves to the use of Kalman filter techniques in determining the correct ambiguity set. This work provides a development and analysis of using multiple model adaptive Kalman filter techniques [22, 25] for the ambiguity resolution problem.

1.2 Problem Definition

The primary goal of this thesis is the development and testing of a new methodology to resolve carrier-phase ambiguities using advanced Kalman filtering techniques. The specific techniques are discussed in detail in Section 2.5.3. The secondary goal is the development and testing of a carrier-phase based DGPS system accurate enough to be used as a navigation truth source for airborne applications. The new methodology must:

- Accurately determine the carrier-phase ambiguities.
- Determine the ambiguities quickly, or with limited data.
- Provide a highly accurate navigation solution at all times.

1.3 Scope

This thesis covers the development and testing (both ground test and flight test) of a new algorithm designed to resolve carrier-phase ambiguities. Performance evaluations of the new algorithm are based on its ability to resolve the carrier-phase ambiguities and its position and velocity accuracy as compared to a nominal “truth” source.

Software development was conducted using MATLAB[®] 5.3 software [23]. Simulated GPS measurements were used to develop and debug the software. Analysis of the new methodology was conducted using actual GPS signals. Ground testing consisted of numerous static data sets collected using Ashtech GPS Z-Surveyor receivers for both the remote and reference receivers. Ground test evaluations are based on Ashtech Office Suite Software-generated truth data [1]. Truth data includes positioning information and the correct carrier-phase ambiguities. Flight test data consists of numerous data sets collected by flying a T-38 aircraft, again using Ashtech GPS Z-Surveyor receivers [2] for

both the reference and remote (airborne) receivers. Flight test evaluations are again based on Ashtech Office Suite Software generated truth data. Flight test truth data includes positioning information and the correct carrier-phase ambiguities.

Detailed information on the data sets used in this research is presented in Chapter 4. A description of the flight test profiles is presented in Appendix A. For more information on Ashtech Office Suite software, the reader is referred to reference [1].

1.4 Related Research

Much of the work in this thesis is based on current research found in industry and academia. This research can be broken down into two main areas: Kalman filtering and GPS (including various types of Differential GPS).

1.4.1 Kalman Filtering

Developed in 1960 by *Kalman*, a linear Kalman filter is an *optimal recursive data processing algorithm* [24, 25]. All Kalman filters are based on a model of the system of interest. The Kalman filter uses information about the model of the system as well as the measurements of the system to generate optimal state estimates. The filter is optimal with respect to virtually any criterion, one aspect being that the filter incorporates all available information. The filter is recursive in that the filter does not require all previous data to be reprocessed every time a new measurement is received. Since the introduction of the linear Kalman filter, new designs have been developed to handle nonlinear models and parallel filter applications [22, 25].

1.4.1.1 Multiple Model Adaptive Estimation

In 1965, Magill [22] presented what is now called a Multiple Model Adaptive Estimator (MMAE). An MMAE is a bank, or set, of individual Kalman filters each based on a particular assumption about the system of interest. Each Kalman filter within the MMAE is called an “elemental filter.” Each elemental filter generates its own optimal estimate of the variables of interest, based not only on the system measurements, but also on its own assumptions (or model) of the system. The characteristics of the residual vector outputs of the elemental filters are used to determine which elemental filter’s system model best matches the true system model [12]. The first practical MMAE was implemented in 1977 by Athens et. al. [3].

Optimality conditions for the MMAE, similar to those of a linear Kalman filter, were proven by Chang and Athans [5], but only if the true system exactly matched the assumption(s) modeled by one of the elemental filters. If the modeled system does not exactly match the real system, research indicates the MMAE will converge to the elemental filter based on “closest to true” system model, in the Barum’s distance-measure sense [4, 25].

The Air Force Institute of Technology (AFIT) has been a major contributor in the area of MMAE research. AFIT has researched and applied MMAE algorithms in various areas including: detection of failed sensors [10, 30], adaptive target tracking [29], adaptive control [39], and GPS spoofing and jamming [43].

In 1985, Maybeck and Suizu [28] addressed the problem of “beta dominance” [3] in a MMAE. Beta dominance is the tendency of the MMAE to weight an elemental filter incorrectly due to erroneous residual contributions. The method developed by Maybeck

and Suizu sets the necessary scalar coefficient to unity; see Equation (2-56). This method greatly improves the performance of the MMAE in certain applications. Additional work on the beta dominance problem known as was done by Menke [30].

In 1987, Maybeck and Hentz [27] reduced the number of necessary elemental filters by using the concept of a *moving bank* of filters. Instead of using a large number of elemental filters, a smaller number of points upon which to base elemental filters are moved as necessary through the appropriate parameter space. Additional moving bank MMAE work was done in 1998 by Vasquez [44]. Continuing the idea was the development of “filter spawning” in 1998 by Fisher [12]. Filter spawning involves using a minimal set of filters until it becomes necessary to use more filters to define the parameter space coverage better [12].

Recent work with MMAE design directly related to GPS started in 1992 with Vasquez [43]. The preliminary work used an MMAE structure for detection of spoofing, jamming or failures in the GPS system. In 1998, Vanek [42] used an MMAE structure for GPS signal offset detection and noise strength estimation.

As shown above, there has been an abundance of research in the area of MMAE design and application, but an MMAE structure has never been used to resolve carrier-phase ambiguities. This thesis uses an MMAE to resolve the carrier-phase ambiguities.

1.4.2 Global Positioning System

The Global Positioning System (GPS) is a constellation of 27 radio navigation satellites (24 primary plus three spares). Each satellite continuously transmits a stream of navigation codes and ranging information providing users with data capable of producing

the position, velocity, and time at the user's location. Currently, most GPS receivers process data from all visible satellites (up to the number of channels in the receiver). For more details on GPS, the reader is referred to references [20, 34, 35].

1.4.2.1 Carrier-Phase Ambiguity Resolution

Resolving the carrier-phase integer ambiguities has been an area of research for many years. The simplest technique is to use code measurements to determine the carrier-phase ambiguities directly. However, due to the large errors associated with code measurements, this technique is usually not adequate. Another early attempt to resolve the carrier-phase ambiguities was the Ambiguity Function Method [7]. The Ambiguity Function Method is a pure position domain search, and is computationally intensive and not commonly used.

The Least Squares Ambiguity Search Technique (LSAST) was developed by Hatch [17] in 1990. In the LSAST method, a given number of ambiguity sets are formed based on the size of the ambiguity search space. Then each ambiguity set is tested by calculating a least-squares position estimate and residual. The integer ambiguity set with residuals (the difference between the true measurement and the predicted measurement) significantly lower than the other ambiguity sets is assumed to be the correct set. This method is also computationally intensive, but is more efficient than the Ambiguity Function Method. This method is also not commonly used.

Other techniques use information about the ambiguities contained in a covariance matrix to help determine the correct ambiguity set. The Fast Ambiguity Search Filter (FASF) was developed by Chen and Lapachelle in 1993 [6]. The FASF method starts with the floating-point ambiguity estimates and covariance. The method next assumes

the best known, smallest covariance, ambiguity is correct and rounds it to the closest integer. Then new conditional covariance and ambiguity estimates are developed for the other ambiguities based on the first ambiguity being “correct.” The process is repeated until a valid ambiguity set is found or an integer ambiguity is not found within the search space. This results in an efficient recursive carrier-phase ambiguity resolution algorithm.

One of the most efficient techniques is known as the Least-squares AMBiguity Decorrelation Adjustment method (LAMBDA) [40, 9]. The LAMBDA method consists of two steps. First, the ambiguities are decorrelated using a linear, volume-preserving integer transform known as a “Z-transform”. Then a sequential conditional least-squares search is performed on the transformed ambiguities. The LAMBDA method was improved by Li and Gao [21], with the ability to construct high dimensional “Z-transforms.”

Some recent research has been performed in applying advanced Kalman filtering techniques to the ambiguity resolution problem. Cox and Brading [8] proposed using the outputs of a Kalman filter to determine the optimal integer ambiguity set and the optimal navigation solution. This approach considers the integer values closest to the Kalman filter estimates as the “the optimal” ambiguity set and does not use MMAE techniques to determine the correct ambiguity set. Finally, in 2000 Williamson and Speyer [45] used an MMAE structure to detect carrier-phase cycle slips in an integrated GPS/INS (Inertial Navigation System), but not to resolve the integer ambiguities.

1.5 Methodology

The research presented in this thesis begins with Kalman filtering and MMAE designs and applications presented in Maybeck [27, 28], Magill [22], Vasquez [44], Miller [31], Vanek [42] and Fisher [12]. This produced the basic MMAE design used in this thesis. In addition, a detailed study was conducted on GPS, DGPS and carrier-phase ambiguity resolution techniques presented by Kaplan [20], Raquet [36, 37], Hatch [17], Chen and Lapachelle [6], and Teunissen [40].

A basic DGPS Kalman filter was implemented in MATLAB[®] [23] using a design similar to the one outlined by Raquet [36]. The filter was expanded to use single or dual frequency data, and other measurement combinations as specified by the user.

The development of the overall algorithm began after verifying the performance of the basic DGPS model. The MMAE model was designed using the basic MMAE structure found in Maybeck [25]. It contains up to 100 elemental filters, each based on a different ambiguity set. Ambiguity set generation for this thesis was developed using a combination of the LAMBDA method “Z-transform” and an FASF subroutine. The combination of these two methods is detailed in Section 2.5.3.1.

All analysis of the new methodology was conducted using actual GPS signals. Ground tests were conducted with Ashtech GPS Z-Surveyor receivers for both the remote and reference receivers. The performance of the algorithm was analyzed based on four different ground test cases, with baselines varying from 250 meters to 100 kilometers. Ground test evaluations are based on Ashtech Office Suite Software-generated “truth” data, which includes positioning information and the correct carrier-phase ambiguities. Flight tests were conducted by flying a T-38A aircraft, also with Ashtech GPS Z-

Surveyor receivers for both the remote and reference receivers. The performance of the algorithm was analyzed based on numerous different flight test cases, with baselines varying from 10 nautical miles to 100 nautical miles at altitudes from 10,000 to 30,000 feet. Flight test evaluations are based on GPS Aided INS Navigation Reference (GAINR) generated truth data, which includes position and velocity information, and Ashtech Office Suite Software truth data containing the correct carrier-phase ambiguities. Finally, analysis and plotting routines were built in MATLAB[®] for a complete tabular and graphical presentation that enabled comparisons of the algorithm to known truth sources, and for side-by-side case comparisons.

1.6 Thesis Overview

Chapter 2 presents the required Kalman Filter, MMAE, and GPS theory used to develop the mathematical models for this research. Kalman filter and MMAE theory are defined and presented as is the theory, mathematical relationships, and measurement types for GPS. Finally, the concepts and methods used for candidate ambiguity set generation, the LAMBDA and FASF methods are described.

Chapter 3 describes the flow of the new algorithm. Detailed model and measurement equations are presented for the DGPS filter and the MMAE design. The method used to generate candidate ambiguity sets is described in detail, as are the calculations required to determine the correct ambiguity set. Finally, concepts necessary to understand the output of the overall algorithm are presented.

Chapter 4 presents a performance analysis of each test case in this research. Position accuracy analysis and ambiguity resolution analysis is presented for ground and flight tests.

Chapter 5 presents a summary of this research effort. In addition, conclusions and recommendations for future research are presented.

2 Theory

2.1 Overview

This chapter describes the linear Kalman filter, the Extended Kalman Filter (EKF) and the Multiple Model Adaptive Estimation (MMAE) structure in more detail. In addition, this chapter develops theory behind GPS, Differential GPS (DGPS) and Carrier-Phase Differential GPS (CPDGPS).

2.2 Kalman Filters

A linear Kalman filter is an *optimal recursive data processing algorithm* [24, 25]. The filter is optimal with respect to virtually any criterion, one aspect being the filter incorporates all available information. The filter is recursive in that the filter computes a new estimate at discrete time intervals whenever a new measurement is available. It does not need all previous measurements to produce an optimal state estimate, as would a batch processing algorithm. In addition, the Kalman filter is a data processing algorithm, meaning it is simply a computer program processing discrete-time measurement samples.

Every Kalman filter is based on a model of the system of interest. The Kalman filter uses system measurements and the system model to generate optimal state estimates. The Kalman filter uses all available measurements, regardless of their accuracy, to generate an optimal estimate of the variables of interest based on knowledge of the system dynamics and measurement characteristics, the statistical description of the system noises, measurement errors, and model uncertainties [46].

The Kalman filter can be described by two stages of operation: the *propagation* stage, and the *update* stage. During the propagation stage, the filter computes a prediction of the system states at some future time based on its own imperfect dynamics model of the system. During the update stage, the filter uses noise-corrupted measurements to refine its predicted state estimates further, generating the optimal state estimate. A complete derivation can be found in *Stochastic Models, Estimation, and Control, Volume 1* [24].

2.2.1 State and Measurement Model Equations

Following the development discussed in references [24, 25, 31], assume that the system dynamics can be modeled as a linear, time-invariant system. The state equation takes the form:

$$\dot{\mathbf{x}}(t) = \mathbf{F}(t)\mathbf{x}(t) + \mathbf{B}(t)\mathbf{u}(t) + \mathbf{G}(t)\mathbf{w}(t) \quad (2-1)$$

where

- $\mathbf{x}(t)$ = the n -dimensional system state vector
- $\mathbf{F}(t)$ = the n -by- n state dynamics matrix
- $\mathbf{B}(t)$ = the n -by- r control input matrix
- $\mathbf{u}(t)$ = the r -dimensional control input vector
- $\mathbf{G}(t)$ = the n -by- s noise input matrix
- $\mathbf{w}(t)$ = the s -dimensional dynamics driving noise vector

The dynamics driving noise vector $\mathbf{w}(t)$ is assumed to be white Gaussian noise with mean and covariance defined by:

$$E\{\mathbf{w}(t)\} = \mathbf{0} \quad (2-2)$$

$$E\{\mathbf{w}(t)\mathbf{w}^T(t+\tau)\} = \mathbf{Q}(t)\delta(\tau) \quad (2-3)$$

where τ has units of time.

Next, assume the measurements can be modeled as a linear, time-invariant, discrete time system. The measurement equation takes the form:

$$\mathbf{z}(t_i) = \mathbf{H}(t_i)\mathbf{x}(t_i) + \mathbf{v}(t_i) \quad (2-4)$$

where

$\mathbf{z}(t_i)$ = the m -dimensional measurement vector

$\mathbf{H}(t_i)$ = the m -by- n system output matrix

$\mathbf{v}(t_i)$ = the m -dimensional discrete time noise input vector

The discrete time noise input vector $\mathbf{v}(t_i)$ is also assumed to be white Gaussian noise. The mean and covariance are defined by:

$$E\{\mathbf{v}(t_i)\} = \mathbf{0} \quad (2-5)$$

$$E\{\mathbf{v}(t_i)\mathbf{v}^T(t_j)\} = \begin{cases} \mathbf{R}(t_i) & \text{for } t_i = t_j \\ \mathbf{0} & \text{for } t_i \neq t_j \end{cases} \quad (2-6)$$

Noises $\mathbf{w}(t)$ and $\mathbf{v}(t_i)$ are assumed independent. Thus:

$$E\{\mathbf{w}(t)\mathbf{v}^T(t_i)\} = \mathbf{0} \quad (2-7)$$

for all t and t_i .

2.2.2 Kalman Filter Equations

The Kalman filter is propagated forward from time t_{i-1} to t , starting from initial conditions $\hat{\mathbf{x}}(t_0)$ and $\mathbf{P}(t_0)$, or from the last update cycle state and covariance estimates.

The Kalman filter is propagated forward by:

$$\dot{\hat{\mathbf{x}}}(t/t_{i-1}) = \mathbf{F}(t)\hat{\mathbf{x}}(t/t_{i-1}) + \mathbf{B}(t)\mathbf{u}(t) \quad (2-8)$$

$$\dot{\mathbf{P}}(t/t_{i-1}) = \mathbf{F}(t)\mathbf{P}(t/t_{i-1}) + \mathbf{P}(t/t_{i-1})\mathbf{F}^T(t) + \mathbf{G}(t)\mathbf{Q}(t)\mathbf{G}^T(t) \quad (2-9)$$

Before being used in the update stage of the Kalman filter the state and covariance differential equations are solved by:

$$\hat{\mathbf{x}}(t_i^-) = \Phi(t_i, t_{i-1})\hat{\mathbf{x}}(t_{i-1}^+) + \int_{t_{i-1}}^{t_i} \Phi(t_i, \tau)\mathbf{B}(\tau)\mathbf{u}(\tau)\delta\tau \quad (2-10)$$

$$\mathbf{P}(t_i^-) = \Phi(t_i, t_{i-1})\mathbf{P}(t_{i-1}^+)\Phi^T(t_i, t_{i-1}) + \int_{t_{i-1}}^{t_i} \Phi(t_i, \tau)\mathbf{G}(\tau)\mathbf{Q}(\tau)\mathbf{G}^T(\tau)\Phi^T(t_i, \tau)\delta\tau \quad (2-11)$$

where $\Phi(t_i, t_{i-1})$ is the state transition matrix from time t_{i-1} to t_i and is calculated by

$$\Phi(t_i, t_{i-1}) = \Phi(\Delta t) = e^{\mathbf{F}\Delta t} \text{ where } \Delta t \equiv t_i - t_{i-1}.$$

In Equations (2-10) and (2-11), the $-$ and $+$ superscripts indicate times immediately before and after measurements are incorporated, respectively.

The Kalman filter is updated by:

$$\mathbf{A}(t_i) = \mathbf{H}(t_i)\mathbf{P}(t_i^-)\mathbf{H}^T(t_i) + \mathbf{R}(t_i) \quad (2-12)$$

$$\mathbf{K}(t_i) = \mathbf{P}(t_i^-)\mathbf{H}^T(t_i)\mathbf{A}(t_i)^{-1} \quad (2-13)$$

$$\mathbf{r}(t_i) = \mathbf{z}_i - \mathbf{H}(t_i)\hat{\mathbf{x}}(t_i^-) \quad (2-14)$$

$$\hat{\mathbf{x}}(t_i^+) = \hat{\mathbf{x}}(t_i^-) + \mathbf{K}(t_i)\mathbf{r}(t_i) \quad (2-15)$$

$$\mathbf{P}(t_i^+) = \mathbf{P}(t_i^-) - \mathbf{K}(t_i)\mathbf{H}(t_i)\mathbf{P}(t_i^-) \quad (2-16)$$

In a properly designed filter the residual vector $\mathbf{r}(t_i)$ is zero mean with a filter-predicted covariance of $\mathbf{A}(t_i)$. The primary outputs of a Kalman filter are the optimal

state estimates $\hat{\mathbf{x}}(t_i^+)$ and their filter computed covariance $\mathbf{P}(t_i^+)$. In MMAE designs, the residual vector $\mathbf{r}(t_i)$ and predicted covariance $\mathbf{A}(t_i)$ are also useful.

2.3 Extended Kalman Filters

A linear Kalman filter is only useful when both the dynamics and measurement equations of a system are a linear combination of the states, known control inputs and noises modeled. However, the equations relating the state and measurement variables for most real system (including the GPS systems in this thesis) are nonlinear. To handle these nonlinearities, the Extended Kalman Filter (EKF) is used.

The concept behind an EKF is to relinearize the nonlinear model about the current best estimate $\hat{\mathbf{x}}(t_i^+)$. This relinearization about each new estimate allows the use of linear assumptions and equations. The EKF is a first-order *approximation* to an optimal nonlinear filter. It is implemented in a very similar manner as the linear Kalman filter through a basic *propagation* stage and an *update* stage. A complete derivation of the EKF can be found in *Stochastic Models, Estimation, and Control, Volume II* [25].

2.3.1 State and Measurement Model Equations

Following the development discussed in reference [25], assume that the system dynamics can be modeled as a nonlinear state equation, which takes the form:

$$\dot{\mathbf{x}}(t) = \mathbf{f}[\mathbf{x}(t), \mathbf{u}(t), t] + \mathbf{G}(t)\mathbf{w}(t) \quad (2-17)$$

where

$\mathbf{x}(t)$ = the n -dimensional state dynamics vector

$\mathbf{f}[\mathbf{x}(t), \mathbf{u}(t), t]$ = the state dynamics vector, which is a linear or nonlinear function of the n -dimensional state vector $\mathbf{x}(t)$, the r -dimensional control input function $\mathbf{u}(t)$ and of continuous-time t .

$\mathbf{G}(t)$ = the n -by- s noise distribution matrix

$\mathbf{w}(t)$ = the s -dimensional dynamics driving noise vector

The dynamics driving noise vector is assumed to be a white Gaussian noise process whose mean and covariance are defined by:

$$E\{\mathbf{w}(t)\} = \mathbf{0} \quad (2-18)$$

$$E\{\mathbf{w}(t)\mathbf{w}^T(t+\tau)\} = \mathbf{Q}(t)\delta(\tau) \quad (2-19)$$

where τ has units of time.

Next, assume the EKF discrete time measurements can be modeled as a nonlinear state equation. It takes the form:

$$\mathbf{z}(t_i) = \mathbf{h}[\mathbf{x}(t_i), t_i] + \mathbf{v}(t_i) \quad (2-20)$$

where

$\mathbf{z}(t_i)$ = the m -dimensional measurement vector at time t_i

$\mathbf{h}[\mathbf{x}(t_i), t_i]$ = a known linear or nonlinear m -dimensional function of $\mathbf{x}(t_i)$ and t_i

$\mathbf{v}(t_i)$ = the m -dimensional discrete-time noise input vector

The discrete-time noise input vector $\mathbf{v}(t_i)$ is also assumed to be white Gaussian noise. The mean and covariance are defined by:

$$E\{\mathbf{v}(t_i)\} = \mathbf{0} \quad (2-21)$$

$$E\{\mathbf{v}(t_i)\mathbf{v}^T(t_j)\} = \begin{cases} \mathbf{R}(t_i) & \text{for } t_i = t_j \\ \mathbf{0} & \text{for } t_i \neq t_j \end{cases} \quad (2-22)$$

2.3.2 State and Measurement Model Linearization

Assuming Equations (2-17) and (2-20) are nonlinear, they must be linearized in order to produce an optimal estimate of the state vector $\mathbf{x}(t)$, to first order. The linearization technique used in reference [25] involves perturbations about a nominal state trajectory to produce a first order linear approximation of Equations (2-17) and (2-20) for use in an EKF [46].

Assume a nominal state trajectory $\mathbf{x}_n(\bullet)$ can be generated from the initial conditions $\mathbf{x}_n(t_0) = \mathbf{x}_{n0}$ using the following differential equation.

$$\dot{\mathbf{x}}_n(t) = \mathbf{f}[\mathbf{x}_n(t), \mathbf{u}(t), t] \quad (2-23)$$

In addition to the nominal state trajectory, assume a sequence of nominal measurements. They can be defined by:

$$\mathbf{z}_n(t_i) = \mathbf{h}[\mathbf{x}_n(t_i), t_i] \quad (2-24)$$

To produce the perturbation state $\delta\mathbf{x}(t)$ the nominal trajectory (2-23) is subtracted from the system model, Equation (2-17), to give:

$$\delta\dot{\mathbf{x}}(t) \equiv [\dot{\mathbf{x}}(t) - \dot{\mathbf{x}}_n(t)] = \mathbf{f}[\mathbf{x}(t), \mathbf{u}(t), t] - \mathbf{f}[\mathbf{x}_n(t), \mathbf{u}(t), t] + \mathbf{G}(t)\mathbf{w}(t) \quad (2-25)$$

A Taylor series expansion of $\mathbf{f}[\mathbf{x}(t), \mathbf{u}(t), t]$ about $\mathbf{x}_n(t)$ gives:

$$\mathbf{f}[\mathbf{x}(t), \mathbf{u}(t), t] = \mathbf{f}[\mathbf{x}_n(t), \mathbf{u}(t), t] + \left. \frac{\partial \mathbf{f}[\mathbf{x}(t), \mathbf{u}(t), t]}{\partial \mathbf{x}} \right|_{\mathbf{x}=\mathbf{x}_n(t)} [\mathbf{x}(t) - \mathbf{x}_n(t)] + h.o.t. \quad (2-26)$$

where "h.o.t." represents the higher order terms in the expansion with powers greater than one. Finally, combining Equations (2-25) and (2-26), subtracting like terms and then reducing it to a first order approximation gives:

$$\delta \dot{\mathbf{x}}(t) = \mathbf{F}[t; \mathbf{x}_n(t)] \delta \mathbf{x}(t) + \mathbf{G}(t) \mathbf{w}(t) \quad (2-27)$$

Here, $\mathbf{F}[t; \mathbf{x}_n(t)]$ is the n -by- n partial derivative matrix of \mathbf{f} with respect to \mathbf{x} , evaluated along the nominal trajectory and defined by:

$$\mathbf{F}[t; \mathbf{x}_n(t)] = \left. \frac{\partial \mathbf{f}[\mathbf{x}, \mathbf{u}(t), t]}{\partial \mathbf{x}} \right|_{\mathbf{x}=\mathbf{x}_n(t)} \quad (2-28)$$

This is an acceptable approximation to the true solution provided the deviations from the nominal solution are small enough that the higher order terms in the Taylor series approximation of Equation (2-26) are negligible.

In a similar manner the measurement perturbation $\delta \mathbf{z}(t_i)$ of the measurement vector $\mathbf{z}(t_i)$ is formed by subtracting Equation (2-24) from (2-20) to yield:

$$\delta \mathbf{z}(t_i) \equiv [\mathbf{z}(t_i) - \mathbf{z}_n(t_i)] = \mathbf{h}[\mathbf{x}(t_i), t_i] - \mathbf{h}[\mathbf{x}_n(t_i), t_i] + \mathbf{v}(t_i) \quad (2-29)$$

A Taylor series expansion of $\mathbf{h}[\mathbf{x}(t_i), t_i]$ about $\mathbf{x}_n(t_i)$ gives:

$$\mathbf{h}[\mathbf{x}(t_i), t_i] = \mathbf{h}[\mathbf{x}_n(t_i), t_i] + \left. \frac{\partial \mathbf{h}[\mathbf{x}(t_i), t_i]}{\partial \mathbf{x}} \right|_{\mathbf{x}(t_i)=\mathbf{x}_n(t_i)} [\mathbf{x}(t_i) - \mathbf{x}_n(t_i)] + h.o.t. \quad (2-30)$$

Combining Equations (2-29) and (2-30), subtracting like terms and then reducing it to a first order approximation gives:

$$\delta \mathbf{z}(t_i) \equiv \mathbf{H}[t_i; \mathbf{x}_n(t_i)] \delta \mathbf{x}(t_i) + \mathbf{v}(t_i) \quad (2-31)$$

Here, $\mathbf{H}[t_i; \mathbf{x}_n(t_i)]$ is the m -by- n partial derivative matrix of \mathbf{h} with respect to \mathbf{x} , evaluated along the nominal trajectory and defined by:

$$\mathbf{H}[t_i; \mathbf{x}_n(t_i)] = \left. \frac{\partial \mathbf{h}[\mathbf{x}, t_i]}{\partial \mathbf{x}} \right|_{\mathbf{x}=\mathbf{x}_n(t_i)} \quad (2-32)$$

Again, this is an acceptable approximation to the true solution provided the deviations from the nominal solution are small enough that the higher order terms in the Taylor series approximation of Equation (2-30) are negligible.

The system model in Equations (2-27) and (2-31) is optimal to first order due to the truncated Taylor Series, and has been linearized to produce *error* state equations. They can now be used to implement a linearized Kalman filter to perform all state propagation and update equations. The total state estimate can be calculated by adding the nominal state value to the error state estimate.

Recall that an EKF relinearizes the nonlinear model about the current best estimate $\hat{\mathbf{x}}(t_i^+)$ and a trajectory emanating from it, as opposed to the nominal state just described. This effectively incorporates a new and better state trajectory into the filter model at each measurement time, allowing the use of linear perturbation techniques.

2.3.3 Extended Kalman Filter Equations

The EKF state and covariance estimates are propagated forward from time t_{i-1} to t_i by integrating from the initial conditions $\hat{\mathbf{x}}(t_0)$ and $\mathbf{P}(t_0)$, or from the last update cycle state and covariance estimates. The propagation equations are given by:

$$\dot{\hat{\mathbf{x}}}(t/t_{i-1}) = \mathbf{f}[\hat{\mathbf{x}}(t/t_{i-1}), \mathbf{u}(t), t] \quad (2-33)$$

$$\dot{\mathbf{P}}(t/t_{i-1}) = \mathbf{F}[t; \hat{\mathbf{x}}(t/t_{i-1})]\mathbf{P}(t/t_{i-1}) + \mathbf{P}(t/t_{i-1})\mathbf{F}^T[t; \hat{\mathbf{x}}(t/t_{i-1})] + \mathbf{G}(t)\mathbf{Q}(t)\mathbf{G}^T(t) \quad (2-34)$$

where the matrix $\mathbf{F}[t; \hat{\mathbf{x}}(t/t_{i-1})]$ is given by:

$$\mathbf{F}[t; \hat{\mathbf{x}}(t/t_{i-1})] \equiv \left. \frac{\partial \mathbf{f}[\mathbf{x}, \mathbf{u}(t), t]}{\partial \mathbf{x}} \right|_{\mathbf{x}=\hat{\mathbf{x}}(t/t_{i-1})} \quad (2-35)$$

In the above equations, the term t / t_{i-1} is the value of a given variable at time t , conditioned on the measurements taken through time t_{i-1} .

If not at time t_0 , the initial conditions at the start of the propagation cycle are defined by:

$$\hat{\mathbf{x}}(t_{i-1} / t_{i-1}) = \hat{\mathbf{x}}(t_{i-1}^+) \quad (2-36)$$

$$\mathbf{P}(t_{i-1} / t_{i-1}) = \mathbf{P}(t_{i-1}^+) \quad (2-37)$$

After integrating Equations (2-33) and (2-34) forward to the next sample time, the following state and covariance values are used in the next measurement update cycle:

$$\hat{\mathbf{x}}(t_i^-) = \hat{\mathbf{x}}(t_i / t_{i-1}) \quad (2-38)$$

$$\mathbf{P}(t_i^-) = \mathbf{P}(t_i / t_{i-1}) \quad (2-39)$$

The EKF is updated by:

$$\mathbf{K}(t_i) = \mathbf{P}(t_i^-) \mathbf{H}^T [t_i; \hat{\mathbf{x}}(t_i^-)] [\mathbf{H} [t_i; \hat{\mathbf{x}}(t_i^-)] \mathbf{P}(t_i^-) \mathbf{H}^T [t_i; \hat{\mathbf{x}}(t_i^-)] + \mathbf{R}(t_i)]^{-1} \quad (2-40)$$

$$\hat{\mathbf{x}}(t_i^+) = \hat{\mathbf{x}}(t_i^-) + \mathbf{K}(t_i) \{z_i - \mathbf{h}[\hat{\mathbf{x}}(t_i^-), t_i]\} \quad (2-41)$$

$$\mathbf{P}(t_i^+) = \mathbf{P}(t_i^-) - \mathbf{K}(t_i) \mathbf{H} [t_i; \hat{\mathbf{x}}(t_i^-)] \mathbf{P}(t_i^-) \quad (2-42)$$

where the matrix $\mathbf{H} [t_i; \hat{\mathbf{x}}(t_i^-)]$ is given by:

$$\mathbf{H} [t_i; \hat{\mathbf{x}}(t_i^-)] \equiv \left. \frac{\partial \mathbf{h}[\mathbf{x}, t_i]}{\partial \mathbf{x}} \right|_{\mathbf{x}=\hat{\mathbf{x}}(t_i^-)} \quad (2-43)$$

The updated state estimate and covariance estimates are used as the new initial conditions for the propagation cycle of the sampling interval:

$$\hat{\mathbf{x}}(t_i / t_i) = \hat{\mathbf{x}}(t_i^+) \quad (2-44)$$

$$\mathbf{P}(t_i / t_i) = \mathbf{P}(t_i^+) \quad (2-45)$$

2.4 Multiple Model Adaptive Estimation

There are many different types of Multiple Model Adaptive Estimators. The MMAE used in this research follows the development of the *multiple model filter algorithm* derived in reference [25]. A block diagram of the *multiple model filter algorithm* is shown below in Figure 2-1.

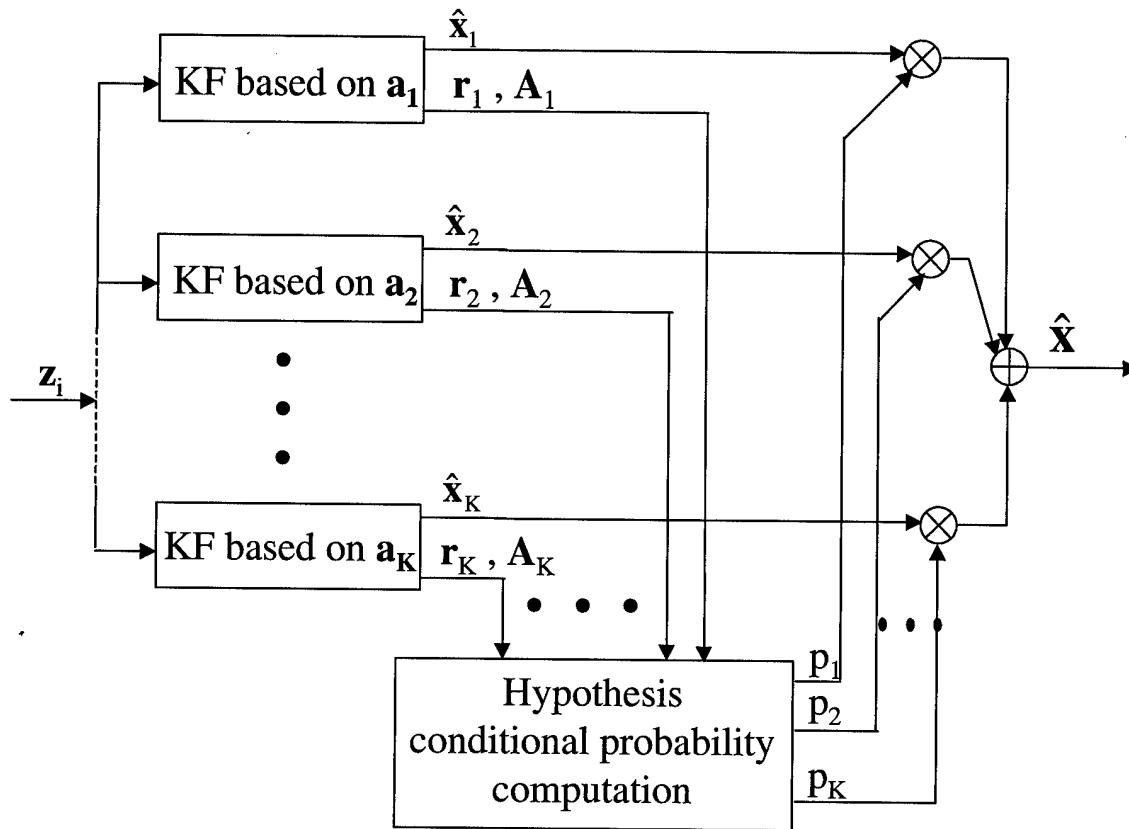


Figure 2-1. Multiple Model Filtering Algorithm

An MMAE is a bank, or set, of K Kalman filters, each designed using a different parameter vector (denoted \mathbf{a}_k), or model, of the system of interest. Each one of the individual Kalman filters is called an elemental filter. The residual vector, $\mathbf{r}_k(t_i)$, and its

covariance, $\mathbf{A}_k(t_i)$, are measures of how well the system modeled in the elemental filter matches the true system. Therefore, if each elemental filter is given the same measurements, then by monitoring the residuals it is possible to determine which elemental filter's model best matches the true system.

2.4.1 Elemental Filters

As stated above, each of the K elemental filters in the MMAE are based on a different parameter vector \mathbf{a} or model of system of interest. For example, the k^{th} filter is based on the parameter vector \mathbf{a}_k . The elemental filters are each propagated forward by:

$$\hat{\mathbf{x}}_k(t_i^-) = \Phi_k(t_i, t_{i-1})\hat{\mathbf{x}}_k(t_{i-1}^+) + \mathbf{B}_{dk}(t_{i-1})\mathbf{u}(t_{i-1}) \quad (2-46)$$

$$\mathbf{P}_k(t_i^-) = \Phi_k(t_i, t_{i-1})\mathbf{P}_k(t_{i-1}^+)\Phi_k^T(t_i, t_{i-1}) + \mathbf{G}_{dk}(t_{i-1})\mathbf{Q}_{dk}(t_{i-1})\mathbf{G}_{dk}^T(t_{i-1}) \quad (2-47)$$

The elemental filters are each updated by:

$$\mathbf{A}_k(t_i) = \mathbf{H}_k(t_i)\mathbf{P}_k(t_i^-)\mathbf{H}_k^T(t_i) + \mathbf{R}_k(t_i) \quad (2-48)$$

$$\mathbf{K}_k(t_i) = \mathbf{P}_k(t_i^-)\mathbf{H}_k^T(t_i)\mathbf{A}_k(t_i)^{-1} \quad (2-49)$$

$$\mathbf{r}_k(t_i) = \mathbf{z}_i - \mathbf{H}_k(t_i)\hat{\mathbf{x}}_k(t_i^-) \quad (2-50)$$

$$\hat{\mathbf{x}}_k(t_i^+) = \hat{\mathbf{x}}_k(t_i^-) + \mathbf{K}_k(t_i)\mathbf{r}_k(t_i) \quad (2-51)$$

$$\mathbf{P}_k(t_i^+) = \mathbf{P}_k(t_i^-) - \mathbf{K}_k(t_i)\mathbf{H}_k(t_i)\mathbf{P}_k(t_i^-) \quad (2-52)$$

where the subscript k refers to the k^{th} elemental filter.

It is important to understand that at every sample time t_i , each elemental filter generates an optimal state estimate $\hat{\mathbf{x}}_k(t_i^+)$, covariance $\mathbf{P}_k(t_i^+)$, residual vector $\mathbf{r}_k(t_i)$, and covariance $\mathbf{A}_k(t_i)$ based on its internal system model and system measurements.

2.4.2 Conditional Probability Generation

The residuals of the elemental filters are evaluated by the conditional probability computation shown in Figure 2-1. The conditional probability of the k^{th} elemental filter at time t_i , is defined as:

$$p_k(t_i) = \text{Prob}(\mathbf{a} = \mathbf{a}_k | \mathbf{Z}(t_i) = \mathbf{Z}_i) \quad (2-53)$$

The conditional probability is the probability that the random variable \mathbf{a} , representing the system characteristics, is the realization of the variable in the k^{th} elemental filter \mathbf{a}_k , given the time history of measurements up to and including that taken at time t_i . The time history of measurements is represented by:

$$\mathbf{Z}(t_i) = [\mathbf{z}(t_1)^T : \mathbf{z}(t_2)^T : \dots : \mathbf{z}(t_i)^T]^T \quad (2-54)$$

As shown in [25], the conditional probabilities can be computed as:

$$p_k(t_i) = \frac{f_{\mathbf{z}(t_i)|\mathbf{a}, \mathbf{Z}(t_{i-1})}(\mathbf{z}_i | \mathbf{a}_k, \mathbf{Z}_{i-1}) p_k(t_{i-1})}{\sum_{j=1}^K f_{\mathbf{z}(t_i)|\mathbf{a}, \mathbf{Z}(t_{i-1})}(\mathbf{z}_i | \mathbf{a}_j, \mathbf{Z}_{i-1}) p_j(t_{i-1})} \quad (2-55)$$

The denominator in Equation (2-55) acts as a scaling function ensuring that the probability of each elemental filter is properly defined in the sense that:

$$p_k(t_i) \geq 0 \text{ for all } K \text{ and } \sum_{k=1}^K p_k(t_i) = 1$$

The conditional density function in Equation (2-55) is for the current measurement based on the elemental filter's parameter vector \mathbf{a}_k and the time history of measurements. This density function is represented and calculated by:

$$f_{\mathbf{z}(t_i)|\mathbf{a},\mathbf{Z}(t_{i-1})}(\mathbf{z}_i|\mathbf{a}_k,\mathbf{Z}_{i-1}) = \frac{1}{(2\pi)^{m/2}|\mathbf{A}_k(t_i)|^{-1/2}} * \exp\{\bullet\} \quad (2-56)$$

$$\{\bullet\} = \left\{ -\frac{1}{2} \mathbf{r}_k^T(t_i) \mathbf{A}_k(t_i)^{-1} \mathbf{r}_k(t_i) \right\}$$

where m = the number of measurements. Equation (2-56) is the conditional density function for the residuals of the k^{th} elemental filter, conditioned on \mathbf{a}_k and the time history of measurements up to time t_{i-1} , where $\mathbf{r}_k(t_i)$ and $\mathbf{A}_k(t_i)$ are given by Equations (2-12) and (2-14). If designed correctly, the elemental filter representing the true system (i.e., having the correct parameter vector \mathbf{a}_k) will have zero-mean white Gaussian residuals, with values consistently more in consonance with that filter's computed $\mathbf{A}_k(t_i)$, than the residuals of other elemental filters. Therefore, based on Equations (2-55) and (2-56), the probability of the *correct* filter will increase while the probability of the other filters will decrease.

2.4.2.1 Lower Probability Bounds

The conditional probability calculation for each elemental filter is recursive in nature. Notice in Equation (2-55) that, if an elemental filter's conditional probability becomes zero, it remains zero for all time. This effect causes the MMAE to ignore information from that particular elemental filter. To avoid this problem, a lower probability bound ϵ (generally $0.001 \leq \epsilon \leq 0.01$) is set for each elemental filter. If the calculated conditional probability for the filter is less than the lower bound, the filter's probability is set to the lower bound ϵ and then all computed $p_k(t_i)$'s are *rescaled* so that they sum to one. Large ϵ values force inappropriate weighting of estimates associated with the wrong

filter, while very small ϵ values slow down the response of the MMAE to true parameter or system changes.

2.4.3 Overall MMAE State Estimate

The output of the multiple model filtering algorithm is a probabilistically weighted average of the outputs of the K elemental filters. The overall state estimate of the MMAE is calculated by:

$$\hat{\mathbf{x}}(t_i^+) = \sum_{k=1}^K \hat{\mathbf{x}}_k(t_i^+) p_k(t_i) \quad (2-57)$$

The conditional covariance of the MMAE is calculated by:

$$\mathbf{P}(t_i^+) = \sum_{k=1}^K p_k(t_i) \{ \mathbf{P}_k(t_i^+) + [\hat{\mathbf{x}}_k(t_i^+) - \hat{\mathbf{x}}(t_i^+)] [\hat{\mathbf{x}}_k(t_i^+) - \hat{\mathbf{x}}(t_i^+)]^T \} \quad (2-58)$$

It is important to understand that the output of the MMAE is a weighted blending of the outputs of *all* of the elemental filters, including filters based on the less correct assumptions.

2.4.4 MMAE Convergence

The ability of the MMAE to converge to the correct hypothesis is guaranteed theoretically under certain specified conditions [5]. Some of these proofs require that the characteristics \mathbf{a}_k modeled by an elemental filter *exactly* match the true system characteristics. Additional research has indicated that, if the modeled system does not exactly match the real system, the MMAE will converge to the elemental filter based on “closest to true” system model [25, 26, 27]. However, none of the work to date gives any guarantee on the convergence rate of the MMAE.

2.5 Global Positioning System

The Global Positioning System (GPS) is a constellation of 27 radio navigation satellites (24 primary plus three spares). Each satellite continuously transmits a stream of navigation codes and ranging information providing users with data capable of producing the position, velocity, and time at the user's location. Currently, most civilian GPS receivers process data from all visible satellites, up to the number of channels in the receiver. The GPS development in this work follows the information provided in references [11, 20, 36, 37]. For a detailed overview of GPS, the reader is referred to reference [20]

2.5.1 The GPS Signal

The GPS signal is transmitted continuously from all satellites on two carrier frequencies: an L1 carrier (1575.42 MHz) and an L2 carrier (1227.6 MHz). Both the L1 and L2 frequencies are modulated with specific pseudorandom noise (PRN) codes unique to each satellite. The coarse/acquisition (C/A) PRN codes are 1023 bit sequences modulating the carrier at 1.023 MHz (repeated every millisecond). The precision (P) code is a much longer code that repeats every 267 days. Each GPS satellite is assigned a one-week segment of the P-code, which modulates the carrier at 10.23 MHz. The Y-code is an encrypted version of the P-code and is referred to as the P(Y)-code. The P(Y)-code is intended for military users and allows for the anti-spoof (AS) mode of operation. The L1 frequency contains both C/A-code and a P(Y)-code, while the L2 frequency only contains P(Y)-code. A 50 Hz navigation message is also modulated onto both carriers.

This navigation message contains information for all satellites such as satellite ephemeris, atmospheric propagation, satellite clock bias, and almanac data. Table 2-1 below summarizes the GPS signals [11].

Table 2-1. GPS Signal Summary

Carrier	Frequency	Wavelength	Modulation	Frequency	Chip Length
L1	1575.42 MHz	19 cm	C/A Code	1.023 MHz	293 m
			P Code	10.23MHz	29.3 m
			Nav Message	50 Hz	
L2	1227.60 MHz	24 cm	P Code	10.23MHz	29.3 m
			Nav Message	50 Hz	

GPS receivers are called single or dual frequency receivers based on their ability to receive either L1 signal or both L1 and L2 signals. Receivers correlate the received code with an internally generated copy of the appropriate PRN code. Single frequency receivers use only C/A code while dual frequency receivers use both C/A and P codes. Receivers that cannot decrypt the P(Y) code signal use semi-codeless techniques to get range information from the encrypted signal [41].

At the start of this research, the GPS signal was intentionally degraded by a process known as selective availability (SA). Selective availability was applied to the signal before being transmitted from the satellite and was either a pseudo-random dither of the satellite GPS clock, or errors added into the ephemeris information broadcast in the navigation message. This denied full position accuracy to users not capable of decrypting the P(Y)-code. SA decreased positioning accuracy to approximately 100 meters (2-D RMS) with SA from approximately 10 meters (2-D RMS) without SA. In the spring of 2000, SA was turned off and full accuracy is available to all users; however civilian users still only have access to C/A code signals.

2.5.2 GPS Measurements

To calculate the user's position, the GPS receiver must measure the range between itself and each satellite in view. The GPS signal contains two main measurement types: code and carrier-phase.

2.5.2.1 Code Measurements

The GPS code measurement is called a pseudorange because it is a combination of the true range to the satellite and errors in the GPS signal. It is essentially the difference between the time of transmission from the satellite of the GPS signal and the time of reception by the GPS receiver. The pseudorange measurement is defined as:

$$\rho = r + c(\delta t_u - \delta t_{sv}) + T + I + m + v + SA \quad (2-59)$$

where

ρ = GPS pseudorange (m)

r = true user to satellite range (m)

c = speed of light (m/s)

δt_u = user (receiver) clock error (s)

δt_{sv} = satellite clock error (s)

T = errors due to tropospheric delay (m)

I = errors due to ionospheric delay (m)

m = errors due to signal multipath (m)

v = errors due to receiver noise (m)

SA = errors due to selective availability (m)

2.5.2.2 GPS Carrier-Phase Measurements

A GPS carrier-phase measurement is the difference between the receiver's internally generated carrier signal, and the carrier signal received from a satellite. The carrier-phase measurement (in cycles) is defined as:

$$\phi = \frac{1}{\lambda} (r + c(\delta t_u - \delta t_{sv}) + T - I + m + v + SA) + N \quad (2-60)$$

where

ϕ = carrier-phase measurement (cycles)

λ = carrier-phase wavelength (m)

N = carrier-phase integer ambiguity (cycles)

The remaining terms $r, c, \delta t_u, \delta t_{sv}, T, I, m, v, SA$ represent the same error types as in Equation (2-59). However, the magnitude of each specific error type in a code measurement will be different from the magnitude of the same error type in the carrier-phase measurement. In addition, the ionospheric term is the same magnitude as in the pseudorange, but is opposite in sign because the ionosphere delays a code measurement but advances a carrier-phase measurement.

A GPS receiver cannot distinguish between one carrier cycle and the next. The receiver only counts the *change* in the number of cycles, or phase, between itself and the satellite. The initial number of cycles between the receiver and satellite is unknown, or ambiguous. To make the carrier-phase measurement a true range measurement, an unknown bias, N , must be added to the basic receiver measurement. The carrier-phase integer ambiguity, N , is essentially a constant unknown integer-valued bias between the

receiver and the satellite, and is different for each receiver-satellite measurement combination. In order to use GPS carrier-phase measurements for positioning, the carrier-phase integer ambiguity must be estimated or resolved. The carrier-phase ambiguity resolution technique used in this research is discussed in Section 2.5.3.

2.5.2.3 Single Differencing

In addition to basic pseudorange and carrier-phase measurements, Differential GPS (DGPS) techniques use measurements created by differencing combinations of receiver to satellite measurements. The concept of a single-difference measurement is shown in Figure 2-2.

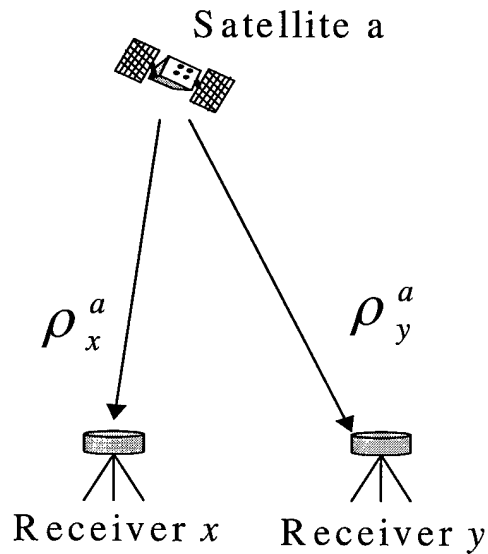


Figure 2-2. Single Differencing

A single-differenced measurement is created by differencing simultaneous measurements between two receivers and one satellite. It is defined as:

$$\Delta\rho_{xy}^a = \rho_x^a - \rho_y^a \quad (2-61)$$

where the superscript identifies the satellite and the subscript identifies the receiver or receivers.

ρ_x^a = pseudorange between satellite a and receiver x

ρ_y^a = pseudorange between satellite a and receiver y

Substituting in the full pseudorange measurement equation, Equation (2-59) into the above equation yields:

$$\begin{aligned} \Delta\rho_{xy}^a = & (r_x^a + c(\delta t_{xu}^a - \delta t_{xsv}^a) + T_x^a + I_x^a + m_x^a + v_x^a + SA_x^a) \\ & - (r_y^a + c(\delta t_{yu}^a - \delta t_{ysv}^a) + T_y^a + I_y^a + m_y^a + v_y^a + SA_y^a) \end{aligned} \quad (2-62)$$

Rearranging the above equation to combine like terms yields

$$\begin{aligned} \Delta\rho_{xy}^a = & (r_x^a - r_y^a) + c(\delta t_{xu}^a - \delta t_{yu}^a) - c(\delta t_{xsv}^a - \delta t_{ysv}^a) + (T_x^a - T_y^a) \\ & + (I_x^a - I_y^a) + (m_x^a - m_y^a) + (v_x^a - v_y^a) + (SA_x^a - SA_y^a) \end{aligned} \quad (2-63)$$

Because the measurements differenced in Equation (2-63) are from the same satellite, the satellite clock errors and the SA errors are eliminated, (i.e. $\delta t_{xsv}^a - \delta t_{ysv}^a = 0$ and $SA_x^a - SA_y^a = 0$). Removing these terms and slightly changing notation to simplify the expression (allow Δ to represent a single-difference) the final single-differenced pseudorange equation becomes:

$$\Delta\rho_{xy}^a = \Delta r_{xy}^a + \Delta c\delta t_{xyu}^a + \Delta T_{xy}^a + \Delta I_{xy}^a + \Delta m_{xy}^a + \Delta v_{xy}^a \quad (2-64)$$

The single-differenced pseudorange measurement is really a measurement of the range between receivers x and y and residual errors. The residual user clock error ($\Delta c\delta t_{xyu}^a$), tropospheric error (ΔT_{xy}^a), and ionospheric error (ΔI_{xy}^a) are reduced by single

differencing, while the multipath errors (Δm_{xy}^a) and the receiver noise errors (Δv_{xy}^a) are slightly increased [37].

In a manner similar to the single-differenced pseudorange measurement, the single-difference carrier-phase measurement can be written as:

$$\Delta \phi_{xy}^a = \phi_x^a - \phi_y^a \quad (2-65)$$

again where the superscript identifies the satellite and the subscript identifies the receiver and

ϕ_x^a = carrier-phase measurement between satellite a and receiver x

ϕ_y^a = carrier-phase measurement between satellite a and receiver y

Substituting in the full carrier-phase measurement equation, Equation (2-60), into the above equation yields:

$$\begin{aligned} \Delta \phi_{xy}^a = & \frac{1}{\lambda} [(r_x^a + c(\delta t_{xu}^a - \delta t_{xsv}^a) + T_x^a + I_x^a + m_x^a + v_x^a + SA_x^a)] + N_x^a \\ & - \frac{1}{\lambda} [(r_y^a + c(\delta t_{yu}^a - \delta t_{ysv}^a) + T_y^a + I_y^a + m_y^a + v_y^a + SA_y^a)] + N_y^a \end{aligned} \quad (2-66)$$

Rearranging the equation to combine like terms yields:

$$\begin{aligned} \Delta \phi_{xy}^a = & \frac{1}{\lambda} [(r_x^a - r_y^a) + c(\delta t_{xu}^a - \delta t_{yu}^a) - c(\delta t_{xsv}^a - \delta t_{ysv}^a) + (T_x^a - T_y^a) \\ & + (I_x^a - I_y^a) + (m_x^a - m_y^a) + (v_x^a - v_y^a) + (SA_x^a - SA_y^a)] + (N_x^a - N_y^a) \end{aligned} \quad (2-67)$$

Again, the satellite clock errors and SA errors are eliminated:

$$\Delta \phi_{xy}^a = \frac{1}{\lambda} (\Delta r_{xy}^a + \Delta c \delta t_{xyu}^a + \Delta T_{xy}^a + \Delta I_{xy}^a + \Delta m_{xy}^a + \Delta v_{xy}^a) + \Delta N_{xy}^a \quad (2-68)$$

The additional term in Equation (2-68), ΔN_{xy}^a , is the difference in the carrier-phase ambiguities between the two receiver's measurements, and it is still an integer value.

2.5.2.4 Differential Corrections

Code based DGPS techniques use differential corrections to improve the relative positioning accuracy of GPS. A differential correction is formed by subtracting the calculated range to a satellite from the measured pseudorange:

$$\Delta\rho_{x_{calc}}^a = \rho_x^a - r_{x_{calc}}^a \quad (2-69)$$

where

$\Delta\rho_{x_{calc}}^a$ = the differential correction between receiver x and satellite a

ρ_x^a = the measured pseudorange between receiver x and satellite a

$r_{x_{calc}}^a$ = the calculated range between receiver x and satellite a

Differential corrections are only used when the receiver's position is known, as it is in a fixed reference receiver. The differential correction is then broadcast or used in post-processing applications to correct the pseudorange measurements of mobile receivers. This effectively achieves a single-difference measurement between the user's receiver and the reference receiver as shown below:

$$\rho_{y_{corr}}^a = \rho_y^a - \Delta\rho_{x_{calc}}^a \quad (2-70)$$

$$\rho_{y_{corr}}^a = r_y^a + c(\delta t_y - \delta t_x) + \Delta T + \Delta I + \Delta v + \Delta m \quad (2-71)$$

As in single-differencing, the satellite clock errors and SA errors are eliminated by the differential corrections.

2.5.2.5 Double Differencing

The concept of double differencing is shown in Figure 2-3 and is very similar to single differencing. A double-difference measurement is created by differencing two single-differenced measurements.

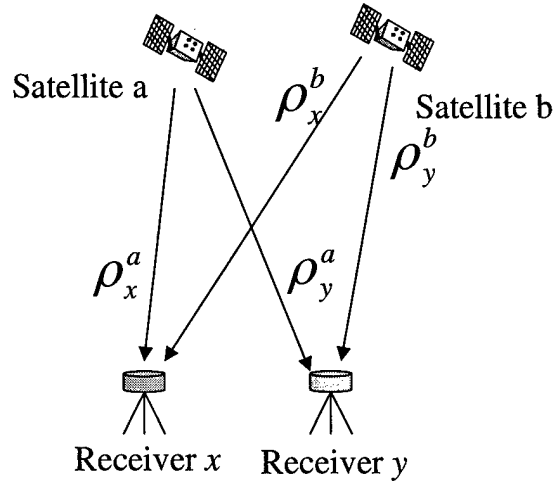


Figure 2-3. Double Differencing

The double-differenced measurement is defined as:

$$\Delta\nabla\rho_{xy}^a = \Delta\rho_{xy}^a - \Delta\rho_{xy}^b = (\Delta\rho_x^a - \Delta\rho_y^a) - (\Delta\rho_x^b - \Delta\rho_y^b) \quad (2-72)$$

Substituting the full pseudorange equation, Equation (2-59), into Equation (2-72) and combining like terms yields:

$$\begin{aligned} \Delta\nabla\rho_{xy}^{ab} = & (r_x^a - r_y^a) - (r_x^b - r_y^b) \\ & + c(\delta t_{xu}^a - \delta t_{yu}^a) - c(\delta t_{xu}^b - \delta t_{yu}^b) \\ & - c(\delta t_{xsv}^a - \delta t_{ysv}^a) + c(\delta t_{xsv}^b - \delta t_{ysv}^b) \\ & + (T_x^a - T_y^a) - (T_x^b - T_y^b) \\ & + (I_x^a - I_y^a) - (I_x^b - I_y^b) \\ & + (m_x^a - m_y^a) - (m_x^b - m_y^b) \\ & + (v_x^a - v_y^a) - (v_x^b - v_y^b) \\ & + (SA_x^a - SA_y^a) - (SA_x^b - SA_y^b) \end{aligned} \quad (2-73)$$

Again, the satellite clock errors and SA errors are eliminated as well as the receiver's clock errors. Removing these terms and using $\Delta\nabla$ to represent double differencing gives the final form of the pseudorange double-differencing measurement equation:

$$\Delta\nabla\rho_{xy}^{ab} = \Delta\nabla r_{xy}^{ab} + \Delta\nabla T_{xy}^{ab} + \Delta\nabla I_{xy}^{ab} + \Delta\nabla m_{xy}^{ab} + \Delta\nabla v_{xy}^{ab} \quad (2-74)$$

The carrier-phase double-difference measurement is created in a similar manner

$$\Delta\nabla\phi_{xy}^a = \Delta\phi_{xy}^a - \Delta\phi_{xy}^b = (\Delta\phi_x^a - \Delta\phi_y^a) - (\Delta\phi_x^b - \Delta\phi_y^b) \quad (2-75)$$

Substituting the full carrier-phase measurement equation, Equation (2-60), into Equation (2-75) and combining like terms yields:

$$\begin{aligned} \Delta\nabla\phi_{xy}^{ab} = & \frac{1}{\lambda} [(r_x^a - r_y^a) - (r_x^b - r_y^b)] \\ & + c(\delta t_{xu}^a - \delta t_{yu}^a) - c(\delta t_{xu}^b - \delta t_{yu}^b) \\ & - c(\delta t_{xsv}^a - \delta t_{ysv}^a) + c(\delta t_{xsv}^b - \delta t_{ysv}^b) \\ & + (T_x^a - T_y^a) - (T_x^b - T_y^b) \\ & + (I_x^a - I_y^a) - (I_x^b - I_y^b) \\ & + (m_x^a - m_y^a) - (m_x^b - m_y^b) \\ & + (v_x^a - v_y^a) - (v_x^b - v_y^b) \\ & + (SA_x^a - SA_y^a) - (SA_x^b - SA_y^b) \\ & + (N_x^a - N_y^a) - (N_x^b - N_y^b) \end{aligned} \quad (2-76)$$

Removing the eliminated terms and using the double difference operator gives the final form of the double-differenced carrier-phase measurement as:

$$\Delta\nabla\phi_{xy}^{ab} = \frac{1}{\lambda} (\Delta\nabla r_{xy}^{ab} + \Delta\nabla T_{xy}^{ab} + \Delta\nabla I_{xy}^{ab} + \Delta\nabla m_{xy}^{ab} + \Delta\nabla v_{xy}^{ab}) + \Delta\nabla N_{xy}^{ab} \quad (2-77)$$

It is important to note that the double-differenced ambiguity term $\Delta\nabla N_{xy}^{ab}$ is still an integer.

2.5.2.6 Widelane Measurements

An additional carrier-phase measurement combination is the widelane measurement. A widelane measurement is a linear combination of L1 and L2 phase measurements defined as:

$$\phi_{WL} = \phi_{L1} - \phi_{L2} \quad (2-78)$$

The widelane measurement has a much longer wavelength than either an L1 or L2 measurement. In addition to its long wavelength, the widelane measurement remains an integer quantity. The longer wavelength of widelane measurements decreases the number of candidate ambiguities in a given search space, making the widelane measurement very useful in ambiguity resolution routines. Table 2-2 below summarizes the different carrier-phase measurements combinations and associated ambiguity terms used in this research.

Table 2-2. Phase Measurement Combinations

Measurement	Wavelength (cm)	Ambiguity
L1	19.03	$\Delta \nabla N_{L1}$ (Integer)
L2	24.42	$\Delta \nabla N_{L2}$ (Integer)
Widelane	86.19	$\Delta \nabla N_{WL} = \Delta \nabla N_{L1} - \Delta \nabla N_{L2}$ (Integer)

In addition to widelane measurements, there are other phase measurement combinations not used in this research, but useful in other GPS applications. For more detail, the reader is referred to references [20, 37].

2.5.3 Carrier-phase Ambiguity Resolution

As stated earlier, in order to use GPS carrier-phase measurements for positioning, the integer ambiguities must be determined. There are many different algorithms used to determine integer ambiguities. However, most algorithms perform two primary operations. First, they determine the ambiguity search space by generating sets of ambiguities. Second, they must determine which set of those generated is the correct ambiguity set.

2.5.3.1 Ambiguity Set Generation

The ambiguity set generation routine used in this research is a combination of the LAMBDA method, developed by Teunissen [40] and the FASF method developed by Chen and Lapachelle [6].

Initial floating-point estimates of the carrier-phase ambiguities and their associated covariance matrix are generated using an EKF. However, these estimates tend to be highly correlated, especially for short time periods, causing problems in determining the correct integer ambiguity set. The basic idea behind the LAMBDA method is to decorrelate the highly correlated carrier-phase ambiguities by applying a decorrelating ambiguity transformation known as the “Z-transformation.” Once the ambiguities are decorrelated, estimating the integer carrier-phase ambiguities can be done rapidly and efficiently.

The Z-transform used in the LAMBDA method must meet certain conditions to be effective in the ambiguity resolution problem. First, to avoid resizing the search space, the Z-Transform must be volume preserving (one-to-one relation). Second, to decorrelate

the ambiguities, it must reduce the product of ambiguity variances. Finally, to preserve the integer nature of ambiguities, the Z-Transform must have integer elements. The Z-Transform used in the LAMBDA method is defined by:

$$\mathbf{z} = \mathbf{Z} \cdot \mathbf{x} \quad , \quad \hat{\mathbf{z}} = \mathbf{Z} \cdot \hat{\mathbf{x}} \quad , \quad \mathbf{Q}_{\hat{\mathbf{z}}} = \mathbf{Z} \mathbf{Q}_{\hat{\mathbf{x}}} \mathbf{Z}^T \quad (2-79)$$

where

\mathbf{z}, \mathbf{x} = transformed and untransformed ambiguities

\mathbf{Z} = Z-Transformation matrix

$\hat{\mathbf{z}}, \hat{\mathbf{x}}$ = transformed and untransformed ambiguity estimates

$\mathbf{Q}_{\hat{\mathbf{z}}}, \mathbf{Q}_{\hat{\mathbf{x}}}$ = transformed and untransformed ambiguity covariance matrices

The Z-Transform (for a two dimensional case) is constructed by the following equations. Assuming

$$\mathbf{Q}_{\hat{\mathbf{x}}} = \begin{bmatrix} \sigma_1^2 & \sigma_{12} \\ \sigma_{21} & \sigma_2^2 \end{bmatrix} \quad (2-80)$$

then

$$\mathbf{Z}_1 = \begin{bmatrix} 1 & \text{int}(-\sigma_{12}\sigma_2^{-2}) \\ 0 & 1 \end{bmatrix} \quad \text{and} \quad \mathbf{Z}_2 = \begin{bmatrix} 1 & 0 \\ \text{int}(-\sigma_{21}\sigma_1^{-2}) & 1 \end{bmatrix} \quad (2-81)$$

where either the upper diagonal form \mathbf{Z}_1 , or the lower diagonal form \mathbf{Z}_2 , of the transform may be used. In the above equation, *int* refers to rounding to the closest integer value, which is necessary to preserve the integer nature of the carrier-phase ambiguities. Without rounding the elements to integer values, Equation (2-81) would fully decorrelate the ambiguities, but the ambiguities would no longer be integer values.

An efficient method to calculate higher order Z-transforms, used in this thesis, was developed by Rizos and Han [38]. The first step in the method is to perform an upper triangular factorization of the ambiguity estimate covariance matrix by:

$$\mathbf{Q}_{\hat{x}} = \mathbf{U}_1 \mathbf{D}_{U_1} \mathbf{U}_1^T \quad (2-82)$$

Next, the integer matrix is calculated by:

$$\mathbf{Z}_{U_1} = [\text{int}(\mathbf{U}_1)]^{-1} \quad (2-83)$$

Then an intermediate covariance matrix is calculated by:

$$\mathbf{Q}_{\hat{z}_{U_1}} = \mathbf{Z}_{U_1} \mathbf{Q}_{\hat{x}} \mathbf{Z}_{U_1}^T \quad (2-84)$$

The second step is to perform a lower triangular factorization of the intermediate covariance matrix by:

$$\mathbf{Q}_{\hat{z}_{L_1}} = \mathbf{L}_1 \mathbf{D}_{L_1} \mathbf{L}_1^T \quad (2-85)$$

Next, the integer matrix is calculated by:

$$\mathbf{Z}_{L_1} = [\text{int}(\mathbf{L}_1)]^{-1} \quad (2-86)$$

Then an intermediate covariance matrix is calculated by:

$$\mathbf{Q}_{\hat{z}_{L_1}} = \mathbf{Z}_{L_1} \mathbf{Q}_{\hat{z}_{U_1}} \mathbf{Z}_{L_1}^T \quad (2-87)$$

This procedure is iterated until both integer matrices $[\text{int}(\mathbf{U}_1)]$ and $[\text{int}(\mathbf{L}_1)]$ become identity matrices. The overall Z-transformation is obtained by:

$$\mathbf{Z} = \mathbf{Z}_{L_{k-1}} \mathbf{Z}_{U_{k-1}} \dots \mathbf{Z}_{L_2} \mathbf{Z}_{U_2} \mathbf{Z}_{L_1} \mathbf{Z}_{U_1} \quad (2-88)$$

The Z-Transform calculated in (2-88) is used to transform, or decorrelate, the floating-point ambiguity estimates and the associated covariance matrix before determining the ambiguity search space. Actual generation of candidate ambiguity sets

for this thesis is accomplished using the transformed ambiguities via the FASF method, but can be done using many of the routines described in Section 1.

The FASF method starts by determining the search space for the best-known single ambiguity. The search space is determined by using a predefined multiple (k) of the standard deviation of the ambiguity. The search space for the ambiguity is:

$$\hat{x}_n - k\sigma_n \leq \nabla\Delta N_{\text{int}} \leq \hat{x}_n + k\sigma_n \quad (2-89)$$

where

\hat{x}_n = floating-point estimate of the n^{th} ambiguity

σ_n = standard deviation of the n^{th} ambiguity

For each possible integer value in this search space, the integer ambiguity is assumed to be the correct value. Then new conditional covariance and ambiguity estimates are calculated, conditioned on the fact that the first ambiguity is known. This process shrinks the covariance terms of the remaining ambiguities. Next, the best-known integer value from the remaining ambiguities is selected, and the process repeated. The method is recursive and will either result in a valid ambiguity set or, if the conditional covariance doesn't allow for a valid integer somewhere, the process will result in an invalid set that will be removed from the candidate ambiguity sets. The new conditional state estimate and covariance are calculated by:

$$\tilde{\mathbf{x}} = \hat{\mathbf{x}} - \mathbf{p}_n (\hat{x}_n - \nabla\Delta N_{\text{int}}) / \sigma_n^2 \quad (2-90)$$

$$\mathbf{P}_{\tilde{\mathbf{x}}} = \mathbf{P}_{\hat{\mathbf{x}}} - (\mathbf{p}_n \mathbf{p}_n^T) / \sigma_n^2 \quad (2-91)$$

where

$\hat{\mathbf{x}}$ = unconditioned estimated parameter vector

$\tilde{\mathbf{x}}$ = estimated parameter vector conditioned upon $\hat{x}_n = \nabla \Delta N_{\text{int}}$

$\mathbf{P}_{\tilde{\mathbf{x}}}$ = covariance matrix conditioned upon $\hat{x}_n = \nabla \Delta N_{\text{int}}$

$\mathbf{p}_n = n^{\text{th}}$ column of the covariance matrix $\mathbf{P}_{\tilde{\mathbf{x}}}$

σ_n^2 = scalar variance of the n^{th} parameter (taken from the diagonal of $\mathbf{P}_{\tilde{\mathbf{x}}}$)

The FASF method can be used to generate ambiguity sets in either the normal or Z-transformed search space. However, the candidate ambiguity sets must be transformed back to the original search space before being used in GPS measurements.

2.5.3.2 Ambiguity Set Determination

Most carrier-phase ambiguity resolution algorithms monitor the measurement residuals for each candidate ambiguity set, by statistically comparing possible solutions, until the correct ambiguity set becomes evident. One method of comparing the residuals is by the ratio test:

$$\text{ratio} = \frac{r^T \mathbf{R}^{-1} r(2^{\text{nd}} \text{best})}{r^T \mathbf{R}^{-1} r(\text{best})} \quad (2-92)$$

where

r = measurement residuals

\mathbf{R} = measurement covariance

The ambiguity set is determined to be the correct ambiguity if the ratio is consistently greater than a given value, typically 2.

This is a common method of determining the correct ambiguity, however it is not the method used in this research. The method used in this research is to base each one of the elemental filters in an MMAE on a different ambiguity set. The conditional probability of each filter being based on the correct ambiguity set is then calculated by Equation (2-55), with the modifications outlined in Section 3.5.2. Based on its convergence properties, the MMAE will converge to the correct ambiguity set, provided the correct ambiguity set is used in one of the elemental filters. If the correct ambiguity set is not available in one of the elemental filters the MMAE will converge to the elemental filter with the ambiguity set “closest” to the correct ambiguity set in the Barum’s distance-measure sense [4].

2.6 Summary

This chapter presented the introduction and theory of linear and Extended Kalman filters, the MMAE and GPS (including carrier-phase ambiguity resolution techniques). Chapter 3 will provide detailed descriptions of the models and algorithm development investigated in this thesis.

3 Methodology and Algorithm Development

3.1 Overview

This chapter provides a complete description of the overall algorithm, system models, and techniques used in this thesis. First, an overall algorithm description is presented, followed by a description of each main subroutine. Detailed descriptions of the system states, models and measurements equations for the Kalman filters used in this research are then presented. Finally, specific techniques are presented that are key to the understanding of this research, including changes made to the theory of Chapter 2.

3.2 Overall Algorithm Structure

The overall structure of the algorithm developed in this thesis is shown in Figure 3-1. The algorithm can easily be divided into three main areas: a floating-point differential filter, carrier-phase ambiguity set generation (Z-transform, FASF and inverse Z-transform), and the MMAE. Each one of these areas is fully described in the following sections.

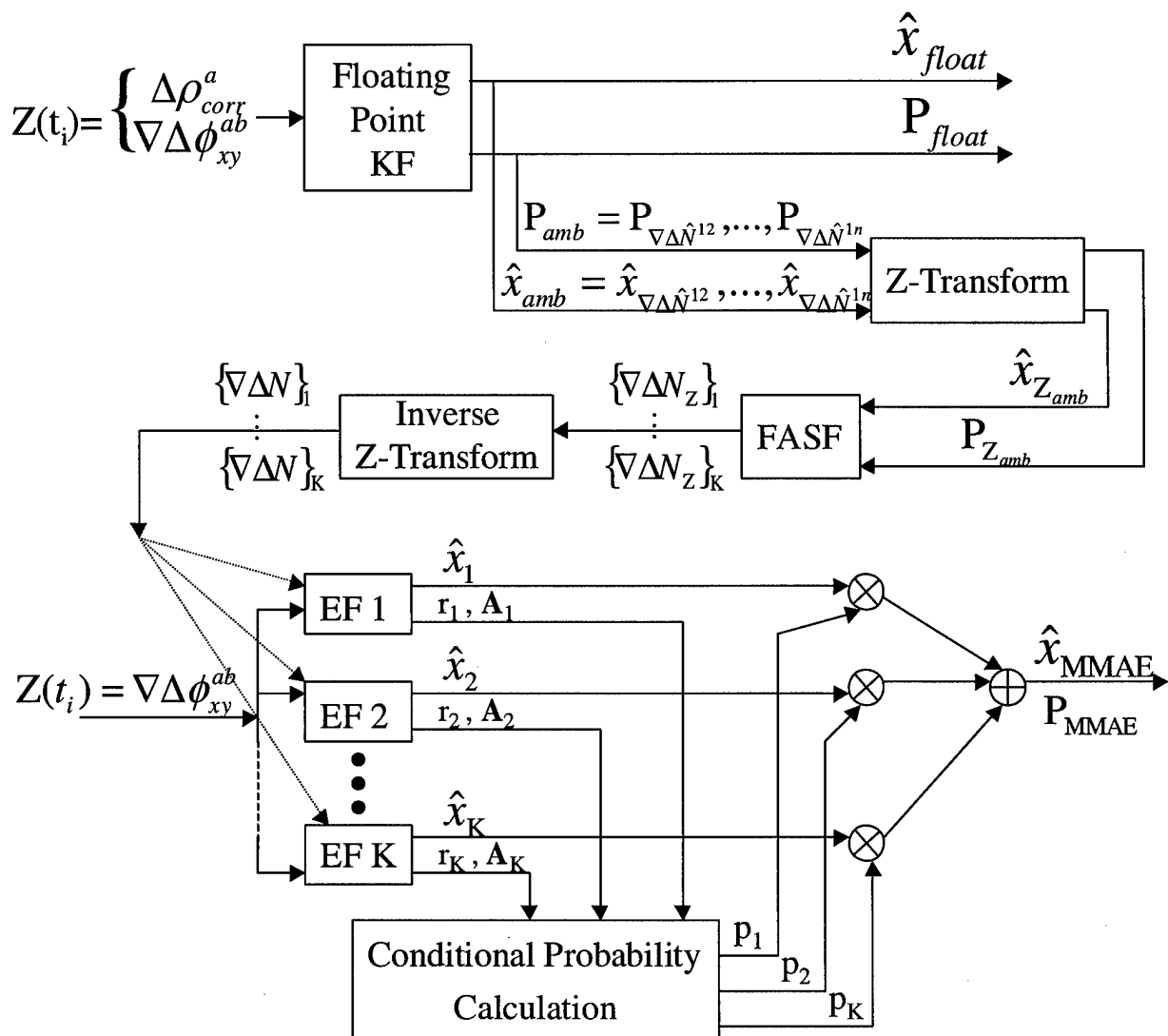


Figure 3-1. Overall Algorithm Description

3.3 Floating-Point Differential GPS Kalman Filter

The initial step in the post-processing algorithm is a floating-point DGPS Kalman filter, and it follows the general development of the filter found in reference [36]. This filter is a DGPS navigation EKF designed to calculate the user's position, velocity, acceleration, and carrier-phase ambiguity estimates. The filter uses both differentially

corrected code measurements and double-differenced carrier-phase measurements. The main purpose of this initial filter is to generate the carrier-phase ambiguity estimates and covariances used by the ambiguity set generation routine. However, the output of this filter is also used, as necessary, to initialize or reinitialize the elemental filters in the MMAE.

A few aspects are critical to implementing this DGPS filter. First, it is assumed that the remote (or airborne) receiver has access to the same satellites as the reference receiver. Second, it is also assumed for modeling purposes that the differential corrections are all timed correctly to correspond to the correct remote receiver pseudorange measurement. Last, when processing DGPS measurements, it is assumed that the differential corrections have been applied to the raw pseudorange measurements from the remote receiver.

All of the above assumptions are easily and properly invoked because the algorithm developed in this thesis is a post-processing algorithm. A simple data preprocessing routine was used to coordinate visible satellites and measurement times between the reference and remote receivers prior to the data being used in the floating-point DGPS Kalman filter. In addition, the data preprocessing routine was used to detect cycle slips, determine a base satellite, and to apply tropospheric corrections to raw pseudorange measurements. The data preprocessing routine does not in any way affect the functioning of the overall algorithm. It simply organizes the available data to improve the efficiency of the floating-point DGPS Kalman filter and the MMAE.

3.3.1 Differential GPS Model Equations

The floating-point Differential GPS Kalman filter is an $11+(n-1)$ state filter (n is the number of satellites in view) with a linear dynamics model. The filter's first nine states consist of three position, three velocity and three acceleration states, based on a First Order Gauss Markov Acceleration (FOGMA) model.

The position and velocity states dynamics are defined as:

$$\begin{aligned}\dot{x}_1 &= \dot{X} = x_4 & \dot{x}_2 &= \dot{Y} = x_5 & \dot{x}_6 &= \dot{Z} = x_6 \\ \dot{x}_4 &= \ddot{X} = x_7 & \dot{x}_5 &= \ddot{Y} = x_8 & \dot{x}_6 &= \ddot{Z} = x_9\end{aligned}$$

To handle unknown accelerations, the acceleration states are modeled as First Order Gauss Markov processes. The acceleration states dynamics are defined as:

$$\begin{aligned}\dot{x}_7 &= (-1/T_a)x_7 + w_{a_1}(t) \\ \dot{x}_8 &= (-1/T_a)x_8 + w_{a_2}(t) \\ \dot{x}_9 &= (-1/T_a)x_9 + w_{a_3}(t)\end{aligned}\tag{3-1}$$

The acceleration states process noises are defined as:

$$\begin{aligned}E\{w_{a_1}(t)w_{a_1}(t+\tau)\} &= E\{w_{a_2}(t)w_{a_2}(t+\tau)\} = E\{w_{a_3}(t)w_{a_3}(t+\tau)\} \\ &= \frac{2\sigma_a^2}{T_a} = q_a\delta(\tau)\end{aligned}\tag{3-2}$$

The time constant, T_a , and the mean squared value, σ_a^2 , are user-defined tuning values, set according to the expected accelerations and time correlations.

The largest error sources in a GPS measurement are due to clock errors in the user's receiver. Therefore, two additional states were added to the first nine states, to represent the user's clock bias and clock bias drift. The clock bias state and drift state dynamics are defined as:

$$\begin{aligned}\dot{x}_{10} &= x_{11} + w_{clk_1} \\ \dot{x}_{11} &= w_{clk_2}\end{aligned}\quad (3-3)$$

The clock bias and drift states process noises are defined as:

$$E\{w_{clk_1}(t)w_{clk_1}(t+\tau)\} = q_{clk_1}\delta(\tau) \quad E\{w_{clk_2}(t)w_{clk_2}(t+\tau)\} = q_{clk_2}\delta(\tau) \quad (3-4)$$

The floating-point DGPS filter uses both single-differenced (differentially corrected) code measurements and double-differenced carrier-phase measurements. The double-differenced carrier-phase measurements may be L1, L2, or widelane measurements. Note, widelane measurements are used for the majority of this research. In order to use double-differenced carrier-phase measurements, the filter must also estimate the carrier-phase ambiguities. By definition, the double-difference carrier-phase integer ambiguities are constant biases in the carrier-phase measurements. However, due to errors in the GPS measurements, if these states were modeled as constant biases the filter may converge to the wrong values, with no way to correct the bias. A bias in the ambiguity estimates will result in a constant bias in the position estimate of the overall algorithm. Therefore, these states were modeled as random walks, and an additional $n-1$ states were added to the filter to represent the double-differenced carrier-phase ambiguities. The double-differenced carrier-phase ambiguity states dynamics are defined as:

$$\dot{x}_{12} = w_{\nabla\Delta N^{12}} \quad \dot{x}_{13} = w_{\nabla\Delta N^{13}} \quad \cdots \quad \dot{x}_{1n} = w_{\nabla\Delta N^{1n}} \quad (3-5)$$

with process noises defined as:

$$\begin{aligned}E\{w_{\nabla\Delta N^{12}}(t)w_{\nabla\Delta N^{12}}(t+\tau)\} &= E\{w_{\nabla\Delta N^{13}}(t)w_{\nabla\Delta N^{13}}(t+\tau)\} \\ &= \cdots = E\{w_{\nabla\Delta N^{1n}}(t)w_{\nabla\Delta N^{1n}}(t+\tau)\} = q_N\delta(\tau)\end{aligned}\quad (3-6)$$

The overall state vector for the floating-point filter is defined by:

$$\mathbf{x} = [X \ Y \ Z \ \dot{X} \ \dot{Y} \ \dot{Z} \ \ddot{X} \ \ddot{Y} \ \ddot{Z} \ c\delta t_{clk} \ c\dot{\delta} t_{clk} \ \nabla\Delta N^{12} \ \nabla\Delta N^{13} \ \dots \ \nabla\Delta N^{1n}]^T \quad (3-7)$$

where

$$\begin{aligned} x_1 &= X = \text{ECEF X position (m)} \\ x_2 &= Y = \text{ECEF Y position (m)} \\ x_3 &= Z = \text{ECEF Z position (m)} \\ x_4 &= \dot{X} = \text{ECEF X velocity (m/s)} \\ x_5 &= \dot{Y} = \text{ECEF Y velocity (m/s)} \\ x_6 &= \dot{Z} = \text{ECEF Z velocity (m/s)} \\ x_7 &= \ddot{X} = \text{ECEF X acceleration (m/s}^2\text{)} \\ x_8 &= \ddot{Y} = \text{ECEF Y acceleration (m/s}^2\text{)} \\ x_9 &= \ddot{Z} = \text{ECEF Z acceleration (m/s}^2\text{)} \\ x_{10} &= c\delta t_{clk} = \text{user's (remote) and reference clock bias (m)} \\ x_{11} &= c\dot{\delta} t_{clk} = \text{user's (remote) and reference clock drift (m/s)} \\ x_{12} &= \nabla\Delta N^{12} = \text{double-difference phase ambiguity between satellites 1 and 2 (cycles)} \\ x_{13} &= \nabla\Delta N^{13} = \text{double-difference phase ambiguity between satellites 1 and 3 (cycles)} \\ &\vdots \\ x_{11+(n-1)} &= \nabla\Delta N^{1n} = \text{double-difference phase ambiguity between satellites 1 and n (cycles)} \end{aligned}$$

Because GPS measurements are in the Earth Centered Earth Fixed (ECEF) reference frame, all of the calculations in the floating-point filter (and the MMAE) were conducted in the ECEF frame.

The linear state-space differential equation for the floating-point filter in the form:

$$\dot{\mathbf{x}}(t) = \mathbf{F}(t)\mathbf{x}(t) + \mathbf{G}(t)\mathbf{w}(t) \quad (3-8)$$

is fully represented by:

$$\begin{bmatrix} \dot{x}_1 \\ \dot{x}_2 \\ \dot{x}_3 \\ \dot{x}_4 \\ \dot{x}_5 \\ \dot{x}_6 \\ \dot{x}_7 \\ \dot{x}_8 \\ \dot{x}_9 \\ \dot{x}_{10} \\ \dot{x}_{11} \\ \dot{x}_{12} \\ \dot{x}_{13} \\ \vdots \\ \dot{x}_{1+(n-1)} \end{bmatrix} = \begin{bmatrix} 0 & 0 & 0 & 1 & 0 & 0 & 0 & 0 & 0 & 0 & 0 & 0 & \cdots & 0 \\ 0 & 0 & 0 & 0 & 1 & 0 & 0 & 0 & 0 & 0 & 0 & 0 & \cdots & 0 \\ 0 & 0 & 0 & 0 & 0 & 1 & 0 & 0 & 0 & 0 & 0 & 0 & \cdots & 0 \\ 0 & 0 & 0 & 0 & 0 & 0 & 1 & 0 & 0 & 0 & 0 & 0 & \cdots & 0 \\ 0 & 0 & 0 & 0 & 0 & 0 & 0 & 1 & 0 & 0 & 0 & 0 & \cdots & 0 \\ 0 & 0 & 0 & 0 & 0 & 0 & 0 & 0 & 1 & 0 & 0 & 0 & \cdots & 0 \\ 0 & 0 & 0 & 0 & 0 & 0 & -1/T_a & 0 & 0 & 0 & 0 & 0 & \cdots & 0 \\ 0 & 0 & 0 & 0 & 0 & 0 & 0 & -1/T_a & 0 & 0 & 0 & 0 & \cdots & 0 \\ 0 & 0 & 0 & 0 & 0 & 0 & 0 & 0 & -1/T_a & 0 & 0 & 0 & \cdots & 0 \\ 0 & 0 & 0 & 0 & 0 & 0 & 0 & 0 & 0 & 1 & 0 & 0 & \cdots & 0 \\ 0 & 0 & 0 & 0 & 0 & 0 & 0 & 0 & 0 & 0 & 0 & 0 & \cdots & 0 \\ 0 & 0 & 0 & 0 & 0 & 0 & 0 & 0 & 0 & 0 & 0 & 0 & \cdots & 0 \\ 0 & 0 & 0 & 0 & 0 & 0 & 0 & 0 & 0 & 0 & 0 & 0 & \cdots & 0 \\ \vdots & \vdots & \vdots & \vdots & \vdots & \vdots & \vdots & \vdots & \vdots & \vdots & \vdots & \vdots & \ddots & 0 \\ 0 & 0 & 0 & 0 & 0 & 0 & 0 & 0 & 0 & 0 & 0 & 0 & 0 & 0 \end{bmatrix} \begin{bmatrix} x_1 \\ x_2 \\ x_3 \\ x_4 \\ x_5 \\ x_6 \\ x_7 \\ x_8 \\ x_9 \\ x_{10} \\ x_{11} \\ x_{12} \\ x_{13} \\ \vdots \\ x_{1+(n-1)} \end{bmatrix} + \begin{bmatrix} 0 \\ 0 \\ 0 \\ 0 \\ 0 \\ 0 \\ w_a \\ w_a \\ w_a \\ w_{clk_1} \\ w_{clk_2} \\ w_{\nabla \Delta N^2} \\ w_{\nabla \Delta N^3} \\ \vdots \\ w_{\nabla \Delta N^{1n}} \end{bmatrix} \quad (3-9)$$

In Equation (3-9), T_a is the time constant associated with the FOGMA acceleration states. For this system, the matrix $\mathbf{G}(t)$ is an identity matrix. Although the floating-point filter does not model all of the possible error sources in a DGPS application, enough are modeled to be accurate enough for the purposes of this research.

The dynamics driving noise matrix \mathbf{Q} defined by:

$$E\{\mathbf{w}(t)\mathbf{w}^T(t+\tau)\} = \mathbf{Q}(t)\delta(\tau) \quad (3-10)$$

must also be specified for the filter. The matrix \mathbf{Q} used in this research was given by:

$$\mathbf{Q} = \begin{bmatrix} 0 & 0 & 0 & 0 & 0 & 0 & 0 & 0 & 0 & 0 & 0 & 0 & \dots & 0 \\ 0 & 0 & 0 & 0 & 0 & 0 & 0 & 0 & 0 & 0 & 0 & 0 & \dots & 0 \\ 0 & 0 & 0 & 0 & 0 & 0 & 0 & 0 & 0 & 0 & 0 & 0 & \dots & 0 \\ 0 & 0 & 0 & 0 & 0 & 0 & 0 & 0 & 0 & 0 & 0 & 0 & \dots & 0 \\ 0 & 0 & 0 & 0 & 0 & 0 & 0 & 0 & 0 & 0 & 0 & 0 & \dots & 0 \\ 0 & 0 & 0 & 0 & 0 & 0 & 0 & 0 & 0 & 0 & 0 & 0 & \dots & 0 \\ 0 & 0 & 0 & 0 & 0 & 0 & q_a & 0 & 0 & 0 & 0 & 0 & \dots & 0 \\ 0 & 0 & 0 & 0 & 0 & 0 & 0 & q_a & 0 & 0 & 0 & 0 & \dots & 0 \\ 0 & 0 & 0 & 0 & 0 & 0 & 0 & 0 & q_a & 0 & 0 & 0 & \dots & 0 \\ 0 & 0 & 0 & 0 & 0 & 0 & 0 & 0 & 0 & q_{clk_1} & 0 & 0 & \dots & 0 \\ 0 & 0 & 0 & 0 & 0 & 0 & 0 & 0 & 0 & 0 & q_{clk_2} & 0 & \dots & 0 \\ 0 & 0 & 0 & 0 & 0 & 0 & 0 & 0 & 0 & 0 & 0 & q_N & \dots & 0 \\ \vdots & \vdots & \vdots & \vdots & \vdots & \vdots & \vdots & \vdots & \vdots & \vdots & \vdots & \vdots & \ddots & 0 \\ 0 & 0 & 0 & 0 & 0 & 0 & 0 & 0 & 0 & 0 & 0 & 0 & 0 & q_N \end{bmatrix} \quad (3-11)$$

The floating-point filter time constant, mean squared value, and noise values used in this thesis, for both ground and flight test, are specified below in Table 3-1.

Table 3-1. Floating-Point Filter Dynamics Driving Noise Values

Term	Definition	Value
σ_a^2	Mean squared value	$(12.25 \text{ m/sec}^2)^2$
T_a	Acceleration time constant	3sec
q_a	Acceleration noise	$100 \text{ m}^2 / \text{sec}^5$
q_{clk_1}	Clock bias noise	$0.036 \text{ m}^2 / \text{sec}$
q_{clk_2}	Clock Drift noise	$0.141 \text{ m}^2 / \text{sec}^3$
q_N	Ambiguity noise	$1.1 \times 10^{-4} \text{ cycles}^2 / \text{sec}$

The initial conditions for the position states (x_1, x_2, x_3) and the clock bias state (x_{10}) are determined using a single point GPS positioning subroutine. The double-differenced ambiguity states $(x_{12}, x_{13}, \dots, x_{1n})$ are initialized using code-carrier difference calculations, by the following equation:

$$x_{1n} = \nabla \Delta N^{1n} \approx \nabla \Delta \phi^{1n} - \frac{\nabla \Delta \rho^{1n}}{\lambda} \quad (3-12)$$

All remaining states were initialized to zero, making the initial state vector:

$$\mathbf{x}(t_0) = [X_0 \ Y_0 \ Z_0 \ 0 \ 0 \ 0 \ 0 \ 0 \ 0 \ 0 \ c\delta t_{clk_0} \ 0 \ \nabla \Delta N_0^{12} \ \nabla \Delta N_0^{13} \ \dots \ \nabla \Delta N_0^{1n}]^T \quad (3-13)$$

The initial covariance matrix for the filter is assumed to be a diagonal matrix with elements shown below. All of the initial cross-covariance terms set to zero. The initial covariance matrix for the filter is given by:

$$\mathbf{P}(t_0) = \begin{bmatrix} \sigma_x^2 & 0 & 0 & 0 & 0 & 0 & 0 & 0 & 0 & 0 & 0 & 0 & 0 & 0 & 0 \\ 0 & \sigma_y^2 & 0 & 0 & 0 & 0 & 0 & 0 & 0 & 0 & 0 & 0 & 0 & 0 & 0 \\ 0 & 0 & \sigma_z^2 & 0 & 0 & 0 & 0 & 0 & 0 & 0 & 0 & 0 & 0 & 0 & 0 \\ 0 & 0 & 0 & \sigma_{\dot{x}}^2 & 0 & 0 & 0 & 0 & 0 & 0 & 0 & 0 & 0 & 0 & 0 \\ 0 & 0 & 0 & 0 & \sigma_{\dot{y}}^2 & 0 & 0 & 0 & 0 & 0 & 0 & 0 & 0 & 0 & 0 \\ 0 & 0 & 0 & 0 & 0 & \sigma_{\dot{z}}^2 & 0 & 0 & 0 & 0 & 0 & 0 & 0 & 0 & 0 \\ 0 & 0 & 0 & 0 & 0 & 0 & \sigma_{\ddot{x}}^2 & 0 & 0 & 0 & 0 & 0 & 0 & 0 & 0 \\ 0 & 0 & 0 & 0 & 0 & 0 & 0 & \sigma_{\ddot{y}}^2 & 0 & 0 & 0 & 0 & 0 & 0 & 0 \\ 0 & 0 & 0 & 0 & 0 & 0 & 0 & 0 & \sigma_{\ddot{z}}^2 & 0 & 0 & 0 & 0 & 0 & 0 \\ 0 & 0 & 0 & 0 & 0 & 0 & 0 & 0 & 0 & \sigma_{clk_1}^2 & 0 & 0 & 0 & 0 & 0 \\ 0 & 0 & 0 & 0 & 0 & 0 & 0 & 0 & 0 & 0 & \sigma_{clk_2}^2 & 0 & 0 & 0 & 0 \\ 0 & 0 & 0 & 0 & 0 & 0 & 0 & 0 & 0 & 0 & 0 & \sigma_{\nabla \Delta N^{12}}^2 & 0 & 0 & 0 \\ 0 & 0 & 0 & 0 & 0 & 0 & 0 & 0 & 0 & 0 & 0 & 0 & \sigma_{\nabla \Delta N^{13}}^2 & 0 & 0 \\ 0 & 0 & 0 & 0 & 0 & 0 & 0 & 0 & 0 & 0 & 0 & 0 & 0 & \ddots & 0 \\ 0 & 0 & 0 & 0 & 0 & 0 & 0 & 0 & 0 & 0 & 0 & 0 & 0 & 0 & \sigma_{\nabla \Delta N^{1n}}^2 \end{bmatrix}$$

The initial covariance values used in this thesis are specified below in Table 3-2.

Table 3-2. Floating-Point Filter Initial Covariance Values

Term	Definition	Value
σ_{x_1, x_2, x_3}^2	Position state variance	$(100m)^2$
σ_{x_4, x_5, x_6}^2	Velocity state variance	$(400m/s)^2$
σ_{x_7, x_8, x_9}^2	Acceleration state variance	$(20m/s^2)^2$
$\sigma_{x_{10}}^2$	Clock bias variance	$(200m/s^2)^2$
$\sigma_{x_{11}}^2$	Clock drift variance	$(1000m/s^2)^2$
$\sigma_{x_{12}}^2 = \dots \sigma_{x_{1n}}^2$	Ambiguity variance	$(\frac{50}{\lambda} cycles)^2$

3.3.2 Differential GPS Measurement Model

The floating-point DGPS Kalman filter uses a nonlinear measurement model consisting of differentially corrected code measurements and double-differenced carrier-phase measurements resulting in a $2n-1$ (n is the number of satellites in view) measurement vector specified by:

$$\mathbf{z}(t_i) = [\rho_{corr}^1 \quad \rho_{corr}^2 \quad \rho_{corr}^3 \quad \dots \quad \rho_{corr}^n \quad \nabla\Delta\phi_{xy}^{12} \quad \nabla\Delta\phi_{xy}^{13} \quad \dots \quad \nabla\Delta\phi_{xy}^{1n}]^T \quad (3-14)$$

where

ρ_{corr}^1 = differentially corrected code measurement between the receiver and satellite 1

ρ_{corr}^2 = differentially corrected code measurement between the receiver and satellite 2

⋮

ρ_{corr}^n = differentially corrected code measurement between the receiver and satellite n

$\nabla\Delta\phi_{xy}^{12}$ = double-differenced carrier-phase measurement satellites 1 and 2

$\nabla\Delta\phi_{xy}^{13}$ = double-differenced carrier-phase measurement satellites 1 and 3

⋮

$\nabla\Delta\phi_{xy}^{1n}$ = double-differenced carrier-phase measurement satellites 1 and n

To be used in an extended Kalman filter the measurement model must be in the form:

$$\mathbf{z}(t_i) = \mathbf{h}[\mathbf{x}(t_i), t_i] + \mathbf{v}(t_i) \quad (3-15)$$

From Section 2.5.2.4, differentially corrected code measurements are defined as:

$$\rho_{y_{corr}}^a = r_y^a + c(\delta t_y - \delta t_x) + \Delta T + \Delta I + \Delta v + \Delta m \quad (3-16)$$

By combining terms, the above equation becomes:

$$\rho_{y_{corr}}^a = r_y^a + c\delta t + v_\rho \quad (3-17)$$

where $c\delta t = c(\delta t_y - \delta t_x)$ and $v_\rho = \Delta T + \Delta I + \Delta v + \Delta m$. In Equation (3-17), the noise term, v_ρ , is modeled as a white noise. Even though the individual residual differential error terms ($\Delta T, \Delta I, \Delta v, \Delta m$) are not white noises, we assume the combination of the four terms can be sufficiently modeled as a white noise due to the central limit theorem. Expanding the range term, to incorporate satellite position and receiver position, and substituting state variables for the appropriate terms gives the following equation:

$$\rho_{y_{corr}}^a = \left[(x_{sv} - x_1)^2 + (y_{sv} - x_2)^2 + (z_{sv} - x_3)^2 \right]^{1/2} + x_{10} + v_\rho \quad (3-18)$$

This measurement equation must be linearized before being used in the gain and covariance calculations of an EKF. The partial derivative matrix \mathbf{H} is defined as:

$$\mathbf{H}[t_i; \mathbf{x}_n(t_i)] = \left. \frac{\partial \mathbf{h}[\mathbf{x}, t_i]}{\partial \mathbf{x}} \right|_{\mathbf{x}=\mathbf{x}_n(t_i)} \quad (3-19)$$

The individual partial derivatives for one row of the differentially corrected code measurements are:

$$\left. \frac{\partial h[x, t_i]}{\partial x_1} \right|_{x=\hat{x}(t_i^-)} = \frac{x_{sv} - x_1}{[(x_{sv} - x_1)^2 + (y_{sv} - x_2)^2 + (z_{sv} - x_3)^2]^{1/2}} \equiv e_1 \quad (3-20)$$

$$\left. \frac{\partial h[x, t_i]}{\partial x_2} \right|_{x=\hat{x}(t_i^-)} = \frac{y_{sv} - x_2}{[(x_{sv} - x_1)^2 + (y_{sv} - x_2)^2 + (z_{sv} - x_3)^2]^{1/2}} \equiv e_2 \quad (3-21)$$

$$\left. \frac{\partial h[x, t_i]}{\partial x_3} \right|_{x=\hat{x}(t_i^-)} = \frac{z_{sv} - x_3}{[(x_{sv} - x_1)^2 + (y_{sv} - x_2)^2 + (z_{sv} - x_3)^2]^{1/2}} \equiv e_3 \quad (3-22)$$

$$\left. \frac{\partial h[x, t_i]}{\partial x_{10}} \right|_{x=\hat{x}(t_i^-)} = 1 \quad (3-23)$$

These can be combined into a vector representing one row of the \mathbf{H} matrix as:

$$\mathbf{H}^a = [\mathbf{e}^a \quad 0 \quad 0 \quad 0 \quad 0 \quad 0 \quad 0 \quad 1 \quad 0 \quad \dots \quad 0] \quad (3-24)$$

where

$$\mathbf{e}^a = [e_1 \quad e_2 \quad e_3] = \text{unit line of sight vector between the receiver and satellite } a.$$

The double-differenced carrier-phase measurements are used in a similar manner.

From Section 2.5.2.5, the double-differenced carrier-phase measurements are defined by:

$$\Delta \nabla \phi_{xy}^{ab} = \frac{1}{\lambda} (\Delta \nabla r_{xy}^{ab} + \Delta \nabla T_{xy}^{ab} + \Delta \nabla I_{xy}^{ab} + \Delta \nabla m_{xy}^{ab} + \Delta \nabla v_{xy}^{ab}) + \Delta \nabla N_{xy}^{ab} \quad (3-25)$$

The λ term in Equation (3-25), represents the wavelength of the carrier-phase measurement and will be different depending on the type of double-differenced carrier-phase measurement (L1, L2, Widelane) being used in the filter.

By expanding the double-differenced range term and combining the residual differential error terms the above equation becomes:

$$\Delta\nabla\phi_{xy}^{ab} = \frac{1}{\lambda} [r_y^a - r_x^a - (r_y^b - r_x^b)] + \Delta\nabla N_{xy}^{ab} + v_{\Delta\nabla\phi} \quad (3-26)$$

In Equation (3-26), $v_{\Delta\nabla\phi}$ is modeled as a white noise, and is the combination of the residual error terms in the double-differenced equation, i.e.

$v_{\Delta\nabla\phi} = \frac{1}{\lambda} (\Delta\nabla T_{xy}^{ab} + \Delta\nabla I_{xy}^{ab} + \Delta\nabla m_{xy}^{ab} + \Delta\nabla v_{xy}^{ab})$. Again, even though the individual residual error terms ($\Delta\nabla T_{xy}^{ab}, \Delta\nabla I_{xy}^{ab}, \Delta\nabla m_{xy}^{ab}, \Delta\nabla v_{xy}^{ab}$) are not white noises, as explained previously, the combination of the four terms can be sufficiently modeled as a white noise. By expanding the range terms and substituting state variables for the appropriate terms gives the following equation:

$$\begin{aligned} \Delta\nabla\phi_{xy}^{ab} = & \frac{1}{\lambda} \left[(x^a - x_1)^2 + (y^a - x_2)^2 + (z^a - x_3)^2 \right]^{1/2} \\ & - \left[(x^b - x_1)^2 + (y^b - x_2)^2 + (z^b - x_3)^2 \right]^{1/2} \\ & + \frac{1}{\lambda} \{ r_x^b - r_x^a \} + \Delta\nabla N_{xy}^{ab} + v_{\Delta\nabla\phi} \end{aligned} \quad (3-27)$$

The individual partial derivatives for one row of the double-differenced widelane carrier-phase measurements are:

$$\begin{aligned}
\left. \frac{\partial h[x, t_i]}{\partial x_1} \right|_{x=\hat{x}(t_i^-)} &= \frac{1}{\lambda} \left\{ \frac{x^a - x_1}{[(x^a - x_1)^2 + (y^a - x_2)^2 + (z^a - x_3)^2]^{1/2}} \right\} \\
&\quad - \frac{1}{\lambda} \left\{ \frac{x^b - x_1}{[(x^b - x_1)^2 + (y^b - x_2)^2 + (z^b - x_3)^2]^{1/2}} \right\} \\
&\equiv \frac{1}{\lambda} \{e_1^a - e_1^b\}
\end{aligned} \tag{3-28}$$

$$\begin{aligned}
\left. \frac{\partial h[x, t_i]}{\partial x_2} \right|_{x=\hat{x}(t_i^-)} &= \frac{1}{\lambda} \left\{ \frac{y^a - x_2}{[(x^a - x_1)^2 + (y^a - x_2)^2 + (z^a - x_3)^2]^{1/2}} \right\} \\
&\quad - \frac{1}{\lambda} \left\{ \frac{y^b - x_2}{[(x^b - x_1)^2 + (y^b - x_2)^2 + (z^b - x_3)^2]^{1/2}} \right\} \\
&\equiv \frac{1}{\lambda} \{e_2^a - e_2^b\}
\end{aligned} \tag{3-29}$$

$$\begin{aligned}
\left. \frac{\partial h[x, t_i]}{\partial x_3} \right|_{x=\hat{x}(t_i^-)} &= \frac{1}{\lambda} \left\{ \frac{z^a - x_3}{[(x^a - x_1)^2 + (y^a - x_2)^2 + (z^a - x_3)^2]^{1/2}} \right\} \\
&\quad - \frac{1}{\lambda} \left\{ \frac{z^b - x_3}{[(x^b - x_1)^2 + (y^b - x_2)^2 + (z^b - x_3)^2]^{1/2}} \right\} \\
&\equiv \frac{1}{\lambda} \{e_3^a - e_3^b\}
\end{aligned} \tag{3-30}$$

$$\left. \frac{\partial h[x, t_i]}{\partial x_{1n}} \right|_{x=\hat{x}(t_i^-)} = 1 \tag{3-31}$$

These can be combined into a vector representing one row of the \mathbf{H} matrix as:

$$\mathbf{H}^{ab} = \left[\frac{1}{\lambda} (\mathbf{e}_y^a - \mathbf{e}_y^b) \quad 0 \quad 0 \quad 0 \quad 0 \quad 0 \quad 0 \quad 0 \quad 0 \quad \dots \quad 1 \quad \dots \quad 0 \right] \tag{3-32}$$

where

$\mathbf{e}^a = [e_1 \quad e_2 \quad e_3] =$ unit line of sight vector between the receiver and satellite a .

$\mathbf{e}^b = [e_1 \quad e_2 \quad e_3] =$ unit line of sight vector between the receiver and satellite b .

The additional "1" in the above equation is placed in the column corresponding to the appropriate ambiguity state.

The entire measurement matrix \mathbf{H} is an $(11+(n-1))$ by $(2n-1)$ matrix defined by:

$$\mathbf{H} = \begin{bmatrix} \mathbf{e}^1 & 0 & 0 & 0 & 0 & 0 & 0 & 1 & 0 & 0 & 0 & \cdots & 0 \\ \mathbf{e}^2 & 0 & 0 & 0 & 0 & 0 & 0 & 1 & 0 & 0 & 0 & \cdots & 0 \\ \vdots & \vdots & \vdots & \vdots & \vdots & \vdots & \vdots & \vdots & \vdots & \vdots & \vdots & \ddots & 0 \\ \mathbf{e}^n & 0 & 0 & 0 & 0 & 0 & 0 & 1 & 0 & 0 & 0 & \cdots & 0 \\ \frac{1}{\lambda}(\mathbf{e}^1 - \mathbf{e}^2) & 0 & 0 & 0 & 0 & 0 & 0 & 0 & 0 & 1 & 0 & \cdots & 0 \\ \frac{1}{\lambda}(\mathbf{e}^1 - \mathbf{e}^3) & 0 & 0 & 0 & 0 & 0 & 0 & 0 & 0 & 0 & 1 & \cdots & 0 \\ \vdots & \vdots & \vdots & \vdots & \vdots & \vdots & \vdots & \vdots & \vdots & \vdots & \vdots & \ddots & \vdots \\ \frac{1}{\lambda}(\mathbf{e}^1 - \mathbf{e}^n) & 0 & 0 & 0 & 0 & 0 & 0 & 0 & 0 & 0 & 0 & \cdots & 1 \end{bmatrix} \quad (3-33)$$

The measurement error covariance matrix \mathbf{R} defined by:

$$E\{\mathbf{v}(t_i) \mathbf{v}^T(t_j)\} = \begin{cases} \mathbf{R}(t_i) & \text{for } t_i = t_j \\ \mathbf{0} & \text{for } t_i \neq t_j \end{cases} \quad (3-34)$$

must also be specified for the filter. The matrix must consider code measurement noise variances, phase measurement noise variances, the code measurement noise covariances, the phase measurement noise covariances, and the cross-covariance of code measurement and phase measurement noise. For this research, the code measurement noise covariance was assumed to be zero based on the assumption that code measurement errors are uncorellated between satellites, and the baseline distances are short enough to cancel the majority of tropospheric errors. In addition, the cross-covariance of code and phase measurement noises was assumed to be zero based on the assumption that double-differenced tropospheric errors are negligible and that phase multipath and noise errors are uncorrelated between measurements. Values for the other measurement error terms are listed in Table 3-3. The \mathbf{R} matrix is a $(2n-1)$ -by- $(2n-1)$ matrix specified by:

$$\mathbf{R} = \begin{bmatrix} r_{\rho^i, \rho^i} & 0 & 0 & \cdots & 0 & 0 & 0 & \cdots & 0 \\ 0 & r_{\rho^i, \rho^i} & 0 & \cdots & 0 & 0 & 0 & \cdots & 0 \\ 0 & 0 & r_{\rho^i, \rho^i} & \cdots & 0 & 0 & 0 & \cdots & 0 \\ \vdots & \vdots & \vdots & \ddots & \vdots & \vdots & \vdots & \ddots & \vdots \\ 0 & 0 & 0 & \cdots & r_{\rho^i, \rho^i} & 0 & 0 & \cdots & 0 \\ 0 & 0 & 0 & \cdots & 0 & r_{\nabla\Delta\phi^{ij}, \nabla\Delta\phi^{ij}} & r_{\nabla\Delta\phi^{ij}, \nabla\Delta\phi^{ik}} & \cdots & r_{\nabla\Delta\phi^{ij}, \nabla\Delta\phi^{jk}} \\ 0 & 0 & 0 & \cdots & 0 & r_{\nabla\Delta\phi^{ij}, \nabla\Delta\phi^{ik}} & r_{\nabla\Delta\phi^{ij}, \nabla\Delta\phi^{jk}} & \cdots & r_{\nabla\Delta\phi^{ij}, \nabla\Delta\phi^{kl}} \\ \vdots & \vdots & \vdots & \ddots & \vdots & \vdots & \vdots & \ddots & \vdots \\ 0 & 0 & 0 & \cdots & 0 & r_{\nabla\Delta\phi^{ij}, \nabla\Delta\phi^{ik}} & r_{\nabla\Delta\phi^{ij}, \nabla\Delta\phi^{jk}} & \cdots & r_{\nabla\Delta\phi^{ij}, \nabla\Delta\phi^{kl}} \end{bmatrix} \quad (3-35)$$

where

r_{ρ^i, ρ^i} = differentially corrected code measurement variance

$r_{\nabla\Delta\phi^{ij}, \nabla\Delta\phi^{ij}}$ = double-differenced carrier-phase measurement variance

$r_{\nabla\Delta\phi^{ij}, \nabla\Delta\phi^{ik}}$ = double-differenced carrier-phase measurement covariance

The floating-point filter measurement error values used in this research are listed below in Table 3-3.

Table 3-3. Floating-Point Filter Measurement Covariance Error Values

Term	Definition	Value
r_{ρ^i, ρ^i}	Differentially corrected code variance error	$2.6m^2$
$r_{\nabla\Delta\phi^{ij}, \nabla\Delta\phi^{ij}}$	Double-differenced carrier-phase variance error	$0.004m^2$
$r_{\nabla\Delta\phi^{ij}, \nabla\Delta\phi^{ik}}$	Double-differenced carrier-phase covariance error	$0.002m^2$

3.3.3 Discrete-Time Models

The equations derived above must be converted into difference equations in order to be implemented in a Kalman filter. The filter model equations must be in the form:

$$\mathbf{x}(t_{k+1}) = \Phi(t_{k+1}, t_k) \mathbf{x}(t_k) + \mathbf{w}_d \quad (3-36)$$

where

$$\begin{aligned} E\{\mathbf{w}_d\} &= \mathbf{0} \\ E\{\mathbf{w}_d(t_k) \mathbf{w}_d^T(t_k)\} &= \mathbf{Q}_d \\ E\{\mathbf{w}_d(t_j) \mathbf{w}_d^T(t_k)\} &= \mathbf{0}, \quad t_j \neq t_k \end{aligned} \quad (3-37)$$

The state transition matrix, $\Phi(\Delta t)$, is calculated by:

$$\Phi(t_{k+1}, t_k) = \Phi(\Delta t) = e^{\mathbf{F}\Delta t} \quad (3-38)$$

where $\Delta t \equiv t_{k+1} - t_k$, resulting in the matrix:

$$\Phi(\Delta t) = \begin{bmatrix} 1 & 0 & 0 & \Delta t & 0 & 0 & A & 0 & 0 & 0 & 0 & 0 & 0 & 0 & 0 \\ 0 & 1 & 0 & 0 & \Delta t & 0 & 0 & A & 0 & 0 & 0 & 0 & 0 & \dots & 0 \\ 0 & 0 & 1 & 0 & 0 & \Delta t & 0 & 0 & A & 0 & 0 & 0 & 0 & \dots & 0 \\ 0 & 0 & 0 & 1 & 0 & 0 & B & 0 & 0 & 0 & 0 & 0 & 0 & \dots & 0 \\ 0 & 0 & 0 & 0 & 1 & 0 & 0 & B & 0 & 0 & 0 & 0 & 0 & \dots & 0 \\ 0 & 0 & 0 & 0 & 0 & 1 & 0 & 0 & B & 0 & 0 & 0 & 0 & \dots & 0 \\ 0 & 0 & 0 & 0 & 0 & 0 & C & 0 & 0 & 0 & 0 & 0 & 0 & \dots & 0 \\ 0 & 0 & 0 & 0 & 0 & 0 & 0 & C & 0 & 0 & 0 & 0 & 0 & \dots & 0 \\ 0 & 0 & 0 & 0 & 0 & 0 & 0 & 0 & C & 0 & 0 & 0 & 0 & \dots & 0 \\ 0 & 0 & 0 & 0 & 0 & 0 & 0 & 0 & 0 & 1 & \Delta t & 0 & 0 & \dots & 0 \\ 0 & 0 & 0 & 0 & 0 & 0 & 0 & 0 & 0 & 0 & 1 & 0 & 0 & \dots & 0 \\ 0 & 0 & 0 & 0 & 0 & 0 & 0 & 0 & 0 & 0 & 0 & 1 & 0 & \dots & 0 \\ 0 & 0 & 0 & 0 & 0 & 0 & 0 & 0 & 0 & 0 & 0 & 0 & 1 & \dots & 0 \\ \vdots & \vdots & \vdots & \vdots & \vdots & \vdots & \vdots & \vdots & \vdots & \vdots & \vdots & \vdots & \vdots & \ddots & 0 \\ 0 & 0 & 0 & 0 & 0 & 0 & 0 & 0 & 0 & 0 & 0 & 0 & 0 & 0 & 1 \end{bmatrix} \quad (3-39)$$

where

$$\begin{aligned} A &= T_a^2 (e^{-\Delta t / T_a} - 1) + T_a \Delta t \\ B &= T_a (1 - e^{-\Delta t / T_a}) \\ C &= e^{-\Delta t / T_a} \end{aligned}$$

The discrete dynamics driving noise matrix is calculated by:

$$\mathbf{Q}_d(t_k) = \int_{t_k}^{t_{k+1}} \Phi(t_{k+1}, \tau) \mathbf{G}(\tau) \mathbf{Q}(\tau) \mathbf{G}^T(\tau) \Phi^T(t_{k+1}, \tau) d\tau \quad (3-40)$$

resulting in the matrix:

$$\mathbf{Q}_d = \begin{bmatrix} D & 0 & 0 & E & 0 & 0 & G & 0 & 0 & 0 & 0 & 0 & 0 & \cdots & 0 \\ 0 & D & 0 & 0 & E & 0 & 0 & G & 0 & 0 & 0 & 0 & 0 & \cdots & 0 \\ 0 & 0 & D & 0 & 0 & E & 0 & 0 & G & 0 & 0 & 0 & 0 & \cdots & 0 \\ E & 0 & 0 & K & 0 & 0 & L & 0 & 0 & 0 & 0 & 0 & 0 & \cdots & 0 \\ 0 & E & 0 & 0 & K & 0 & 0 & L & 0 & 0 & 0 & 0 & 0 & \cdots & 0 \\ 0 & 0 & E & 0 & 0 & K & 0 & 0 & L & 0 & 0 & 0 & 0 & \cdots & 0 \\ G & 0 & 0 & L & 0 & 0 & M & 0 & 0 & 0 & 0 & 0 & 0 & \cdots & 0 \\ 0 & G & 0 & 0 & L & 0 & 0 & M & 0 & 0 & 0 & 0 & 0 & \cdots & 0 \\ 0 & 0 & G & 0 & 0 & L & 0 & 0 & M & 0 & 0 & 0 & 0 & \cdots & 0 \\ 0 & 0 & 0 & 0 & 0 & 0 & 0 & 0 & 0 & N & S & 0 & 0 & \cdots & 0 \\ 0 & 0 & 0 & 0 & 0 & 0 & 0 & 0 & 0 & S & T & 0 & 0 & \cdots & 0 \\ 0 & 0 & 0 & 0 & 0 & 0 & 0 & 0 & 0 & 0 & 0 & U & 0 & \cdots & 0 \\ 0 & 0 & 0 & 0 & 0 & 0 & 0 & 0 & 0 & 0 & 0 & 0 & U & \cdots & 0 \\ \vdots & \vdots & \vdots & \vdots & \vdots & \vdots & \vdots & \vdots & \vdots & \vdots & \vdots & \vdots & \vdots & \ddots & 0 \\ 0 & 0 & 0 & 0 & 0 & 0 & 0 & 0 & 0 & 0 & 0 & 0 & 0 & 0 & U \end{bmatrix} \quad (3-41)$$

where

$$\begin{aligned} D &= \frac{1}{2} T_a^5 q_a (1 - e^{-2\Delta t / T_a}) + T_a^4 q_a \Delta t (1 - 2e^{-\Delta t / T_a}) - T_a^3 q_a (\Delta t)^2 + \frac{1}{3} T_a^2 q_a (\Delta t)^3 \\ E &= T_a^4 q_a \left(\frac{1}{2} e^{-2\Delta t / T_a} - e^{-\Delta t / T_a} + \frac{1}{2} \right) + T_a^3 q_a \Delta t (e^{-\Delta t / T_a} - 1) + \frac{1}{2} T_a^2 q_a (\Delta t)^2 \\ G &= \frac{1}{2} T_a^3 q_a (1 - e^{-2\Delta t / T_a}) - T_a^2 q_a \Delta t e^{-\Delta t / T_a} \\ K &= \frac{1}{2} T_a^3 q_a \left(-e^{-2\Delta t / T_a} + 4e^{-\Delta t / T_a} + 2\frac{\Delta t}{T_a} - 3 \right) \\ L &= -\frac{1}{2} T_a^2 q_a (-e^{-2\Delta t / T_a} + 2e^{-\Delta t / T_a} - 1) \\ M &= -\frac{1}{2} T_a q_a (e^{-2\Delta t / T_a} - 1) \\ N &= q_{c1} \Delta t + \frac{1}{3} q_{c2} (\Delta t)^3 \end{aligned} \quad \left| \begin{aligned} S &= \frac{1}{2} q_{c2} (\Delta t)^2 \\ T &= q_{c2} \Delta t \\ U &= q_N \Delta t \end{aligned} \right.$$

3.4 Carrier-phase Ambiguity Set Generation

The carrier-phase ambiguity set generation routine consists of the Z-transform, FASF and inverse Z-transforms subroutines. The double-differenced ambiguity states and their associated covariance output from the floating-point filter are used in the carrier-phase ambiguity set generation routine.

The first step in generating candidate ambiguity sets is to generate the Z-transform. The Z-transform is the linear, volume preserving, integer transform described in Section 2.5.3.1. The Z-transform used in this algorithm is based on the higher order transformations detailed in Equations (2-82) through (2-88). Once generated, the Z-transform is used to decorrelate the floating-point DGPS filter ambiguity estimates before being used in the FASF subroutine.

These transformed estimates are then used by the FASF subroutine also described in Section 2.5.3.1 and Equations (2-89) through (2-91). The FASF subroutine generates a user-defined number of candidate ambiguity sets, picked to be 250 sets for this thesis. Then the routine picks the K best candidate sets (where K is the number of elemental filters used in the MMAE, between 15 and 100, as described in Section 3.5) by using the ratio test in Equation (2-92). The K candidate ambiguity sets are transformed back into the original measurement space using the inverse of the Z-transform before being used in the elemental filters of the MMAE.

New candidate ambiguity sets are only generated and provided to the elemental filters in the MMAE under certain conditions:

- ❑ During initialization, candidate ambiguity sets are generated after a *single propagate and update cycle* of the floating-point filter.
- ❑ New candidate ambiguity sets are generated after uncorrected cycle slips in either the reference or remote receivers.
- ❑ New candidate ambiguity sets are generated when a satellite is lost from view or a new satellite comes into view.

The above conditions, although simplistic and overly restrictive, were implemented to validate the “proof of concept” algorithm developed in this thesis. An operational system would have advanced logic routines capable of more efficiently handling cycle slips and satellites changes.

3.5 Multiple Model Adaptive Estimator Design

As stressed throughout this thesis, the MMAE design is the key to determining the correct carrier-phase ambiguity set, and the generation of accurate GPS navigation data. The MMAE design used in this thesis is the design described in Section 2.4, with minor changes to the conditional probability generation calculations. In addition, a filter pruning routine was added to allow the MMAE to converge to the true fixed-point solution.

3.5.1 *Elemental Filter Design*

The elemental filters in the MMAE are nine-state (3 position, 3 velocity, and 3 acceleration) FOGMA filters, described below. The additional clock or ambiguity states used in the floating-point filter are not necessary because the elemental filters only use double-difference carrier-phase measurements. All of the elemental filters are identical, i.e. they use the same system dynamics, the same states, the same process noises and the same tuning values. This means there is only one dynamics “model” in the Multiple Model Adaptive Estimator (MMAE). The only difference between elemental filters is that each filter “corrects” the double-differenced carrier-phase measurements based on a different double-differenced ambiguity set. At every sample time, each elemental filter receives (n-1) double-difference carrier-phase measurements, corrects them according to its own double-differenced ambiguity set. Each elemental filter then uses the “ambiguity corrected” double-difference carrier-phase measurements to generate state estimates and residuals.

Because each elemental filter uses a fixed ambiguity set to correct the carrier-phase measurement, at every sample time each elemental filter generates a fixed-point solution. The elemental filter’s state estimates and residuals are used in the conditional probability calculations to determine which elemental filter’s solution is the true fixed-point solution.

3.5.1.1 *Elemental Filter Model Equations*

The state vector for the elemental filters are given by:

$$\mathbf{x} = [X \ Y \ Z \ \dot{X} \ \dot{Y} \ \dot{Z} \ \ddot{X} \ \ddot{Y} \ \ddot{Z}] \quad (3-42)$$

where

$$\begin{aligned}
x_1 &= X = \text{ECEF X position (m)} \\
x_2 &= Y = \text{ECEF Y position (m)} \\
x_3 &= Z = \text{ECEF Z position (m)} \\
x_4 &= \dot{X} = \text{ECEF X velocity (m/s)} \\
x_5 &= \dot{Y} = \text{ECEF Y velocity (m/s)} \\
x_6 &= \dot{Z} = \text{ECEF Z velocity (m/s)} \\
x_7 &= \ddot{X} = \text{ECEF X acceleration (m/s}^2\text{)} \\
x_8 &= \ddot{Y} = \text{ECEF Y acceleration (m/s}^2\text{)} \\
x_9 &= \ddot{Z} = \text{ECEF Z acceleration (m/s}^2\text{)}
\end{aligned}$$

The dynamics and process noises for the elemental filter were derived in the same manners as the first nine states of the floating-point filter. The linear state space differential equation for the elemental filters is fully represented by:

$$\begin{bmatrix} \dot{x}_1 \\ \dot{x}_2 \\ \dot{x}_3 \\ \dot{x}_4 \\ \dot{x}_5 \\ \dot{x}_6 \\ \dot{x}_7 \\ \dot{x}_8 \\ \dot{x}_9 \end{bmatrix} = \begin{bmatrix} 0 & 0 & 0 & 1 & 0 & 0 & 0 & 0 & 0 \\ 0 & 0 & 0 & 0 & 1 & 0 & 0 & 0 & 0 \\ 0 & 0 & 0 & 0 & 0 & 1 & 0 & 0 & 0 \\ 0 & 0 & 0 & 0 & 0 & 0 & 1 & 0 & 0 \\ 0 & 0 & 0 & 0 & 0 & 0 & 0 & 1 & 0 \\ 0 & 0 & 0 & 0 & 0 & 0 & 0 & 0 & 1 \\ 0 & 0 & 0 & 0 & 0 & 0 & -1/T_a & 0 & 0 \\ 0 & 0 & 0 & 0 & 0 & 0 & 0 & -1/T_a & 0 \\ 0 & 0 & 0 & 0 & 0 & 0 & 0 & 0 & -1/T_a \end{bmatrix} \begin{bmatrix} x_1 \\ x_2 \\ x_3 \\ x_4 \\ x_5 \\ x_6 \\ x_7 \\ x_8 \\ x_9 \end{bmatrix} + \begin{bmatrix} 0 \\ 0 \\ 0 \\ 0 \\ 0 \\ 0 \\ w_a \\ w_a \\ w_a \end{bmatrix} \quad (3-43)$$

Again, T_a is the time constant associated with the FOGMA acceleration states. For this system, the matrix $\mathbf{G}(t)$ is an identity matrix. The dynamics driving noise vector matrix \mathbf{Q} must also be specified for the elemental filters and is given by:

$$\mathbf{Q} = \begin{bmatrix} 0 & 0 & 0 & 0 & 0 & 0 & 0 & 0 & 0 & 0 \\ 0 & 0 & 0 & 0 & 0 & 0 & 0 & 0 & 0 & 0 \\ 0 & 0 & 0 & 0 & 0 & 0 & 0 & 0 & 0 & 0 \\ 0 & 0 & 0 & 0 & 0 & 0 & 0 & 0 & 0 & 0 \\ 0 & 0 & 0 & 0 & 0 & 0 & 0 & 0 & 0 & 0 \\ 0 & 0 & 0 & 0 & 0 & 0 & 0 & 0 & 0 & 0 \\ 0 & 0 & 0 & 0 & 0 & 0 & q_a & 0 & 0 & 0 \\ 0 & 0 & 0 & 0 & 0 & 0 & 0 & q_a & 0 & 0 \\ 0 & 0 & 0 & 0 & 0 & 0 & 0 & 0 & q_a & 0 \end{bmatrix} \quad (3-44)$$

The elemental filter time constant, mean squared value, and noise values used in this thesis, for both ground and flight test are specified below in Table 3-4. The mean squared value and hence the acceleration noises were increased when processing flight test data to account for unknown accelerations not present during the static ground tests.

Table 3-4. Elemental Filter Dynamics Driving Noise Values

Term	Definition	Ground Test Value	Flight Test Value
σ_a^2	Mean squared value	$(3.873 \text{ m/sec}^2)^2$	$(12.25 \text{ m/sec}^2)^2$
T_a	Acceleration time constant	3sec	3sec
q_a	Acceleration noise	$10 \text{ m}^2/\text{sec}^5$	$100 \text{ m}^2/\text{sec}^5$

At the start of the algorithm, or whenever the MMAE is reset, the elemental filters are initialized to the output of the floating-point filter.

$$\hat{\mathbf{x}}_k(t_0) = \hat{\mathbf{x}}_{(1-9)}(t_0) \quad (3-45)$$

$$\mathbf{P}_k(t_0) = \mathbf{P}_{(1-9),x(1-9)}(t_0) \quad (3-46)$$

3.5.1.2 Elemental Filter Measurement Model

The elemental filters use a discrete-time, nonlinear measurement model consisting only of double-differenced carrier-phase measurements. Before being used by the elemental filters, the double-differenced carrier-phase measurements are corrected by the candidate ambiguity set being tested by the elemental filter. This results in an $n-1$ measurement vector specified by:

$$\mathbf{z}(t_i) = \begin{bmatrix} (\nabla\Delta\phi_{xy}^{12})' & (\nabla\Delta\phi_{xy}^{13})' & \cdots & (\nabla\Delta\phi_{xy}^{1n})' \end{bmatrix} \quad (3-47)$$

where

$(\nabla\Delta\phi_{xy}^{12})' =$ ambiguity corrected double-differenced carrier-phase measurement between satellites 1 and 2

$(\nabla\Delta\phi_{xy}^{13})' =$ ambiguity corrected double-differenced carrier-phase measurement between satellites 1 and 3

\vdots

$(\nabla\Delta\phi_{xy}^{1n})' =$ ambiguity corrected double-differenced carrier-phase measurement between satellites 1 and n

The ambiguity-corrected double-difference carrier-phase measurements are given by:

$$(\nabla\Delta\phi_{xy}^{ab})' = \nabla\Delta\phi_{xy}^{ab} - \nabla\Delta\tilde{N}_{xy}^{ab} \quad (3-48)$$

where

$\nabla\Delta\phi_{xy}^{ab} =$ the normal (or uncorrected) double-differenced carrier-phase measurement between satellites a and b

$\nabla\Delta\tilde{N}_{xy}^{ab} =$ the double-differenced candidate ambiguity term between satellites a and b

The candidate double-differenced ambiguity *set* ($n-1$ ambiguities) being tested by an elemental filter is made of candidate ambiguity *terms*, $\nabla\Delta\tilde{N}_{xy}^{ab}$, one ambiguity for each of

the double-differenced measurements. The candidate ambiguity terms, $\nabla\Delta\tilde{N}_{xy}^{ab}$, are by definition constant values, but are different constant values for each elemental filter. In fact, the difference in the candidate ambiguity sets is *the only* difference between the elemental filters.

By substituting in the full double-differenced widelane carrier-phase measurement equation into Equation (3-48), the ambiguity corrected measurement becomes:

$$(\Delta\nabla\phi_{xy}^{ab})' = \frac{1}{\lambda}(\Delta\nabla r_{xy}^{ab} + \Delta\nabla T_{xy}^{ab} + \Delta\nabla I_{xy}^{ab} + \Delta\nabla m_{xy}^{ab} + \Delta\nabla v_{xy}^{ab}) + \Delta\nabla N_{xy}^{ab} - \Delta\nabla\tilde{N}_{xy}^{ab} \quad (3-49)$$

As outlined in Section 3.3.2, the measurement model must be represented in the form:

$$\mathbf{z}(t_i) = \mathbf{h}[\mathbf{x}(t_i), t_i] + \mathbf{v}(t_i) \quad (3-50)$$

By expanding the double-differenced range term and combining terms Equation (3-49) becomes:

$$(\Delta\nabla\phi_{xy}^{ab})' = \frac{1}{\lambda}[r_y^a - r_x^a - (r_y^b - r_x^b)] + v_{\Delta\nabla\phi} \quad (3-51)$$

where now

$$v_{\Delta\nabla\phi} = \frac{1}{\lambda}(\Delta\nabla T_{xy}^{ab} + \Delta\nabla I_{xy}^{ab} + \Delta\nabla m_{xy}^{ab} + \Delta\nabla v_{xy}^{ab}) + \Delta\nabla N_{xy}^{ab} - \Delta\nabla\tilde{N}_{xy}^{ab} \quad (3-52)$$

The term $v_{\Delta\nabla\phi}$, modeled as a white noise, is the combination of the residual error terms in the double-differenced equation and the difference in the ambiguity terms. As explained previously, even though the individual residual error terms $(\Delta\nabla T_{xy}^{ab}, \Delta\nabla I_{xy}^{ab}, \Delta\nabla m_{xy}^{ab}, \Delta\nabla v_{xy}^{ab})$ are not white noises, we assume the combination of the four terms can be sufficiently modeled as a white noise.

As long as the ambiguity terms in Equation (3-52) and (3-49) cancel, i.e. $\Delta \nabla N_{xy}^{ab} - \Delta \nabla \tilde{N}_{xy}^{ab} = 0$, modeling $v_{\Delta \nabla \phi}$ as a white noise is a good assumption. However, if the two ambiguity terms are not equal, a constant bias equal to the difference in the ambiguity terms will remain in the ambiguity corrected double-differenced carrier-phase measurements. The presence, or absence, of this bias, $\Delta \nabla N_{xy}^{ab} - \Delta \nabla \tilde{N}_{xy}^{ab}$, will be apparent in the elemental filter's residuals. This bias in the residuals is the key to determining which elemental filter contains the correct ambiguity set.

Expanding the range terms and substituting state variables for the appropriate terms as described in Section (3.3.2) gives the following equation:

$$\begin{aligned} \Delta \nabla \phi_{xy}^{ab} = & \frac{1}{\lambda} \left[(x^a - x_1)^2 + (y^a - x_2)^2 + (z^a - x_3)^2 \right]^{1/2} \\ & - \left[(x^b - x_1)^2 + (y^b - x_2)^2 + (z^b - x_3)^2 \right]^{1/2} \\ & + \frac{1}{\lambda} \{ r_x^b - r_x^a \} + v_{\Delta \nabla \phi} \end{aligned} \quad (3-53)$$

Again, the partial derivative matrix \mathbf{H} must be calculated. The individual partial derivatives for a row of the double-differenced widelane carrier-phase measurements are:

$$\begin{aligned} \left. \frac{\partial h[x, t_i]}{\partial x_1} \right|_{x=\hat{x}(t_i^-)} &= \frac{1}{\lambda} \left\{ \frac{x^a - x_1}{\left[(x^a - x_1)^2 + (y^a - x_2)^2 + (z^a - x_3)^2 \right]^{1/2}} \right\} \\ &- \frac{1}{\lambda} \left\{ \frac{x^b - x_1}{\left[(x^b - x_1)^2 + (y^b - x_2)^2 + (z^b - x_3)^2 \right]^{1/2}} \right\} \\ &\equiv \frac{1}{\lambda} \{ e_1^a - e_1^b \} \end{aligned} \quad (3-54)$$

$$\begin{aligned}
\left. \frac{\partial h[x, t_i]}{\partial x_2} \right|_{x=\hat{x}(t_i^-)} &= \frac{1}{\lambda} \left\{ \frac{y^a - x_2}{[(x^a - x_1)^2 + (y^a - x_2)^2 + (z^a - x_3)^2]^{1/2}} \right\} \\
&\quad - \frac{1}{\lambda} \left\{ \frac{y^b - x_2}{[(x^b - x_1)^2 + (y^b - x_2)^2 + (z^b - x_3)^2]^{1/2}} \right\} \\
&\equiv \frac{1}{\lambda} \{e_2^a - e_2^b\}
\end{aligned} \tag{3-55}$$

$$\begin{aligned}
\left. \frac{\partial h[x, t_i]}{\partial x_3} \right|_{x=\hat{x}(t_i^-)} &= \frac{1}{\lambda} \left\{ \frac{z^a - x_3}{[(x^a - x_1)^2 + (y^a - x_2)^2 + (z^a - x_3)^2]^{1/2}} \right\} \\
&\quad - \frac{1}{\lambda} \left\{ \frac{z^b - x_3}{[(x^b - x_1)^2 + (y^b - x_2)^2 + (z^b - x_3)^2]^{1/2}} \right\} \\
&\equiv \frac{1}{\lambda} \{e_3^a - e_3^b\}
\end{aligned} \tag{3-56}$$

These can be combined into a vector representing one row of the \mathbf{H} matrix as:

$$\mathbf{H}^{ab} = \begin{bmatrix} \frac{1}{\lambda}(\mathbf{e}_y^a - \mathbf{e}_y^b) & 0 & 0 & 0 & 0 & 0 & 0 \end{bmatrix} \tag{3-57}$$

where

$\mathbf{e}^a = [e_1 \quad e_2 \quad e_3] =$ unit line of sight vector between the receiver and satellite a .
 $\mathbf{e}^b = [e_1 \quad e_2 \quad e_3] =$ unit line of sight vector between the receiver and satellite b .

The entire measurement matrix \mathbf{H} is an $(n-1)$ -by-9 matrix defined by:

$$\mathbf{H} = \begin{bmatrix} \frac{1}{\lambda}(\mathbf{e}^1 - \mathbf{e}^2) & 0 & 0 & 0 & 0 & 0 & 0 \\ \frac{1}{\lambda}(\mathbf{e}^1 - \mathbf{e}^3) & 0 & 0 & 0 & 0 & 0 & 0 \\ \vdots & \vdots & \vdots & \vdots & \vdots & \vdots & \vdots \\ \frac{1}{\lambda}(\mathbf{e}^1 - \mathbf{e}^n) & 0 & 0 & 0 & 0 & 0 & 0 \end{bmatrix} \tag{3-58}$$

The measurement error covariance matrix for the elemental filters defined by:

$$E\{\mathbf{v}(t_i) \mathbf{v}^T(t_j)\} = \begin{cases} \mathbf{R}(t_i) & \text{for } t_i = t_j \\ \mathbf{0} & \text{for } t_i \neq t_j \end{cases} \quad (3-59)$$

The \mathbf{R} matrix is a $(n-1)$ -by- $(n-1)$ matrix specified by:

$$\mathbf{R} = \begin{bmatrix} r_{\phi^{ij}, \phi^{ij}} & r_{\phi^{ij}, \phi^{ik}} & \cdots & r_{\phi^{ij}, \phi^{ik}} \\ r_{\phi^{ij}, \phi^{ik}} & r_{\phi^{ij}, \phi^{ij}} & \cdots & r_{\phi^{ij}, \phi^{ik}} \\ \vdots & \vdots & \ddots & \vdots \\ r_{\phi^{ij}, \phi^{ik}} & r_{\phi^{ij}, \phi^{ik}} & r_{\phi^{ij}, \phi^{ik}} & r_{\phi^{ij}, \phi^{ij}} \end{bmatrix} \quad (3-60)$$

where

$r_{\nabla\Delta\phi^{ij}, \nabla\Delta\phi^{ij}}$ = double-differenced carrier-phase measurement variance

$r_{\nabla\Delta\phi^{ij}, \nabla\Delta\phi^{ik}}$ = double-differenced carrier-phase measurement covariance

The double-differenced carrier-phase measurement variances were all set to the same value as were the double-differenced carrier-phase measurement covariances. The elemental filter measurement error values used in this research, for both ground and flight test, are listed in Table 3-5. Due to the dynamics associated with the flight test data the measurement covariance error values were reduced to allow the conditional probability to more rapidly shift between elemental filters.

Table 3-5. Elemental Filter Measurement Covariance Error Values

Term	Definition	Ground Test Value	Flight Test Value
$r_{\nabla\Delta\phi^{ij}, \nabla\Delta\phi^{ij}}$	Double-differenced carrier-phase variance error	$(0.75\text{m})^2$	$(0.075\text{m})^2$
$r_{\nabla\Delta\phi^{ij}, \nabla\Delta\phi^{ik}}$	Double-differenced carrier-phase covariance error	$0.5*(0.75\text{m})^2$	$0.5*(0.075\text{m})^2$

3.5.1.3 Discrete-Time Models

The elemental filter model equations derived above must be converted into difference equations in order to be implemented easily in a Kalman filter. Following the procedure described in Section 3.3.3, again assuming $\Delta t \equiv t_{k+1} - t_k$, the elemental filter state transition matrix is defined as:

$$\Phi(\Delta t) = \begin{bmatrix} 1 & 0 & 0 & \Delta t & 0 & 0 & A_e & 0 & 0 \\ 0 & 1 & 0 & 0 & \Delta t & 0 & 0 & A_e & 0 \\ 0 & 0 & 1 & 0 & 0 & \Delta t & 0 & 0 & A_e \\ 0 & 0 & 0 & 1 & 0 & 0 & B_e & 0 & 0 \\ 0 & 0 & 0 & 0 & 1 & 0 & 0 & B_e & 0 \\ 0 & 0 & 0 & 0 & 0 & 1 & 0 & 0 & B_e \\ 0 & 0 & 0 & 0 & 0 & 0 & C_e & 0 & 0 \\ 0 & 0 & 0 & 0 & 0 & 0 & 0 & C_e & 0 \\ 0 & 0 & 0 & 0 & 0 & 0 & 0 & 0 & C_e \end{bmatrix} \quad (3-61)$$

where

$$\begin{aligned} A_e &= T_a^2 (e^{-\Delta t/T_a} - 1) + T_a \Delta t \\ B_e &= T_a (1 - e^{-\Delta t/T_a}) \\ C_e &= e^{-\Delta t/T_a} \end{aligned}$$

and the discrete dynamics driving noise matrix:

$$\mathbf{Q}_d = \begin{bmatrix} D_e & 0 & 0 & E_e & 0 & 0 & G_e & 0 & 0 \\ 0 & D_e & 0 & 0 & E_e & 0 & 0 & G_e & 0 \\ 0 & 0 & D_e & 0 & 0 & E_e & 0 & 0 & 0 \\ E_e & 0 & 0 & K_e & 0 & 0 & L_e & 0 & G_e \\ 0 & E_e & 0 & 0 & K_e & 0 & 0 & L_e & 0 \\ 0 & 0 & E_e & 0 & 0 & K_e & 0 & 0 & L_e \\ G_e & 0 & 0 & L_e & 0 & 0 & M_e & 0 & 0 \\ 0 & G_e & 0 & 0 & L_e & 0 & 0 & M_e & 0 \\ 0 & 0 & G_e & 0 & 0 & L_e & 0 & 0 & M_e \end{bmatrix} \quad (3-62)$$

where

$$\begin{aligned}
D_e &= \frac{1}{2}T_a^5 q_a (1 - e^{-2\Delta t/T_a}) + T_a^4 q_a \Delta t (1 - 2e^{-\Delta t/T_a}) - T_a^3 q_a (\Delta t)^2 + \frac{1}{3}T_a^2 q_a (\Delta t)^3 \\
E_e &= T_a^4 q_a \left(\frac{1}{2}e^{-2\Delta t/T_a} - e^{-\Delta t/T_a} + \frac{1}{2} \right) + T_a^3 q_a \Delta t (e^{-\Delta t/T_a} - 1) + \frac{1}{2}T_a^2 q_a (\Delta t)^2 \\
G_e &= \frac{1}{2}T_a^3 q_a (1 - e^{-2\Delta t/T_a}) - T_a^2 q_a \Delta t e^{-\Delta t/T_a} \\
K_e &= \frac{1}{2}T_a^3 q_a \left(-e^{-2\Delta t/T_a} + 4e^{-\Delta t/T_a} + 2\frac{\Delta t}{T_a} - 3 \right) \\
L_e &= -\frac{1}{2}T_a^2 q_a (-e^{-2\Delta t/T_a} + 2e^{-\Delta t/T_a} - 1) \\
M_e &= -\frac{1}{2}T_a q_a (e^{-2\Delta t/T_a} - 1)
\end{aligned}$$

3.5.2 Conditional Probability Calculations

The conditional probability generation block shown in Figure 3-1 is based on Equations (2-55) and (2-56), derived in Section 2.4.2, with some slight modifications. Equations (2-55) and (2-56) are repeated here for clarity.

$$p_k(t_i) = \frac{f_{\mathbf{z}(t_i)|\mathbf{a}, \mathbf{Z}(t_{i-1})}(\mathbf{z}_i | \mathbf{a}_k, \mathbf{Z}_{i-1}) p_k(t_{i-1})}{\sum_{j=1}^K f_{\mathbf{z}(t_i)|\mathbf{a}, \mathbf{Z}(t_{i-1})}(\mathbf{z}_i | \mathbf{a}_j, \mathbf{Z}_{i-1}) p_j(t_{i-1})} \quad (2-55)$$

$$\begin{aligned}
f_{\mathbf{z}(t_i)|\mathbf{a}, \mathbf{Z}(t_{i-1})}(\mathbf{z}_i | \mathbf{a}_k, \mathbf{Z}_{i-1}) &= \frac{1}{(2\pi)^{m/2} |\mathbf{A}_k(t_i)|^{-1/2}} * \exp\{\bullet\} \\
\{\bullet\} &= \left\{ -\frac{1}{2} \mathbf{r}_k^T(t_i) \mathbf{A}_k(t_i)^{-1} \mathbf{r}_k(t_i) \right\}
\end{aligned} \quad (2-56)$$

where

$$\begin{aligned}
\mathbf{A}_k(t_i) &= \mathbf{H}_k(t_i) \mathbf{P}_k(t_i^-) \mathbf{H}_k^T(t_i) + \mathbf{R}_k(t_i) \\
\mathbf{r}_k(t_i) &= \mathbf{z}_i - \mathbf{h}[\hat{\mathbf{x}}_k(t_i^-), t_i]
\end{aligned}$$

The success of the MMAE depends on the conditional probability calculations being able to distinguish between correct and incorrect solutions, i.e. the correct ambiguity set. The conditional probability calculations are very sensitive to differences in the residuals of the elemental filters. Any error, or noise, in the state estimates and covariances of each of the elemental filters increases their residual values and degrades the overall performance of the MMAE. Therefore, Equations (2-55) and (2-56) were modified to incorporate the latest measurement; i.e. $\mathbf{P}_k(t_i^-) \Rightarrow \mathbf{P}_k(t_i^+)$ and $\hat{\mathbf{x}}_k(t_i^-) \Rightarrow \hat{\mathbf{x}}_k(t_i^+)$. Using the updated state estimate and covariance values, or “post-fit” residuals, instead of the propagated estimates means the conditional probability density function in Equation (2-56) is now conditioned on the time history of measurements up to and including measurements at time t_i . The post-fit residuals reduce the effect of propagation errors within the elemental filters on the conditional probability calculations. The propagation errors during *static* ground tests were small enough that the algorithm performed well without using post-fit residuals. However, during flight tests, without these post-fit residuals, the propagation errors caused the measurement residuals to be large enough that the conditional probability calculations could not determine which elemental filter contained the correct ambiguity set. However, careful consideration must be taken before modifying the residual calculations so as not to disrupt the beneficial qualities of an MMAE. The new equations using the post-fit residuals are shown below in Equations (3-63) and (3-64).

$$p_k(t_i) = \frac{f_{\mathbf{z}(t_i)|\mathbf{a}, \mathbf{Z}(t_i)}(\mathbf{z}_i | \mathbf{a}_k, \mathbf{Z}_i) p_k(t_{i-1})}{\sum_{j=1}^K f_{\mathbf{z}(t_i)|\mathbf{a}, \mathbf{Z}(t_i)}(\mathbf{z}_i | \mathbf{a}_j, \mathbf{Z}_i) p_j(t_{i-1})} \quad (3-63)$$

$$f_{\mathbf{z}(t_i)|\mathbf{a}, \mathbf{Z}(t_i)}(\mathbf{z}_i | \mathbf{a}_k, \mathbf{Z}_i) = \frac{1}{(2\pi)^{m/2} |\mathbf{A}_k(t_i)|^{-1/2}} * \exp\{\bullet\} \quad (3-64)$$

$$\{\bullet\} = \left\{ -\frac{1}{2} \mathbf{r}_k^T(t_i) \mathbf{A}_k(t_i)^{-1} \mathbf{r}_k(t_i) \right\}$$

where

$$\mathbf{A}_k(t_i) = \mathbf{H}_k(t_i) \mathbf{P}_k(t_i^+) \mathbf{H}_k^T(t_i) + \mathbf{R}_k(t_i)$$

$$\mathbf{r}_k(t_i) = \mathbf{z}_i - \mathbf{h}[\hat{\mathbf{x}}_k(t_i^+), t_i]$$

Recall that the elemental filters are identical, except for the candidate ambiguity set being evaluated. This lead to the value of $|\mathbf{A}_k(t_i)|^{-1/2}$ being the same for all elemental filters, out to ten significant digits. Therefore, the leading coefficient, $\frac{1}{(2\pi)^{m/2} |\mathbf{A}_k(t_i)|^{-1/2}}$, was removed from the conditional probability calculations, and the conditional probability calculations are only based on the $\exp\left\{-\frac{1}{2} \mathbf{r}_k^T(t_i) \mathbf{A}_k(t_i)^{-1} \mathbf{r}_k(t_i)\right\}$ in Equation (2-56). By removing the leading coefficient, Equation (2-56) is no longer a proper conditional probability density, and tests showed there was no significant effect on the final probability weights, other than simplifying the necessary calculations.

3.5.2.1 Lower Probability Bounds

As discussed in Section 2.4.2.1, a conditional probability lower bound must be set to ensure the MMAE does not prematurely ignore information from a particular elemental

filter. The lower probability bound (ϵ) for each elemental filter was set at 0.001. A smaller lower probability bound ($\epsilon = 0.0005$) yielded a sluggish response in the calculated probabilities due to changes in the elemental filters. A larger lower probability bound ($\epsilon = 0.01$) reduced the accuracy of the overall MMAE estimate by inappropriately forcing large weights to be associated with incorrect solutions. The lower probability bound of $\epsilon = 0.001$ proved to be a good compromise between providing a quick enough response to changes in the MMAE and not overly weighting the MMAE estimate toward a wrong elemental filter.

3.5.3 Filter Pruning

An important aspect of the overall algorithm not depicted in Figure 3-1 is the concept of filter pruning. Most MMAEs are designed to look constantly for a change, or changes (failed sensor or actuator, etc.) in the system of interest. Because the MMAE is constantly looking for this change, each elemental filter must be checked at every sample time to determine if it represents the correct change to the system. However, in the integer ambiguity resolution problem, each elemental filter is used to check a constant bias, or ambiguity set. Because integer ambiguities are, by definition, constants once an ambiguity set is determined wrong, it will always be wrong. There is then no benefit to keeping that particular elemental filter within the MMAE.

In addition, to generate an accurate navigation solution, the MMAE must converge to the true fixed-point solution, meaning the elemental filter based on the correct ambiguity set must absorb the entire probability weight. However, based on Equation (2-57) this cannot happen unless there is only one elemental filter in the MMAE. Therefore, logic

was added to the algorithm to remove an elemental filter from the MMAE if the elemental filter's probability remained at or below the lower bound ϵ for more than a predetermined number of consecutive sample periods. The number of consecutive sample periods was determined empirically and can be varied for specific applications. For ground tests, elemental filters were removed from the MMAE after 10 consecutive sample periods below the lower bound (at a 1Hz data rate). For flight tests, elemental filters were removed from the MMAE after 40 consecutive samples below the lower bound periods (at a 2Hz data rate). The additional time during flight test was necessary for the MMAE to determine the correct ambiguity set due to the larger errors caused by the dynamics of the flight tests. The overall MMAE state estimate is then simply an application of Equation (2-57) on the elemental filters still left in the algorithm.

By adding pruning logic to the overall algorithm design, the MMAE is now similar to some forms of moving bank MMAE designs [26, 27]. However, instead of moving a constant number of elemental filters through a search space this new design changes the number of elemental filters used to examine the search space.

The Bayesian method described in Equation (2-57) uses *all* of the remaining elemental filters to provide an overall state estimate. This ensures that until the pruning logic deletes all but the correct elemental filter, the filters based on a wrong ambiguity set will have some affect on the overall MMAE state estimate. Although the wrong elemental filters associated conditional probabilities may be small, their solutions can only degrade the performance of the MMAE.

A different approach would be to use the *maximum a posteriori*, or MAP, design of the MMAE. The MAP design uses the same conditional probability calculations as a

normal MMAE design. However, in the MAP design, the overall MMAE state estimate is the state estimate of the elemental filter that has the highest conditional probability. If the elemental filter with the highest probability is the correct filter then the MMAE estimate is not degraded by the solution of wrong elemental filters. However, this approach ignores the information available in the other elemental filters. In addition, if the filter with the highest probability is the wrong filter, as it occasionally is in this research as shown in Section 4, then the overall state estimate may be worse than the Bayesian approach.

3.6 *Summary*

This chapter discussed the overall algorithm, system models, and techniques used in this thesis. The floating-point DGPS Kalman fitter and the MMAE structure are based on previous AFIT research. The carrier-phase ambiguity set generation routine was a combination of the LAMBDA and FASF methods. The floating-point DGPS Kalman filter model and the elemental filter models used in the MMAE were presented and described in detail. In addition, changes made to the MMAE theory presented in Chapter 2, necessary for the development of the overall algorithm, were described. Chapter 4 will discuss the completed results based on both ground and flight tests.

4 Results and Analysis

4.1 Overview

This chapter presents the results and analysis of the algorithm developed in this thesis. The first section covers four static ground tests cases, and the second section covers the three flight tests cases. The results presented here represent the best possible tuning within the scope of this research. Note that, the purpose of this research is to analyze the use of a MMAE structure to determine carrier-phase ambiguities and generate an accurate GPS navigation solution, not to design a production quality flight-worthy system.

4.2 Ground Tests

Ground tests were conducted at Wright-Patterson Air Force Base (AFB) Ohio, from 1 October 99 to 31 October 99. Results are presented for four different cases, with baseline distances ranging from 250 m to 100 km. Dual frequency Ashtech Z-Surveyor receivers were used to collect data at both the reference and remote sites. The reference station was located at a surveyed site on the roof of the Air Force Institute of Technology. The remote site was a tripod-mounted antenna and receiver placed at various distances from the reference station.

4.2.1 Case Definitions

Each ground test case consisted of approximately 30 minutes of data collected at a 1-Hz rate. The data included L1 C/A pseudorange and carrier-phase measurements, and L2 pseudorange (semi-codeless) and carrier-phase measurements. In all cases the lower probability bound for each elemental filter was 0.001, as justified in Section 3.5.2.1, and each had an equal initial probability weighting. The pruning logic was set to delete elemental filters if their conditional probability remained below the lower limit for more than 10 consecutive sample periods. The floating-point and elemental filters were tuned in accordance with the values specified in Chapter 3. The MMAE used between 15 and 100 filters, and was manually picked depending on the case. More elemental filters were used as the expected difficulty of resolving the carrier-phase ambiguities increased, due to increased baseline distances. Eventually, the algorithm would automatically pick the number of elemental filters based on an expected level of difficulty.

The first two ground test cases were chosen to demonstrate the ability of the MMAE to “instantaneously” resolve the carrier-phase ambiguities, using either widelane or L1 carrier-phase measurements. The last two cases were chosen to demonstrate the ability of the MMAE to correctly resolve the carrier-phase ambiguities at medium and long baseline distances. Ground test case specifics are shown below in Table 4-1.

Table 4-1. Ground Test Case Parameter Description

Case	Baseline Distance	Carrier-Phase Measurement Type	Elemental Filters	Data Rate	Length of Data Set
1	250 m	Widelane	15	1 Hz	~ 30 Minutes
2	250 m	L1	25	1 Hz	~ 30 Minutes
3	28.1 km	Widelane	100	1 Hz	~ 30 Minutes
4	100.7km	Widelane	100	1 Hz	~ 30 Minutes

For the ground tests, the truth position and the true carrier-phase ambiguities were determined by the Ashtech Office Suite software [1]. The position errors are defined as:

$$\hat{x}_{error} = \hat{x}_{filter} - \hat{x}_{true} \quad (4-1)$$

where the subscript “*filter*” refers to either the floating-point filter or the MMAE solution, as appropriate, and the subscript “*true*” refers to the Ashtech Office Suite solution. Note that \hat{x}_{true} is not the absolute truth but it is the solution the MMAE is striving to achieve, namely the fixed-integer solution.

4.2.2 Case 1: 250 m Baseline, Widelane Measurements

Case 1 is designed to demonstrate the near instantaneous ambiguity resolution capability of the MMAE. The time history position performance of the floating-point filter and the MMAE, for the entire data run, are shown in Figure 4-1 and Figure 4-2, respectively. In both figures, the solid line represents the computed position error as described by Equation (4-1). The dashed line represents the filter-predicted standard deviation, not the actual standard deviation of the results. At the beginning of the data run, the MMAE was initialized to the floating-point filter, which had initial position errors between 0.2-0.7 meters. As shown in Figure 4-2, the MMAE corrected these errors to less than 0.1 meters in one sample period. The steps in the filter-predicted standard deviation within the first 100 seconds are due to the algorithm pruning bad elemental filters as described in Section 3.5.3. The filter-predicted standard deviations for the Up direction in Figure 4-2 are at approximately $\pm 0.6\text{m}$, just outside the plot limits.

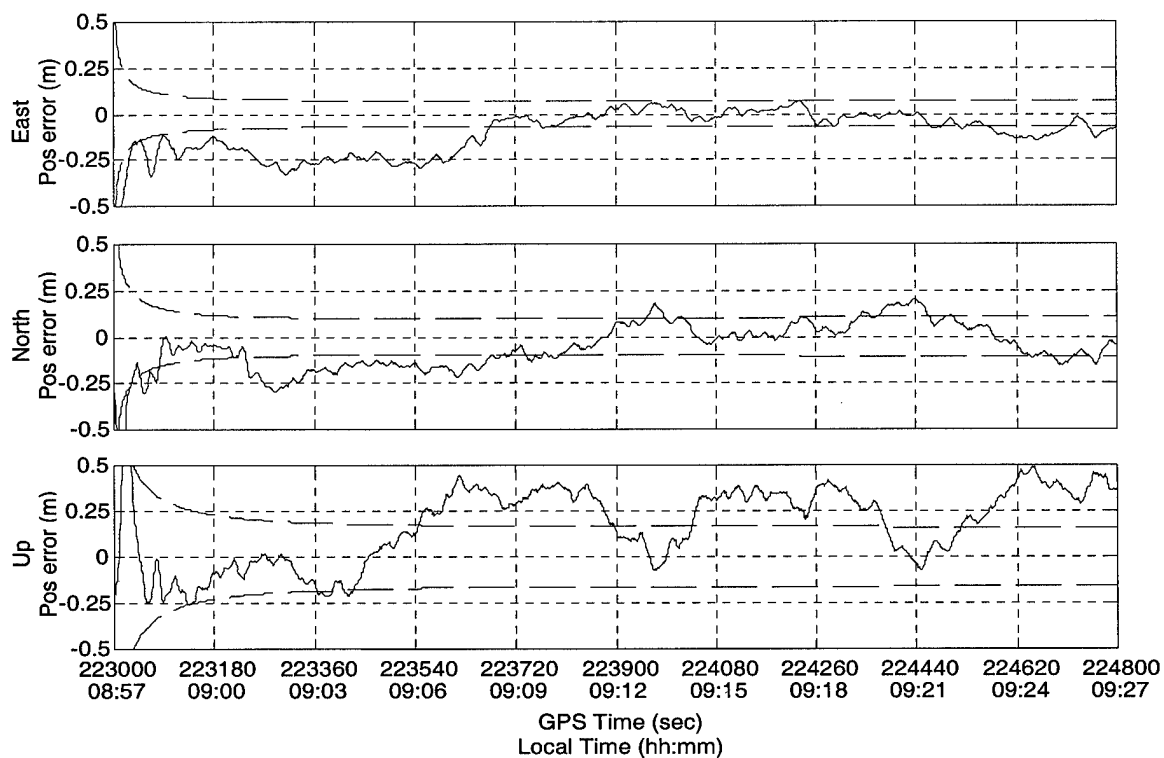


Figure 4-1. Case 1 - Floating-Point Filter Position Errors

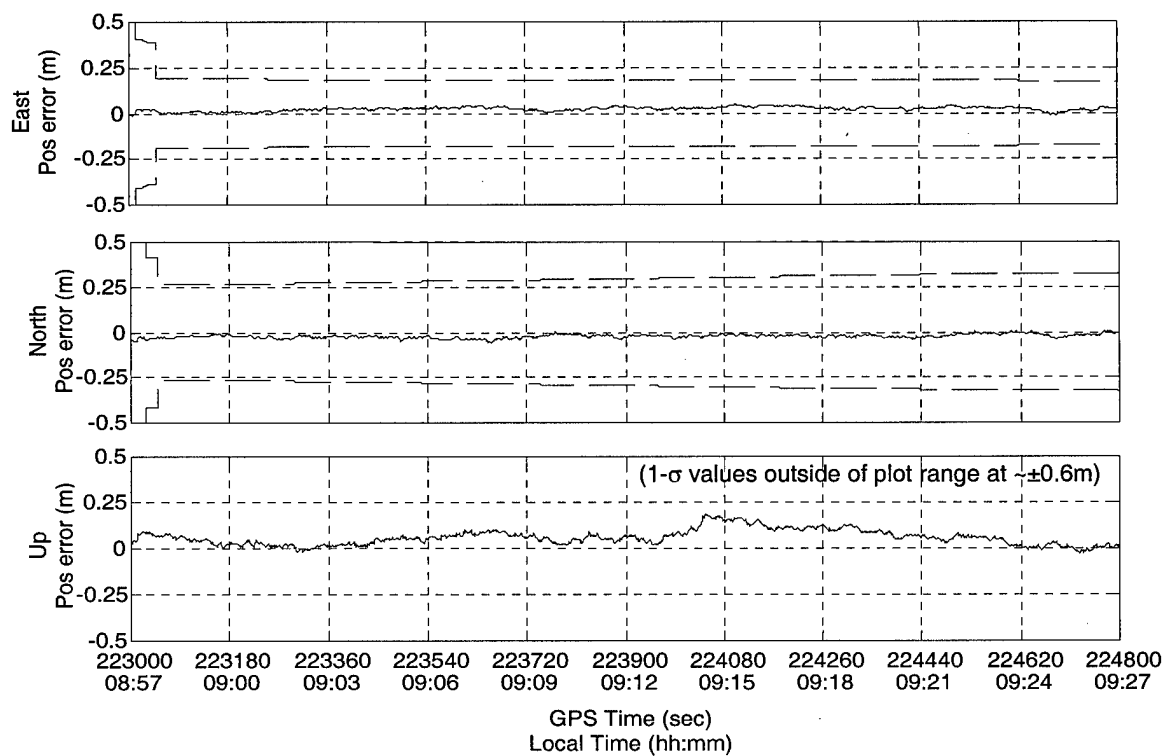


Figure 4-2. Case 1 - MMAE Position Errors

The time averaged mean position error and standard deviation of the floating-point filter solution and the MMAE solution are listed below in Table 4-2. The results are represented in the geodetic (East, North, Up (ENU)) reference frame. These results show that the MMAE solution was an order of magnitude more accurate than the floating-point filter solution.

Table 4-2. Case 1 - Position Solution Error Comparison

	East		North		Up	
	Mean Error (m)	Std (m)	Mean Error (m)	Std (m)	Mean Error (m)	Std (m)
Floating-Point Filter	-0.107	0.118	-0.059	0.138	-0.172	0.205
MMAE	0.023	0.019	-0.024	0.010	0.059	0.042

The first minute of the conditional probability time histories for two of the 15 elemental filters are shown in Figure 4-3. In Figure 4-3, elemental filter 4 (EF 4) contains the correct carrier-phase ambiguity set, and elemental filter 3 (EF 3) contains an incorrect carrier-phase ambiguity set. After the first probability calculation, elemental filter 4 absorbs approximately 98% of the conditional probability, essentially instantaneously resolving the ambiguity. The remaining 2% of the conditional probability is distributed among the other 14 incorrect elemental filters. The conditional probability of 12 of the 14 incorrect elemental filters is small enough that the filters conditional probability had to be artificially set at the lower bound of 0.001. Ten seconds later the filter pruning logic deletes 12 of the 14 incorrect elemental filters (those whose probability stayed at the lower bound) and elemental filter 4 absorbs approximately

99.8% of the conditional probability. Within 25 seconds, the filter pruning logic deletes the remaining 2 incorrect elemental filters. Elemental filter 4 is the only remaining elemental filter in the MMAE, and because it contains the correct ambiguity set, the MMAE converges to the true fixed-integer solution.

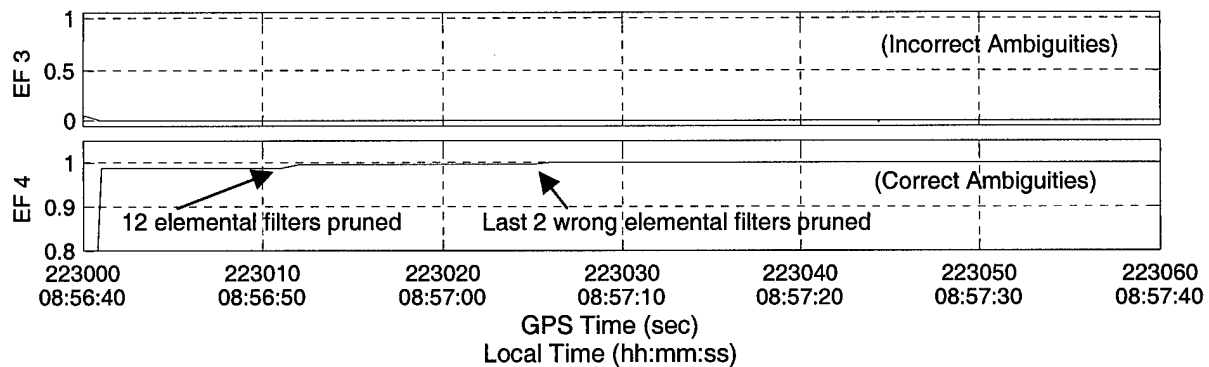


Figure 4-3. Case 1 - Sample Elemental Filter Conditional Probability Time Histories, First Minute

4.2.3 Case 2: 250 m Baseline, L1 Measurements

Case 2 is identical to Case 1, except the algorithm uses L1 carrier-phase measurements instead of widelane measurements. The wavelength of an L1 cycle (~19 cm) is approximately one-fourth the wavelength of a widelane measurement (~86 cm). This increases the number of candidate ambiguity sets within a given search space, making the correct ambiguity set harder to resolve. However, once resolved, an L1 fixed-integer solution is more accurate than a widelane fixed-integer solution, due to amplification of multipath and ionospheric errors in the widelane measurements.

The performance of the floating-point filter and the MMAE are shown in Figure 4-4 and Figure 4-5, respectively. Again, the solid line represents the computed position error and the dashed line represents the filter-predicted standard deviation.

In this case, the floating-point filter initializes with position errors of less than 0.2 meters, and the MMAE corrects these errors to less than 0.03 meters within one sample period. Note that the vertical scale in Figure 4-5 is five times smaller than in Figure 4-4.

The floating-point filter uses the same tuning values for this case as Case 1, even though different carrier-phase measurements are used. This might explain why the floating-point filter solutions are consistently outside of the filter predicted covariance bounds. For this case the floating-point filter performance is satisfactory, however, an operational algorithm would use separate tuning values for different measurement types.

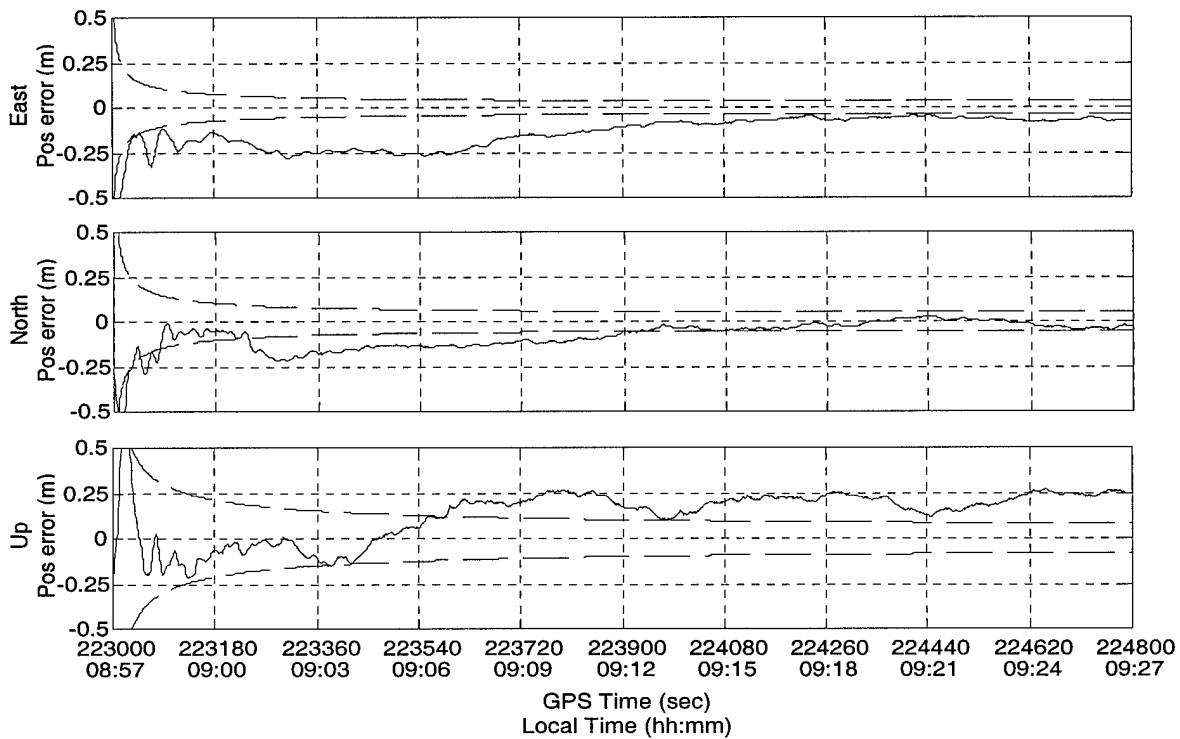


Figure 4-4. Case 2 - Floating-Point Filter Position Errors

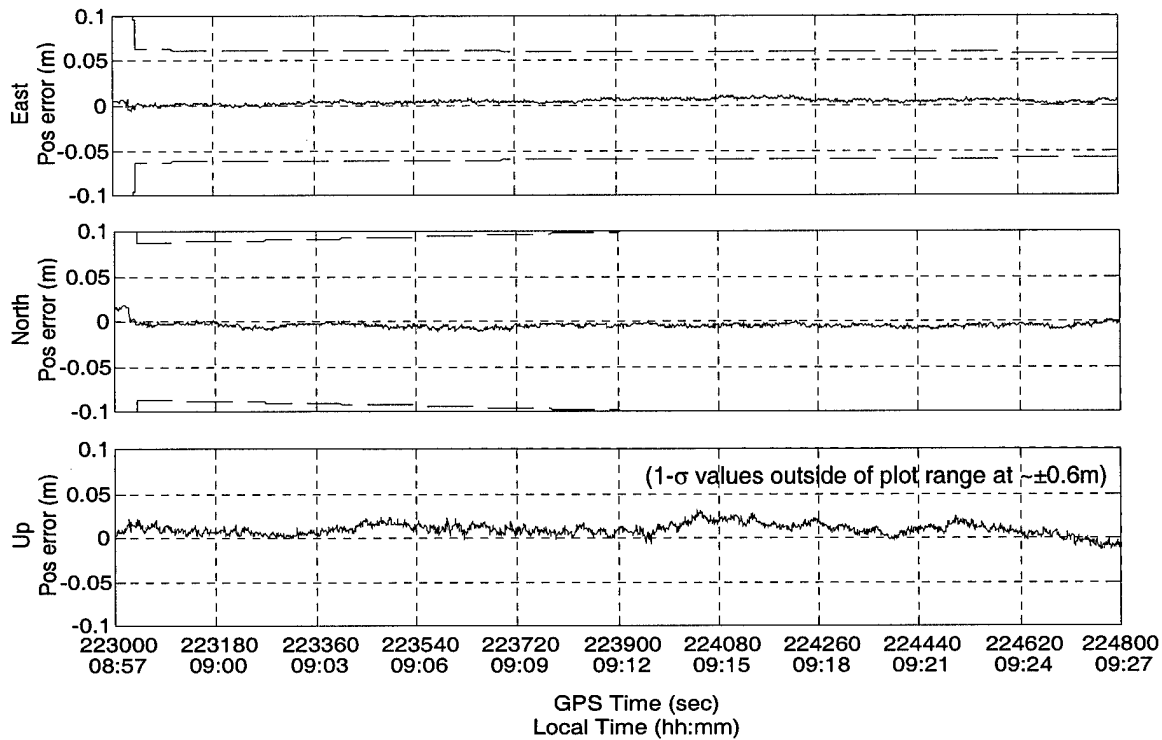


Figure 4-5. Case 2 - MMAE Position Errors

The time averaged mean position error and standard deviation of the floating-point filter solution and the MMAE solution (ENU frame) are shown in Table 4-3. As expected, the results indicate that the MMAE solution is at least an order of magnitude more accurate than the floating-point filter solution, and the L1 solution is more accurate than the widelane solution shown in Case 1.

Table 4-3. Case 2 - Position Solution Error Comparison

	East		North		Up	
	Mean Error (m)	Std (m)	Mean Error (m)	Std (m)	Mean Error (m)	Std (m)
Floating-Point Filter	-0.142	0.088	-0.082	0.097	0.130	0.140
MMAE	0.004	0.015	-0.002	0.004	0.011	0.008

The conditional probability time history, and two of the measurement residual (post-fit residual) time histories for elemental filters 21 and 24 are shown below in Figure 4-6 and Figure 4-7, respectively. Only the first two minutes of the data run are shown.

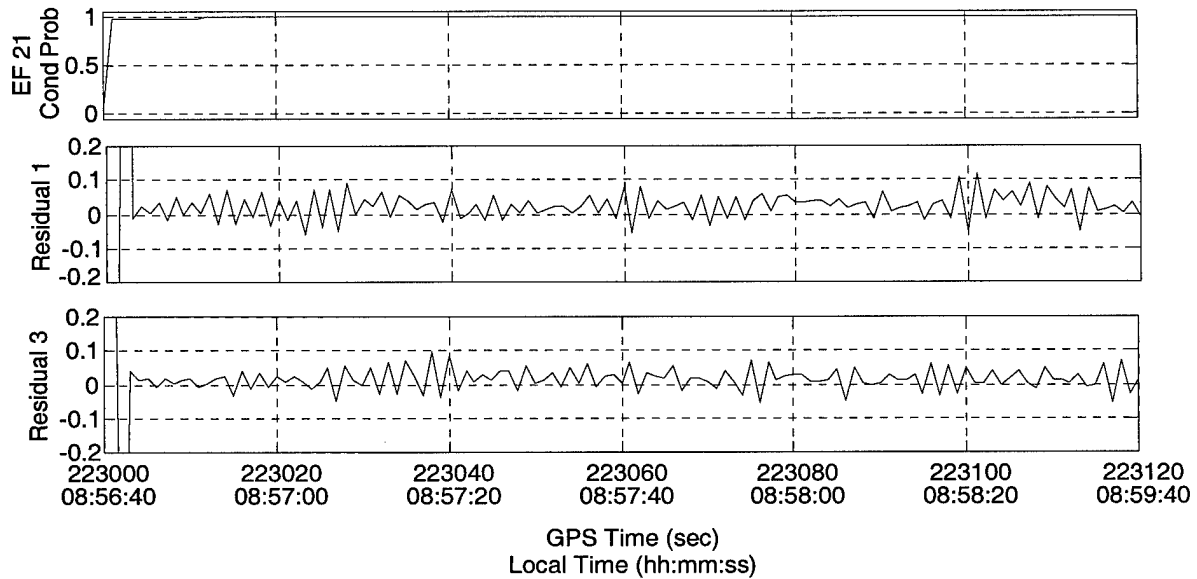


Figure 4-6. Case 2 - Elemental Filter 21 Probability and Residual Time History (Correct Ambiguities)

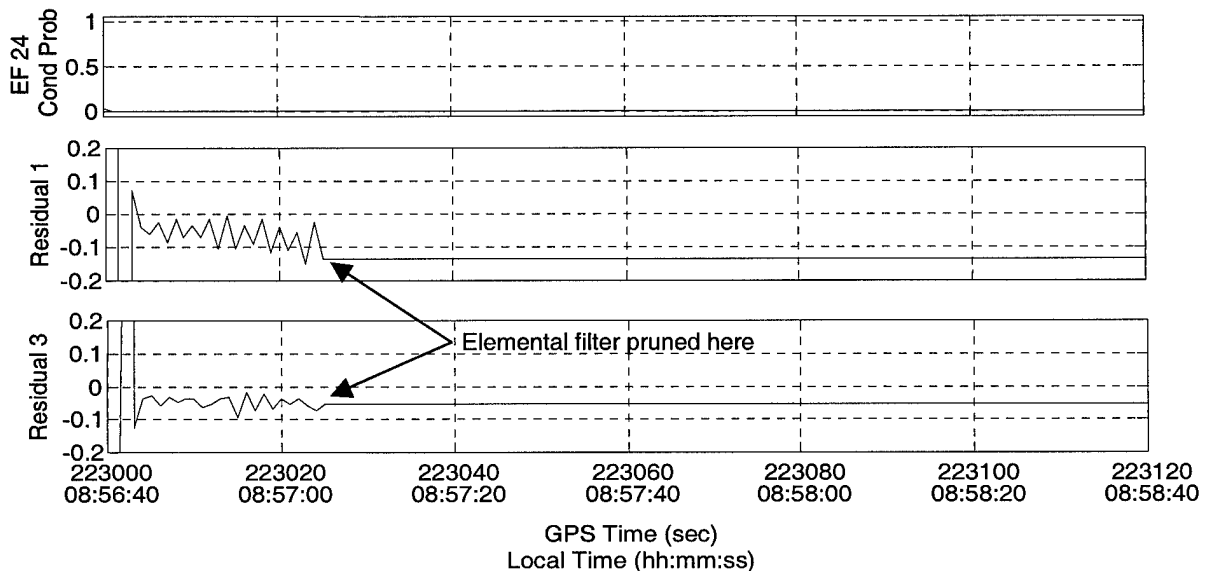


Figure 4-7. Case 2 - Elemental Filter 24 Probability and Residual Time History (Incorrect Ambiguities)

Both of the residuals shown in Figure 4-6 for elemental filter 21 appear almost zero-mean and white; characteristics of a residual in a properly designed and tuned Kalman filter. However, in Figure 4-7 the first residual for elemental filter 24 appears to be growing more negative, while measurement residual 3 shows a small but noticeable bias. These small differences in residuals are enough to cause the conditional probability to shift rapidly toward elemental filter number 21. The straight horizontal line in the elemental filter 21 residual plots, approximately 25 seconds after the start of the data run, are due to the pruning logic, which deleted the elemental filter from the MMAE at that point.

Because of the small value of its residuals, elemental filter 21 (the correct elemental filter) absorbs approximately 97% of the probability during the first conditional probability calculation. The remaining 3% is divided among the other 24 incorrect elemental filters. In a manner very similar to Case 1, the pruning logic starts deleting elemental filters with probabilities at the lower bound for 10 consecutive samples. Within 40 seconds, the pruning logic deletes all of the incorrect elemental filters, and the MMAE converges to the true fixed-integer solution.

The results from the first two cases show that for short baselines, an MMAE almost instantly determines which elemental filter contains the correct carrier-phase ambiguity set. In addition, the MMAE solution is less erratic and at least an order of magnitude more accurate than the DGPS floating-point filter solution.

4.2.4 Case 3: 28.1 km Baseline, Widelane Measurements

Case 3 is designed to demonstrate the performance of the MMAE using a medium baseline distance. The performance of the floating-point filter and the MMAE are shown in Figure 4-8 and Figure 4-9. The floating-point filter (and hence the MMAE) initializes with a much larger than expected position error (~ 0.5 - 2.5 meters), due to residual differential errors not canceled in the floating-point filter. These residual differential errors are a problem, because they are used by the FASF routine to generate candidate ambiguity sets, and they decrease the ability of the MMAE to determine which elemental filter contains the correct ambiguity set. Consequently, the correct elemental filter is not instantly obvious to the MMAE in the conditional probability calculations. For the first 3 minutes of the data run, the conditional probability shifts between an incorrect elemental filter and the correct elemental filter, causing the transients in the MMAE position errors seen in Figure 4-9. Even though initially the MMAE heavily weights an incorrect elemental filter, its position solution accuracy is comparable to the floating-point filter solution during the initial transients.

The other advantage of the MMAE solution is that it transitions very smoothly from a floating-point filter like solution to the true fixed-integer solution. There are no discontinuities, or jumps, in its position solution (typical in other ambiguity resolution routines) as it approaches the fixed-integer solution. The MMAE is reset after it lost lock on a satellite (at $\sim 19:01$), and even though the transients are not as large as the initial transients, the MMAE again transitions very rapidly and smoothly from the floating-point solution to the fixed-integer solution.

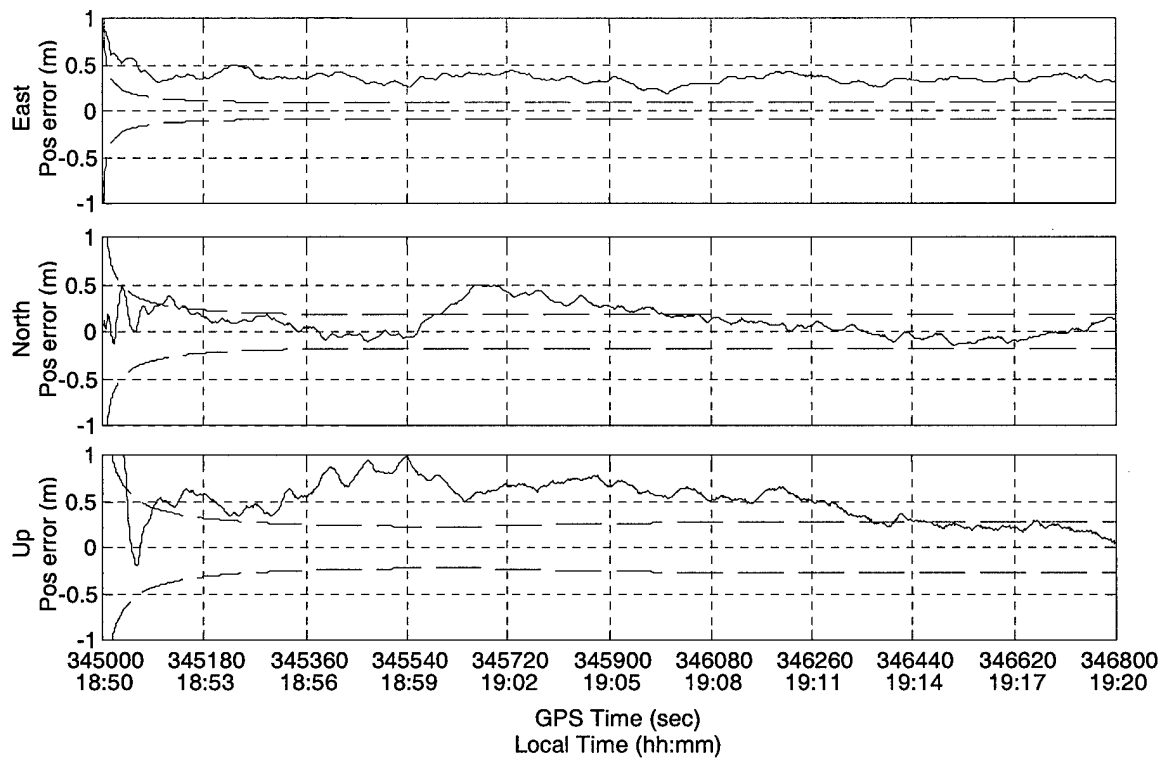


Figure 4-8. Case 3 - Floating-Point Position Errors

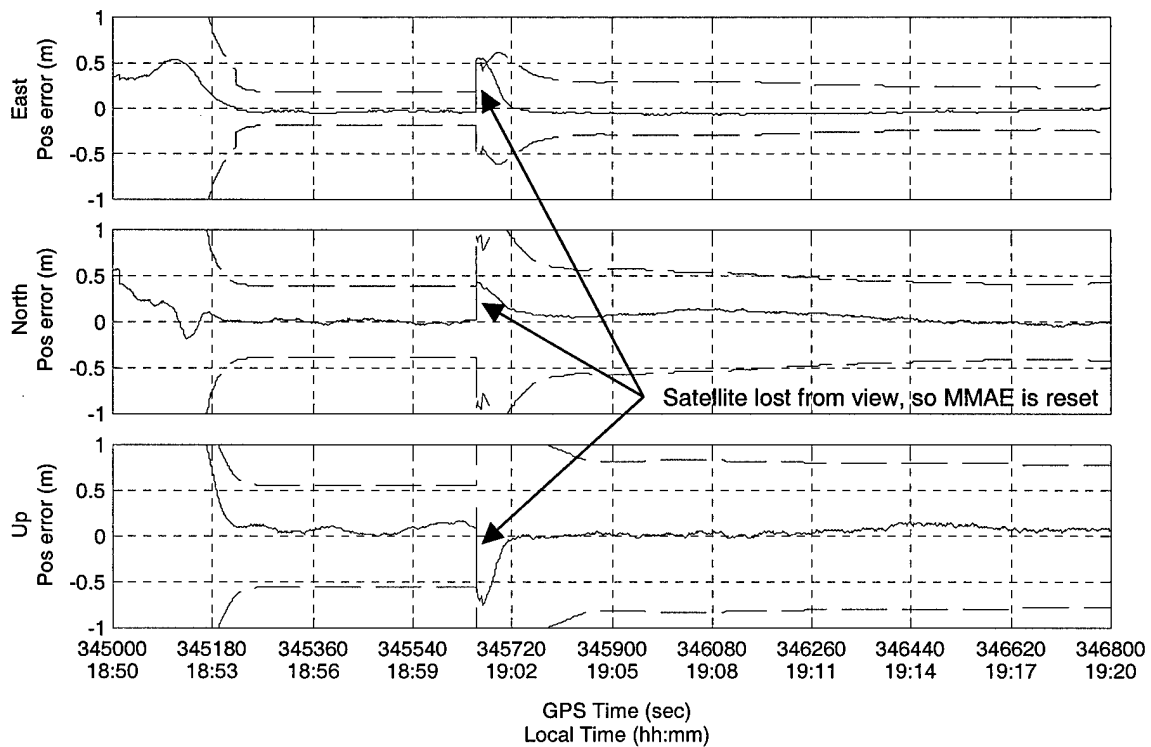


Figure 4-9. Case 3 - MMAE Position Errors

As in the previous cases, position error comparisons between floating-point filter solution and the MMAE solution are shown in Table 4-4. Again, as expected, the MMAE solution is significantly more accurate than the floating-point solution, even with the large transient errors averaged into the overall MMAE accuracy. The large initial transient errors are also the cause of the larger than expected standard deviation in the MMAE solution listed in Table 4-4.

Table 4-4. Case 3 - Position Solution Error Comparison

	East		North		Up	
	Mean Error (m)	Std (m)	Mean Error (m)	Std (m)	Mean Error (m)	Std (m)
Floating-Point Filter	0.355	0.074	0.112	0.159	0.533	0.327
MMAE	0.018	0.151	0.060	0.098	0.205	0.500

The conditional probability time histories for the four elemental filters of interest in this case are shown Figure 4-10. Initially elemental filter 68 (EF 68) contains the correct carrier-phase ambiguity set, and elemental filter 5 (EF 5) contains an incorrect carrier-phase ambiguity set. At approximately 19:01 local time, the mobile receiver lost lock on a low elevation satellite. At this time the algorithm reset all of the elemental filters in the MMAE to the floating filter solution, generated new candidate ambiguity sets for each elemental filter, and reset the elemental filter probabilities to equal values. After being reset elemental filter 77 (EF 77) contains the correct ambiguity set, and elemental filter 58 (EF 58) contains an incorrect ambiguity set. Resetting the probabilities explains the instant probability drop in elemental filter 68, and the probability spikes in elemental filters 58 and 77.

Note that resetting the MMAE was done for programming simplicity, and is not characteristic of an operational algorithm. Completely reinitializing the MMAE removes any information or advantage already gained by the MMAE. The performance of the algorithm could be improved by using the information already available in the MMAE to reset the elemental filter and more efficiently handle changes in the satellite constellation.

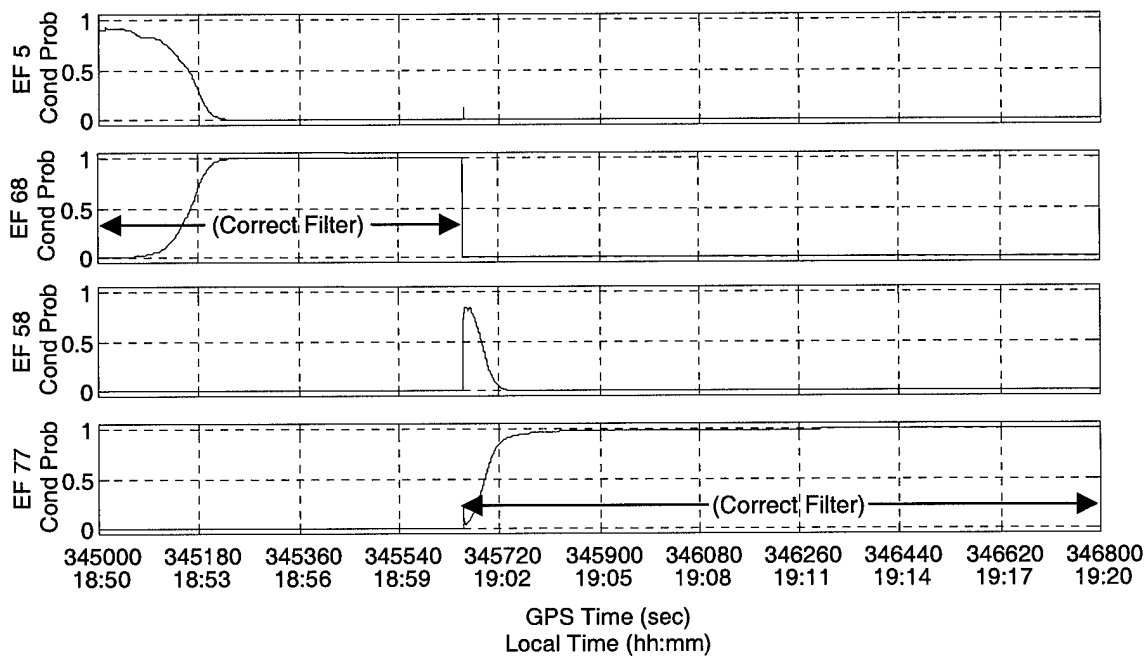


Figure 4-10. Case 3 - Sample Elemental Filter Conditional Probability Time Histories

The first six minutes of conditional probability time history, and four representative measurement residual time histories for elemental filters 5 and 68 are shown in Figure 4-11 and Figure 4-12, respectively. As shown in Figure 4-10 and Figure 4-11, the MMAE initially shifts the probability weight to elemental filter 5. Even though two of the four measurement residuals (residuals 2 and 3) are relatively large, the other two residuals are small enough to cause this initial probability shift toward elemental filter 5. However, the 2nd and 3rd residuals in elemental filter 5 are slowly increasing in

magnitude. This increase causes the conditional probability to shift away from elemental filter 5. Eventually, the elemental filter 5 residuals are consistently large, which reduces the probability to near zero and causes the pruning logic to remove the filter from the MMAE. Because the elemental filter 68 residuals are much closer to zero mean and white, the MMAE quickly starts to weight elemental filter 68 (which contains the correct ambiguity set). In approximately 3.5 minutes, the pruning logic deletes the incorrect elemental filters and the MMAE converges to the correct filter and the true fixed-integer solution.

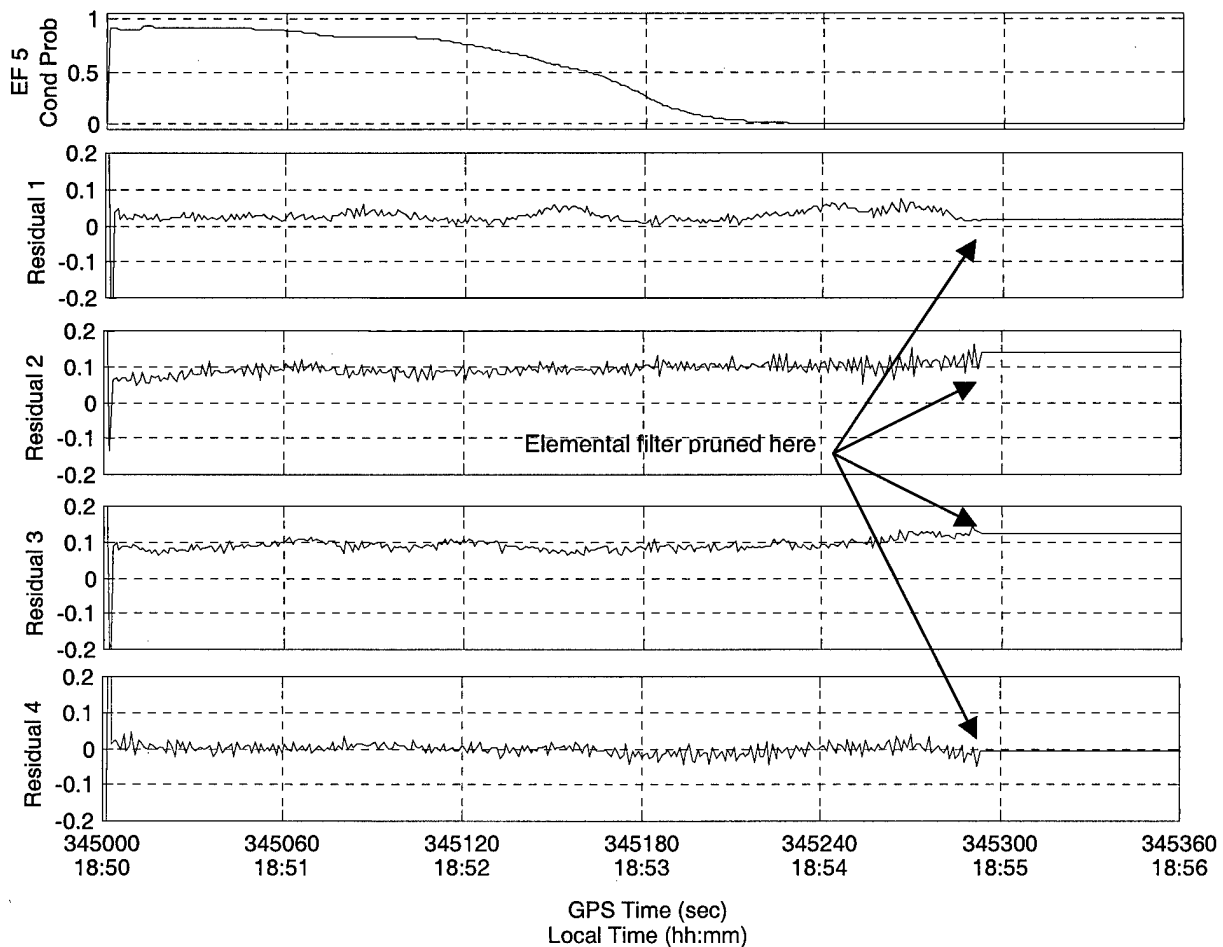


Figure 4-11. Case 3 - Elemental Filter 5 Probability and Residual Time History (Incorrect Ambiguities), First Six Minutes

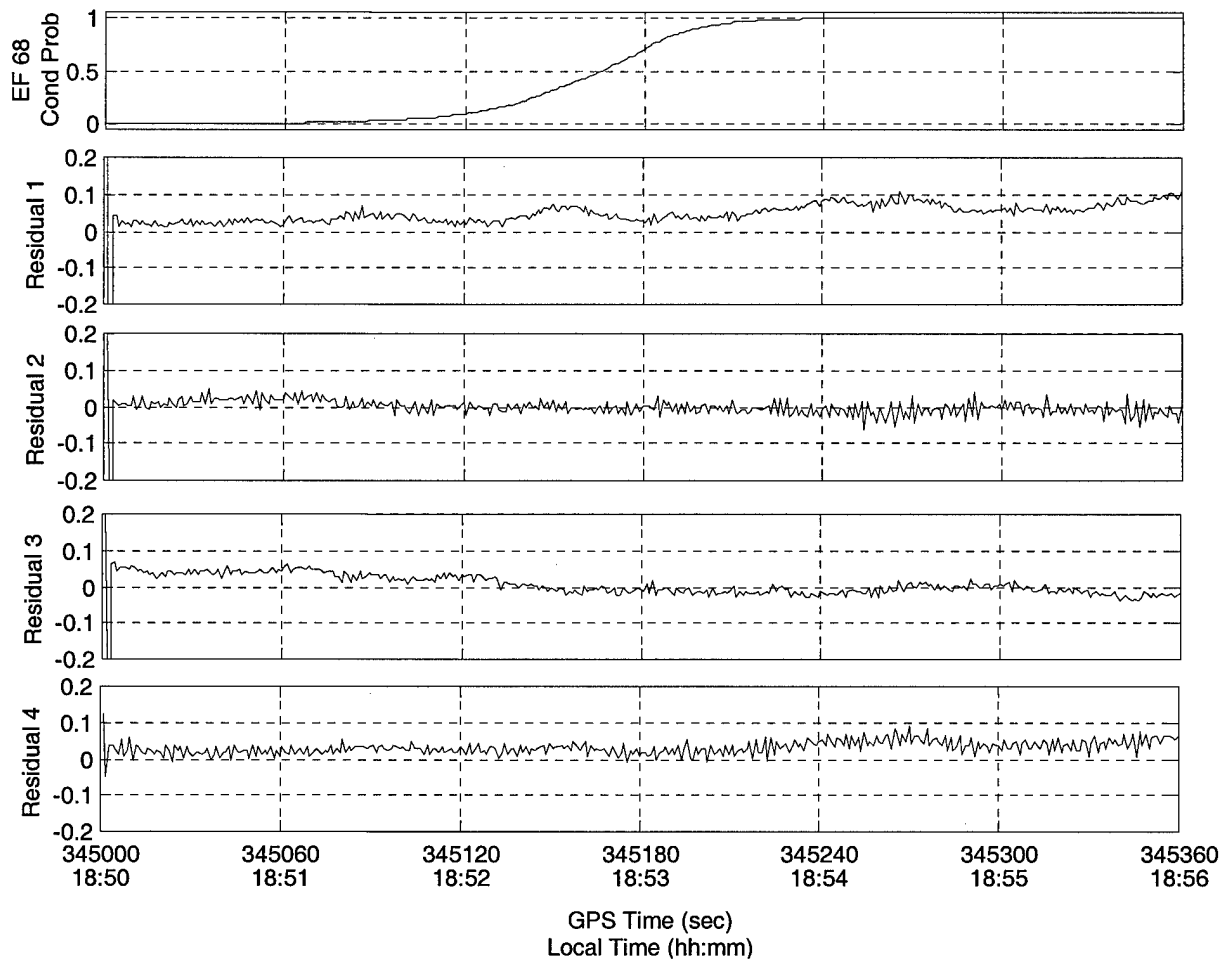


Figure 4-12. Case 3 - Elemental Filter 68 Probability and Residual Time History (Correct Ambiguities), First Six Minutes

4.2.5 Case 4: 100 km Baseline, Widelane Measurements

The purpose of Case 4 is to demonstrate the ability of the MMAE to determine the correct ambiguity set under the more difficult conditions associated with long a baseline distance. The baseline distance was increased to ~100 km to increase the affect of the residual differential errors in the ambiguity set generation routine and the conditional probability calculations.

The initialization errors from the floating-point filter for this case were large like Case 3, and had a major effect on the candidate ambiguity sets generated by the FASF subroutine. In fact, none of the 100 candidate ambiguity sets initially generated by the FASF routine were the correct ambiguity set. This meant the MMAE could not converge to the correct solution, as the correct solution was not in one of the elemental filters.

Similar to Case 3, the transients in the MMAE position solution in Figure 4-14 are due to the initial high weighting of an incorrect elemental filter (elemental filter 3 as shown in Figure 4-15). However, elemental filter 3 does not contain the correct ambiguity set, and the MMAE quickly shifts the probability weight to elemental filter 62. The MMAE converges to elemental filter 62 in approximately 6 minutes, even though *elemental filter 62 does not contain the correct ambiguity set*. Recall that none of the elemental filters contain the correct ambiguity set.

The MMAE is reset at approximately 22:06:30 local time when the remote receiver losses lock on a low elevation satellite. At this time, the correct ambiguity set is in one of the 100 elemental filters (filter 67) and the MMAE converges to this filter and the correct solution within 90 seconds of being reset.

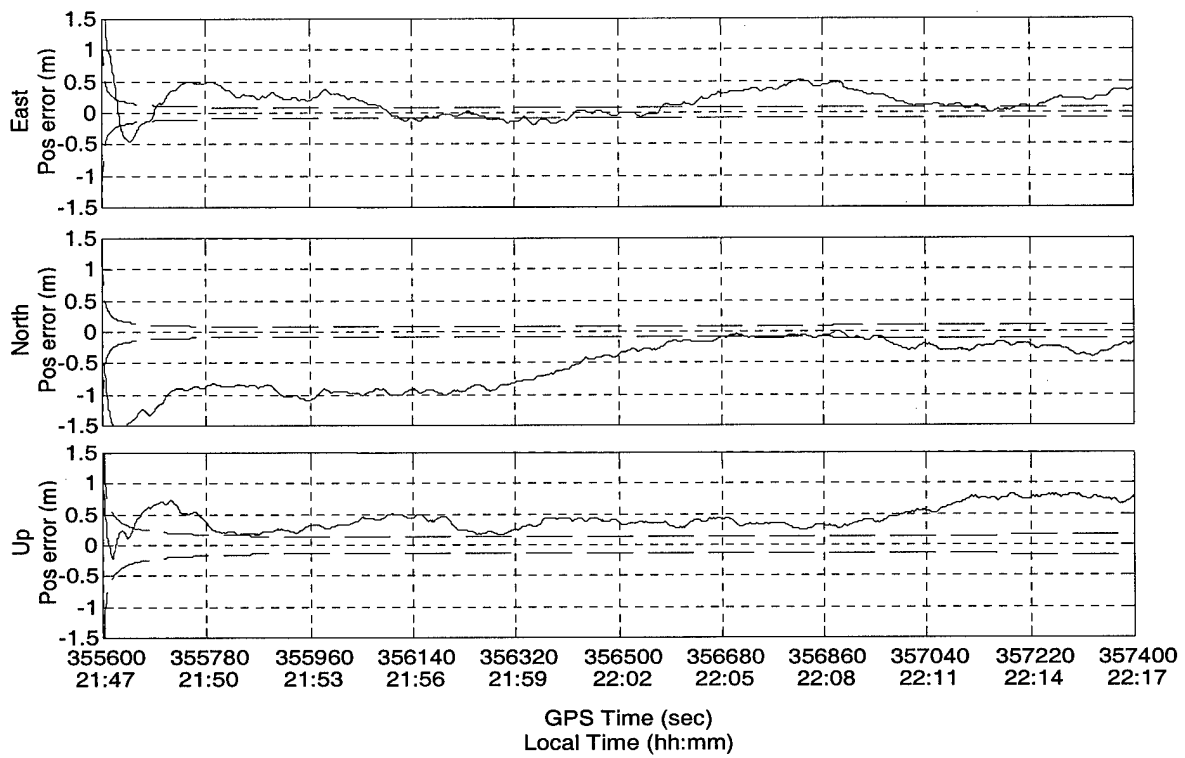


Figure 4-13. Case 4 - Floating-Point Filter Position Errors

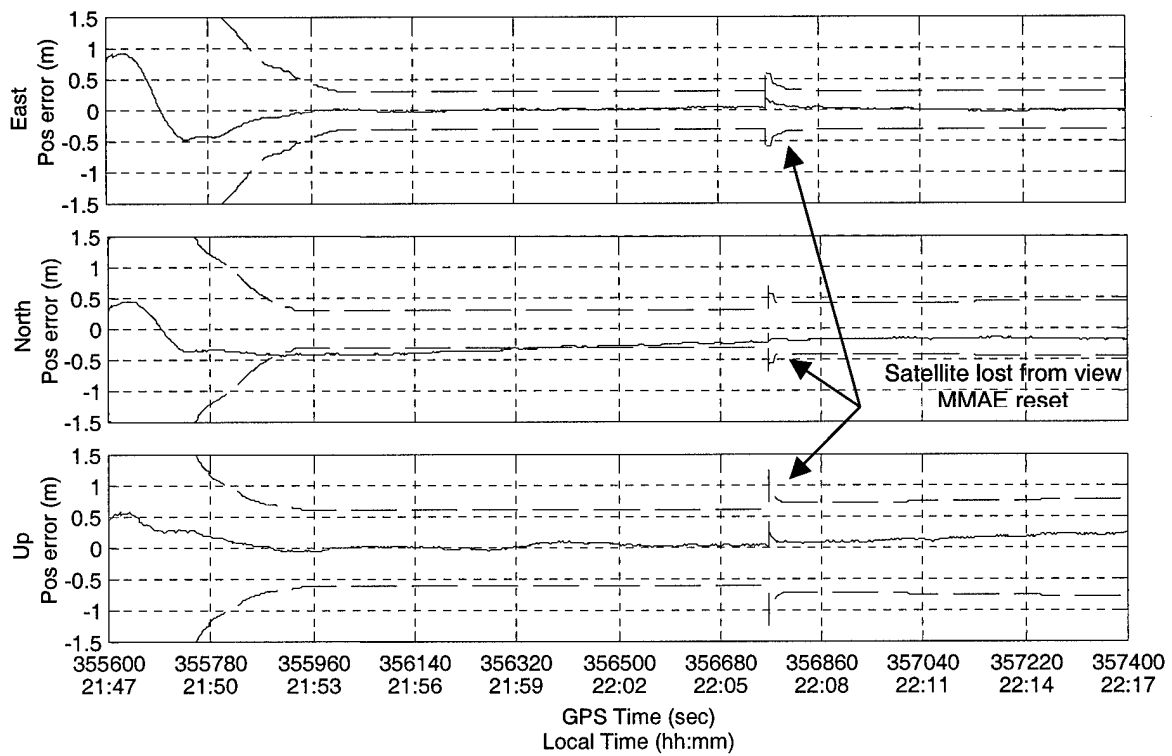


Figure 4-14. Case 4 - MMAE Position Errors

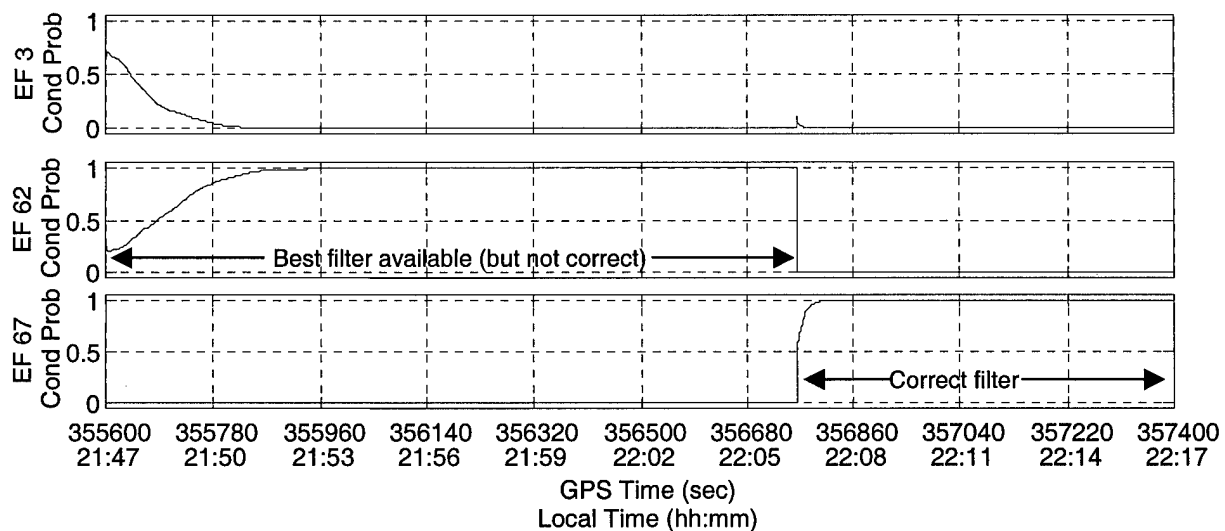


Figure 4-15. Case 4 - Sample Elemental Filter Conditional Probability Time Histories

The true ambiguities and the ambiguities used by the elemental filters are shown below in Table 4-5. Elemental filter 3 contains three incorrect ambiguities (each one cycle off the correct value), while elemental filter 62 only contains one incorrect ambiguity. Although it contains an incorrect ambiguity set, *elemental filter 62 was the best ambiguity set available*, among the 100 elemental filters (remember, the correct ambiguity set was not included in the 100 elemental filters). The ambiguity set in elemental filter 62 is considered the best set, as it is the ambiguity set closest to the true ambiguity set. The other elemental filters contain ambiguity sets with more than one incorrect ambiguity or an ambiguity set with one incorrect ambiguity more than one cycle off the correct value. The difference between the ambiguity set in an elemental filter and the true ambiguity set determines the size of the measurement bias in the ambiguity corrected double-differenced carrier-phase measurements described in Section 3.5.1.2. In general, the larger the difference between the two ambiguity sets, the larger the error in

the computed position solution. The underlined and italicized entries are the incorrect ambiguity values, and the N/A for elemental filter 67 is due to a satellite being lost from view, and therefore that measurement (and associated ambiguity term) being lost.

Table 4-5. Case 4 - True Ambiguities vs. Elemental Filter Ambiguities

True Ambiguity	1094483	2268285	3812363	4213446	4210673	3709768	7338024
EF #3	1094483	<u>2268286</u>	3812363	4213446	<u>4210672</u>	3709768	<u>7338023</u>
EF #62	1094483	2268285	3812363	4213446	4210673	3709768	<u>7338023</u>
EF #67	1094483	2268285	3812363	4213446	4210673	3709768	<u>N/A</u>

The time averaged mean error and standard deviations of the floating filter compared to those of the MMAE design are shown in Table 4-6. Again, the MMAE performance produced much better results than the floating-point filter, even though the MMAE could not initially converge to the true fixed-integer solution.

Table 4-6. Case 4 - Position Solution Error Comparison

	East		North		Up	
	Mean Error (m)	Std (m)	Mean Error (m)	Std (m)	Mean Error (m)	Std (m)
Floating-Point Filter	0.167	0.223	-0.545	0.400	0.437	0.192
MMAE	0.014	0.207	-0.055	0.167	0.253	0.121

This case clearly demonstrates some of the strengths of using an MMAE to resolve carrier-phase ambiguities and in the process generate a navigation position solution. Figure 4-14 clearly shows the MMAE solution transitioning very smoothly from a floating-point filter like solution to a fixed-integer solution. Even though the true fixed-integer solution is not reached (it is not initially available) the MMAE transitions to the

best solution available. Also notice, that the MMAE fixed-integer solution is more accurate and more stable than the floating-point solution even though it is using and incorrect ambiguity set. After the MMAE is reset, due to the loss of a satellite from view, the correct ambiguity set is available and the MMAE again transitions very quickly and smoothly to the true fixed-integer solution.

None of the initial candidate ambiguity sets generated by the algorithm contain the correct ambiguity set. As described in Section 3.4 the initial candidate ambiguity sets are generated after only one cycle of the floating-point filter. After one cycle the floating-point filter may not have an accurate estimate of the carrier-phase ambiguities. However, after the MMAE is reset the correct ambiguity set was generated by the Z-transform and FASF subroutines. By this time the floating-point filter has a more accurate estimate of the carrier-phase ambiguities, which increases the probability of the correct ambiguity set being included in one of the elemental filters. Allowing the floating-point filter a few propagate and update cycles before using its ambiguity estimates to generate the candidate ambiguity sets may improve the performance of the carrier-phase ambiguity set generation routine and the overall algorithm.

4.3 *Flight Tests*

Flight tests were conducted at Edwards AFB CA, from 5 October 2000 to 17 October 2000. Appendix A describes the complete series of flight tests. Out of the twelve flight conditions outlined in Appendix A, results are presented for three different cases. Due to flight limitations, data was only collected for the primary data points described in Appendix A.

The reference receiver station was a dual frequency Ashtech Z-Surveyor receiver located at a surveyed site at the Air Force Flight Test Center (AFFTC) Range Division, Edwards AFB, CA. Data presented in this section is represented in a geodetic (East, North, Up (ENU)) reference frame with the origin located at the reference receiver location. The coordinates of the reference receiver station are listed in Appendix A. The test aircraft was a T-38A aircraft, modified to carrier an Ashtech Z-surveyor receiver in the rear cockpit.

4.3.1 *Case Definitions*

Each flight test case consisted of 4 to 20 minutes of data collected at a 2 Hz rate as outlined in Appendix A. For each case, the test aircraft was flown in an arc at a constant speed, distance and altitude from the reference receiver. L1 C/A - code pseudorange and carrier-phase measurements and L2 pseudorange (semi-codeless) and carrier-phase measurements were collected by both the reference receiver and the receiver onboard the test aircraft. The reference receiver was at an altitude of ~690 m while the aircraft was flown at an altitude of at least 3,400 m. In all cases, the lower probability bound for each elemental filter was set at 0.001 and each had an equal initial probability weighting. The

pruning logic in the algorithm was set to delete elemental filters if their conditional probability remained below the lower limit for more than 40 consecutive sample periods (20 seconds). The pruning time was increased to allow the MMAE more time to determine which elemental filter contained the correct ambiguity set, and was necessary due to the additional errors added by the aircraft dynamics, not present during the ground tests. The floating-point filter and the elemental filters were tuned in accordance with the values specified in Chapter 3. For all flight test cases, the MMAE within the algorithm used 50 elemental filters. The number of elemental filters was chosen based on the expected difficulty of resolving the carrier-phase ambiguities. However, as discussed in the next section, the carrier-phase ambiguity set generation subroutine did not perform well under flight test conditions.

The first flight test case was chosen to demonstrate the performance of the MMAE using a nominal flight test profile. The second case uses the same flight profile but demonstrates the problems associated with removing elemental filters from an MMAE. The last case was chosen to demonstrate the ability of the MMAE to correctly resolve the carrier-phase ambiguities at an increased baseline distance. The flight test case specifics are shown below in Table 4-7.

Table 4-7. Flight Test Case Parameter Description

Case	Baseline Distance	Pressure Altitude	Carrier-Phase Measurement Type	Elemental Filters	Data Rate	Length of Data Set
1	16.1 km (10 naut. mi)	3,400 m (10,000 ft)	Widelane	50	2 Hz	~ 4 minutes
2	16.1 km (10 naut. mi)	3,400 m (10,000 ft)	Widelane	50	2 Hz	~ 4 minutes
3	32.2 km (20 naut. mi)	3,400 m (10,000 ft)	Widelane	50	2 Hz	~ 6 minutes

For the flight tests, the true carrier-phase ambiguities were determined by the Ashtech Office Suite software [1]. The truth position was then calculated using a fixed-integer carrier-phase DGPS routine, using the true ambiguities determined by Ashtech Office Suite software. For all flight test cases, the position errors are defined as:

$$\hat{x}_{error} = \hat{x}_{filter} - \hat{x}_{true} \quad (4-2)$$

where the subscript “*filter*” refers to either the floating-point filter or the MMAE solution, and the subscript “*true*” refers to the fixed-integer calculated truth position. The “truth” position generated by using the correct carrier-phase ambiguities and a fixed-integer carrier-phase DGPS routine is not an absolute truth position solution, but it is the solution the MMAE is striving to achieve.

The position errors described above are only used to generate the position error plots in the following sections. They are not used to calculate time averaged mean errors and standard deviations. Because of the way the “truth” is generated for the flight tests, once the MMAE converges to the fixed-integer solution the two solutions (“truth” and MMAE), are virtually identical, and it is impossible to determine if the errors are due to the MMAE solution or the truth solution. In addition, the small amount of data used in each flight test case, along with the initial transients of the MMAE solution, limits the usefulness of a time averaged mean error. Therefore, no time averaged mean error or standard deviations are presented for the flight test cases.

4.3.1.1 Ambiguity Set Generation

For the flight test cases analyzed, none of the 50 candidate ambiguity sets initially generated by the carrier-phase ambiguity set generation routine (Z-transform, FASF and inverse Z-transforms sub-routines) were the correct ambiguity set. This meant the MMAE could not converge to the correct solution, as the correct solution was not in one of the elemental filters. Although not changed for this research, allowing the floating-point filter a few propagate and update cycles before using its ambiguity estimates to generate the candidate ambiguity sets may improve the performance of the carrier-phase ambiguity set generation routine.

The main emphasis of this research is to investigate the ability of an MMAE to distinguish the correct ambiguity set; therefore, the correct ambiguity set was *artificially* placed in the first elemental filter. In addition, an ambiguity set with one incorrect ambiguity (one cycle off the correct ambiguity) was *artificially* placed in the second elemental filter.

Placing these ambiguity sets in the elemental filters allowed the performance of the MMAE to be analyzed in two ways. First, the ability of the MMAE to determine which ambiguity set is correct could be analyzed. Second, the ability of the MMAE to distinguish between closely related solutions could also be determined.

The above modification was implemented to validate the “proof of concept” algorithm developed in this thesis. An operational system would require advanced routines to increase the probability that the correct ambiguity set is in one of the elemental filters.

4.3.2 Case 5: 16.1 km Baseline, 10,000 ft Altitude, Widelane Measurements

The purpose of this flight test case is to demonstrate the performance of the MMAE using a nominal flight test profile. The time history position performance of the floating-point filter and the MMAE, for the entire data run, are shown in Figure 4-16 and Figure 4-17 respectively. The errors are represented in a geodetic ENU reference frame with the origin at the reference receiver location. In both figures, the solid line represents the computed position error as described in Equation (4-2). The dashed line represents the filter-predicted standard deviation, and not the actual standard deviation of the errors.

As discussed in Section 4.3.1.1, the correct ambiguity set was not generated by the FASF subroutine, so the correct ambiguity set was artificially placed in elemental filter 1. The conditional probability time histories for elemental filters 1, 2, 14, and 41 are shown in Figure 4-18. The conditional probability shifts back and forth between elemental filters 14 and 41 for the first 45 seconds of the data run. At approximately 45 seconds, elemental filter 1 rapidly absorbs the conditional probability and within 75 seconds, the pruning logic deleted all of the other elemental filters. The probability shifts between elemental filters is the reason for the large errors initially present in the MMAE position solution. However, once the MMAE converges to the correct elemental filter, the position solution is very stable and within a few centimeters of the true position solution.

The large “spike” in the floating-point filter solution at 8:07:00 is due to a bad pseudorange measurement. Because the MMAE only uses carrier phase measurements, the bad pseudorange measurement only affected the floating-point filter solution.

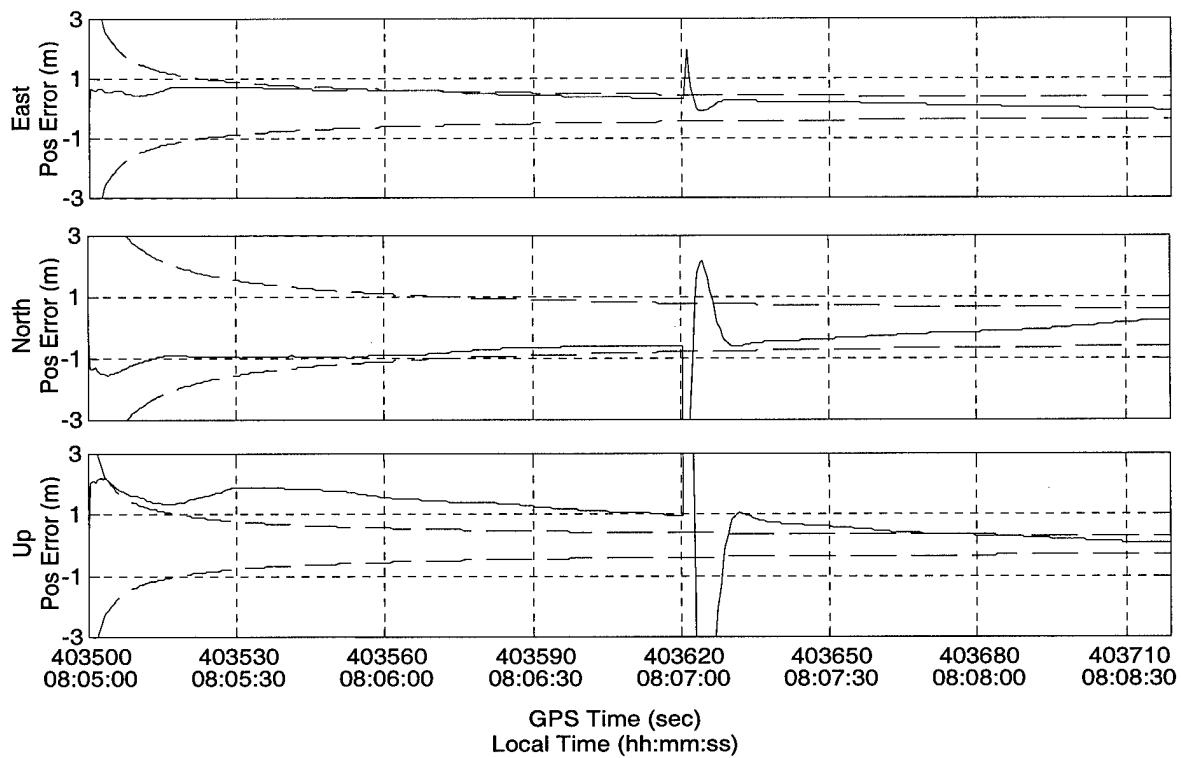


Figure 4-16. Case 5 – Floating-Point Filter Position Errors

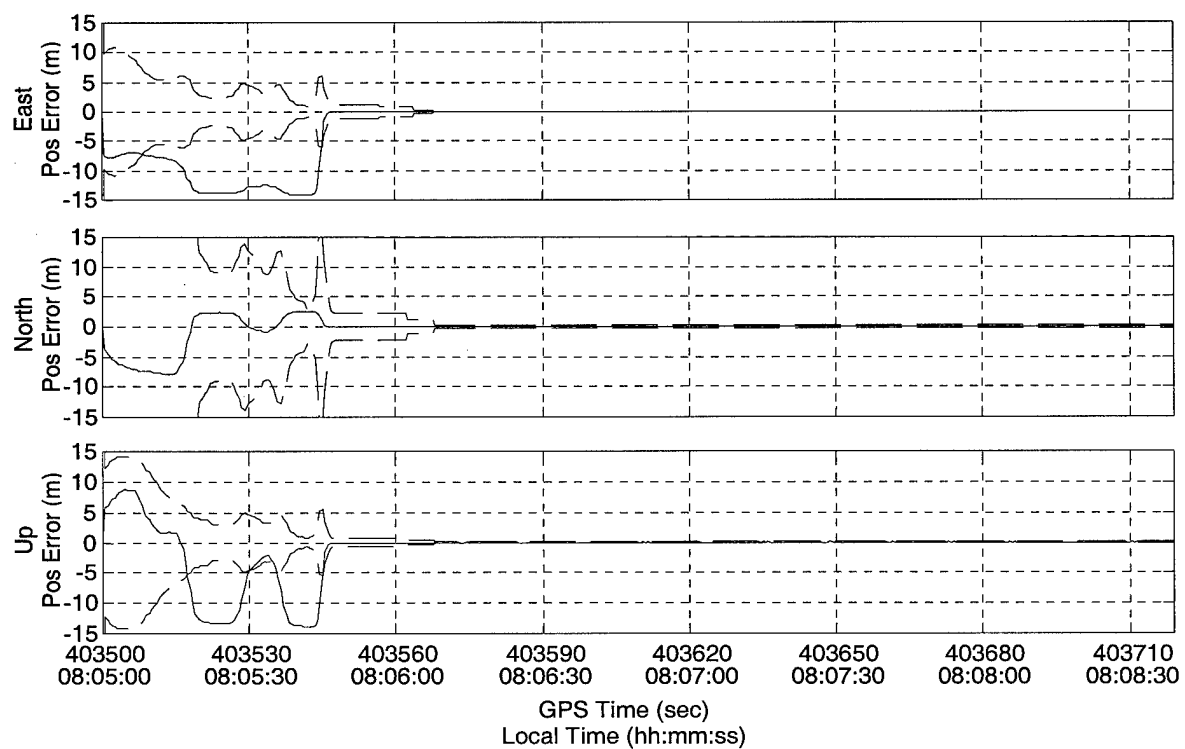


Figure 4-17. Case 5 - MMAE Position Errors

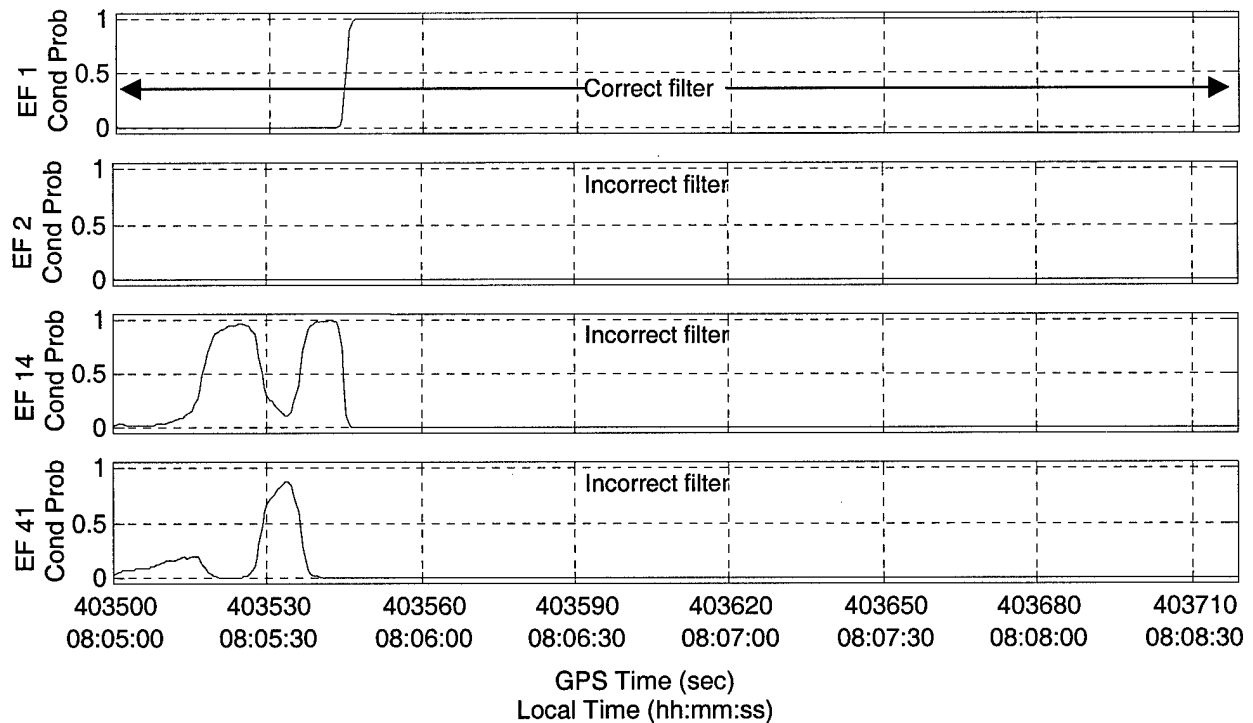


Figure 4-18. Case 5 - Sample Elemental Filter Conditional Probability Time Histories

The true ambiguities and the ambiguities used by the elemental filters are shown in Table 4-8. The underlined and italicized values represent incorrect ambiguity values. Elemental filter 1 contains the correct ambiguity set, while elemental filter 2 contains only one incorrect ambiguity. Elemental filter 14, which twice manages to absorb over 95% of the conditional probability, contains only one correct ambiguity. Elemental filter 14 even contains one ambiguity 17 cycles off the correct value. Finally, elemental filter 41 does not contain any correct ambiguities. The ambiguity sets contained in the elemental filter are much further off of the true ambiguity set than expected. This causes the initial transients to have much larger errors than in the ground test cases. The ambiguity sets are a direct result of allowing the floating-point filter only one propagate and update cycle before its estimates are used to generate candidate ambiguity sets.

Table 4-8. Case 5 - True Ambiguities vs. Elemental Filter Ambiguities

True Ambiguity	-2320781	-1205221	210188	1885413	12121638	5587938
EF #1	-2320781	-1205221	210188	1885413	12121638	5587938
EF #2	-2320781	-1205221	210188	1885413	<u>12121639</u>	5587938
EF #14	<u>-2320798</u>	<u>-1205218</u>	210188	<u>1885417</u>	<u>12121629</u>	<u>5587916</u>
EF #41	<u>-2320792</u>	<u>-1205219</u>	<u>210191</u>	<u>1885425</u>	<u>12121636</u>	<u>5587925</u>

The conditional probability time histories and three of the measurement residual time histories for elemental filters 1 and 14 are shown in Figure 4-19 and Figure 4-20, respectively.

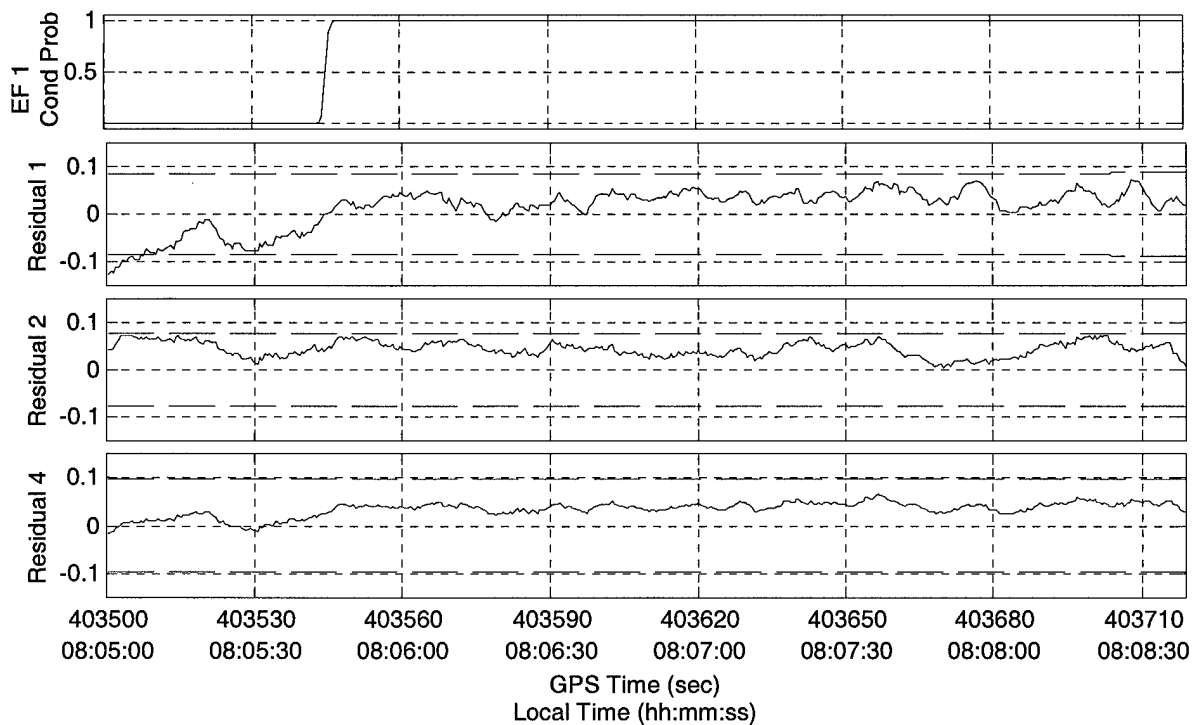


Figure 4-19. Case 5 - Elemental Filter 1 Probability and Residual Time History (Correct Ambiguities)

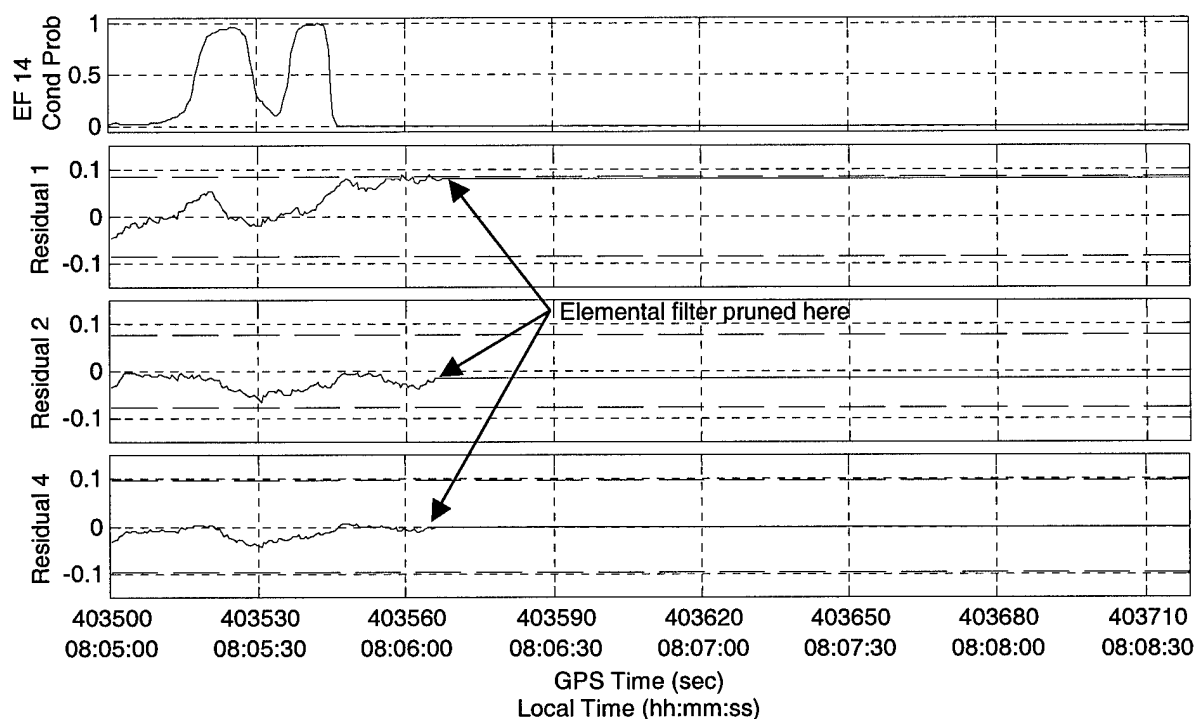


Figure 4-20. Case 5 - Elemental Filter 14 Probability and Residual Time History (Incorrect Ambiguities)

For the first 10 to 15 seconds of the data run, none of the elemental filter residuals are small enough for the conditional probability calculations to determine which elemental filter contains the correct ambiguity set. Then the value of the 2nd and 4th residuals in elemental filter 14 become very small, even though it contains an ambiguity set with ambiguities far from the correct values. In fact, the elemental filter 14 residuals are smaller than the same residuals in elemental filter 1, demonstrating how residual DGPS errors can make it difficult to distinguish the true ambiguity set. After approximately 45 seconds, the first residual in elemental filter 14 starts to increase in value. It is this increase (along with an increase in the residuals not shown) that causes the conditional probability weight to shift away from elemental filter 14 and toward elemental filter 1.

Although elemental filter 2 contained only one incorrect ambiguity, its residuals (not shown) were initially larger than the residuals of elemental filter 1, 14 or 41. The pruning logic quickly deleted elemental filter 2 from the MMAE, because its probability was below the lower bound for the first 20 seconds.

Although the MMAE transitions smoothly to the true fixed-integer solution it emphasizes the affect of a poorly performing candidate ambiguity set generation routine on the overall performance of the algorithm. The candidate ambiguity generation routine did not generate ambiguity sets close to the true ambiguity set, and for demonstration purposes the correct set was artificially placed in the MMAE. Because the incorrect candidate ambiguity sets are so far from the correct values, they cause much larger errors and more rapid position shifts in the overall solution than would incorrect ambiguity sets closer to the true ambiguity set. This case also emphasizes the problem of rapidly shifting the probability to an elemental filter whose probabilities look “good” for a short period of time. Tuning the MMAE to slow down the conditional probability shifts, or adding additional tests on the elemental filter residuals, such as a whiteness test [15, 25], may also improve the overall performance of the algorithm.

4.3.3 Case 6: 16.1 km Baseline, 10,000 ft Altitude, Widelane Measurements

Case 6 is a separate data run, but it is the same flight profile as Case 5. This case, although not specifically designed too, demonstrates the problems associated with removing elemental filters from and MMAE. The time history position performance of the floating-point filter and the MMAE, for the entire data run, are shown in Figure 4-21 and Figure 4-22, respectively. In both figures, the solid line represents the computed position error and the dashed line represents the filter predicted standard deviation.

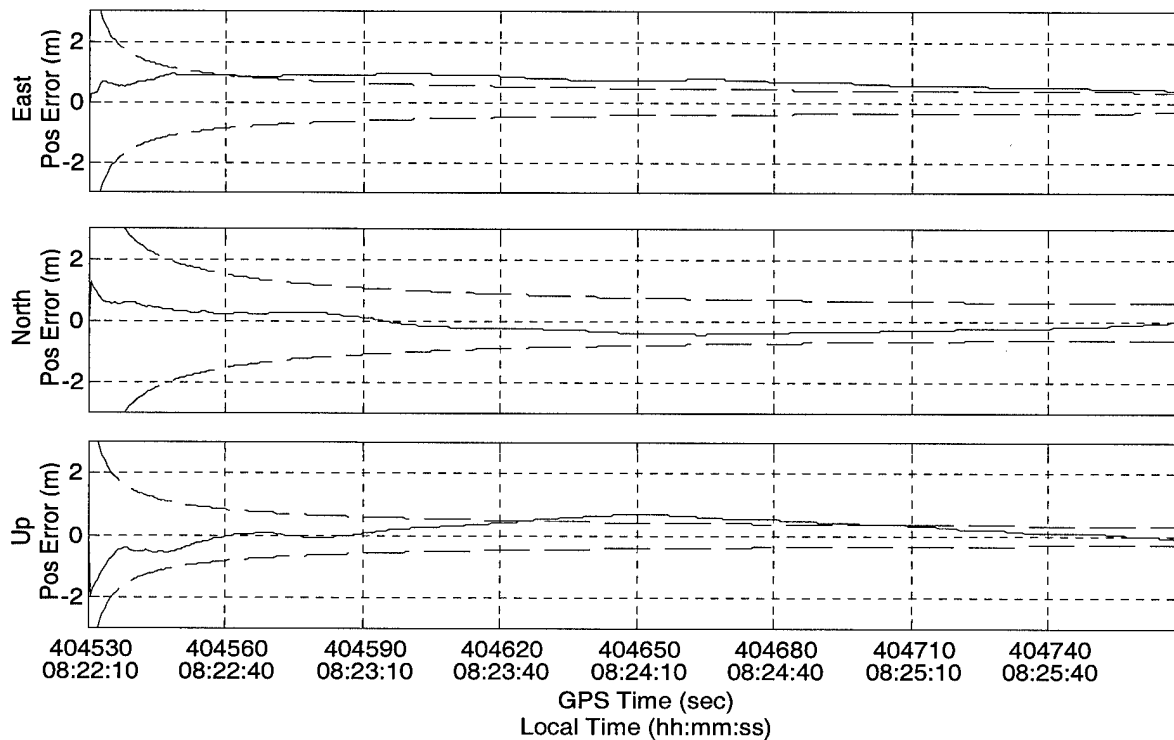


Figure 4-21. Case 6 – Floating-Point Filter Position Errors

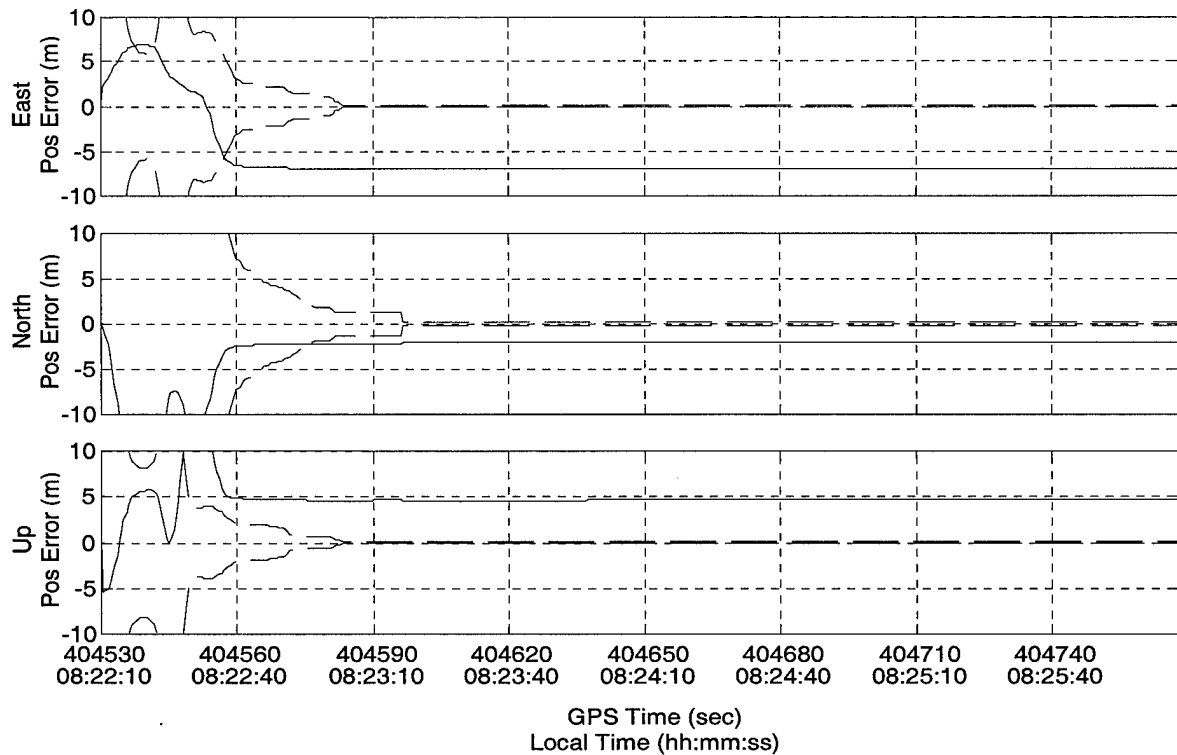


Figure 4-22. Case 6 - MMAE Position Errors

As seen in the previous cases, the initial transients in the solution are due to the MMAE shifting the probability weight to an incorrect elemental filter. However, unlike previous cases, the MMAE converges to a solution with a significant bias from the true solution. This large bias in the position solution of the MMAE is because *the MMAE converged to the wrong elemental filter*, even though the correct ambiguity set is available in elemental filter 1.

The conditional probability time histories for elemental filters 1, 2, 34, 38 and 45 are shown in Figure 4-23. The conditional probability calculations never shift the probability weight toward elemental filter 1. Elemental filter 1 is deleted from the MMAE 23 seconds from the start of the data run. Because the correct ambiguity set is no longer available, the MMAE can never converge to the correct fixed-integer solution. The

conditional probability shifts between elemental filters 45 and 34 before being completely shifted to elemental filter 38. The MMAE converges to elemental filter 38, and the wrong solution, 53 seconds after the start of the data run.

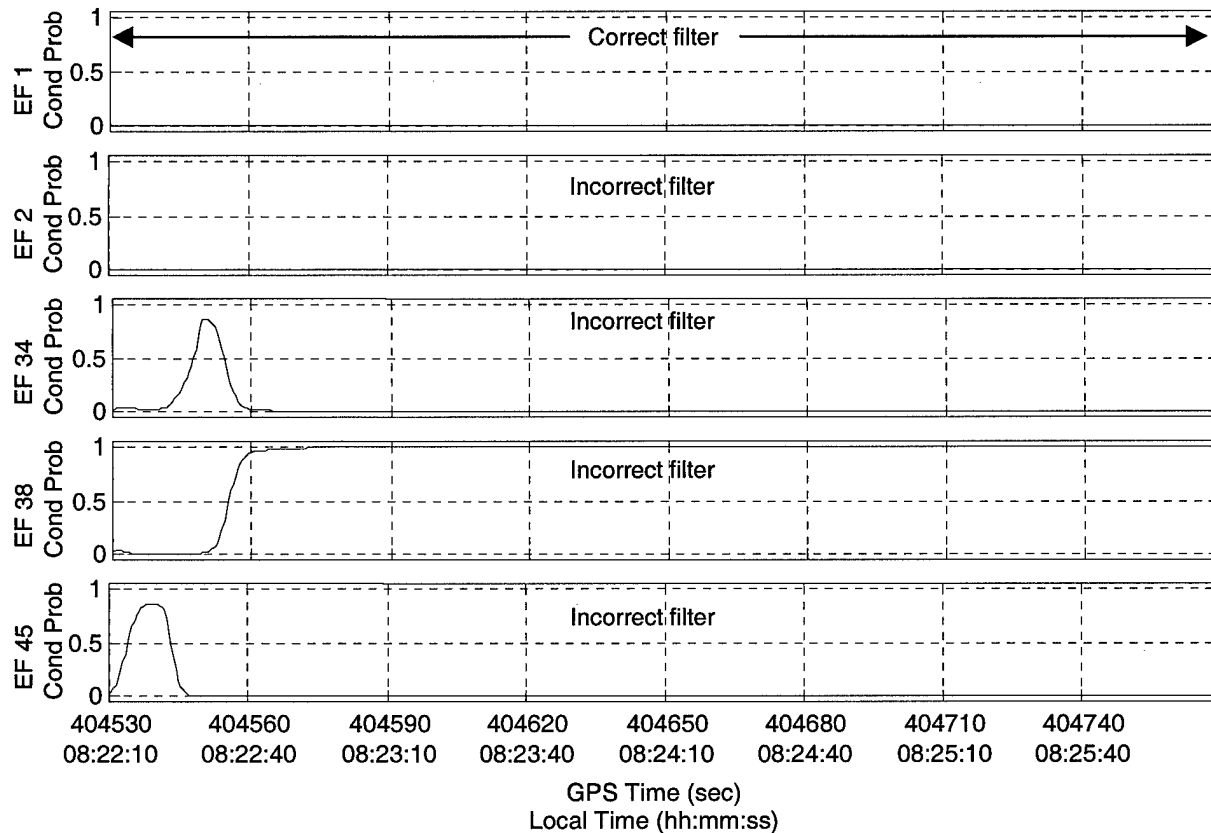


Figure 4-23. Case 6 - Conditional Probability Time Histories

The true ambiguities and the ambiguities used by the elemental filters are shown in Table 4-9. Elemental filter 1 contains the correct ambiguity set, while elemental filter 38, the filter the MMAE converges to, has four incorrect ambiguities, one ten cycles off the correct value.

Table 4-9. Case 6 - True Ambiguities vs. Elemental Filter Ambiguities

True Ambiguity	-2320781	-1205221	210188	-3181105	12121638	5587938
EF #1	-2320781	-1205221	210188	-3181105	12121638	5587938
EF #2	-2320781	-1205221	210188	-3181105	<u>12121639</u>	5587938
EF #34	<u>-2320780</u>	<u>-1205228</u>	<u>210193</u>	<u>-3181092</u>	<u>12121635</u>	<u>5587947</u>
EF #38	<u>-2320786</u>	-1205221	<u>210191</u>	<u>-3181095</u>	12121638	<u>5587932</u>
EF #45	<u>-2320793</u>	<u>-1205234</u>	<u>210191</u>	<u>-3181109</u>	<u>12121614</u>	<u>5587943</u>

The probability time history and three of the measurement residual time histories for elemental filters 1, 38 and 45 are shown below in Figure 4-24, Figure 4-25, and Figure 4-26 respectively. As shown in Figure 4-26, the elemental filter 45 measurement residuals at the start of the data run, are small enough that the MMAE shifts the conditional probability to elemental filter 45. However, this shift is only for a few seconds, because the residuals rapidly increase in value, causing the MMAE to shift the probability to elemental filter 34.

The elemental filter 1 measurement residuals are large enough at the beginning of the data run to shift the conditional probability away from the filter. Measurement residual 3 in Figure 4-24 is actually getting larger at the start of the data run. In contrast, two of the elemental filter 38 residuals (residuals 2 and 4) are very close to zero. Approximately 20 seconds after the start of the data run all six (even the three not shown) of the elemental filter 38 residuals are very close to zero. This causes the rapid shift in probability toward the filter. None of the other elemental filter's residuals are small enough to cause the MMAE to shift the probability away from elemental filter 38. The pruning logic eventually deletes the other elemental filters and the MMAE is forced to converge to elemental filter 38.

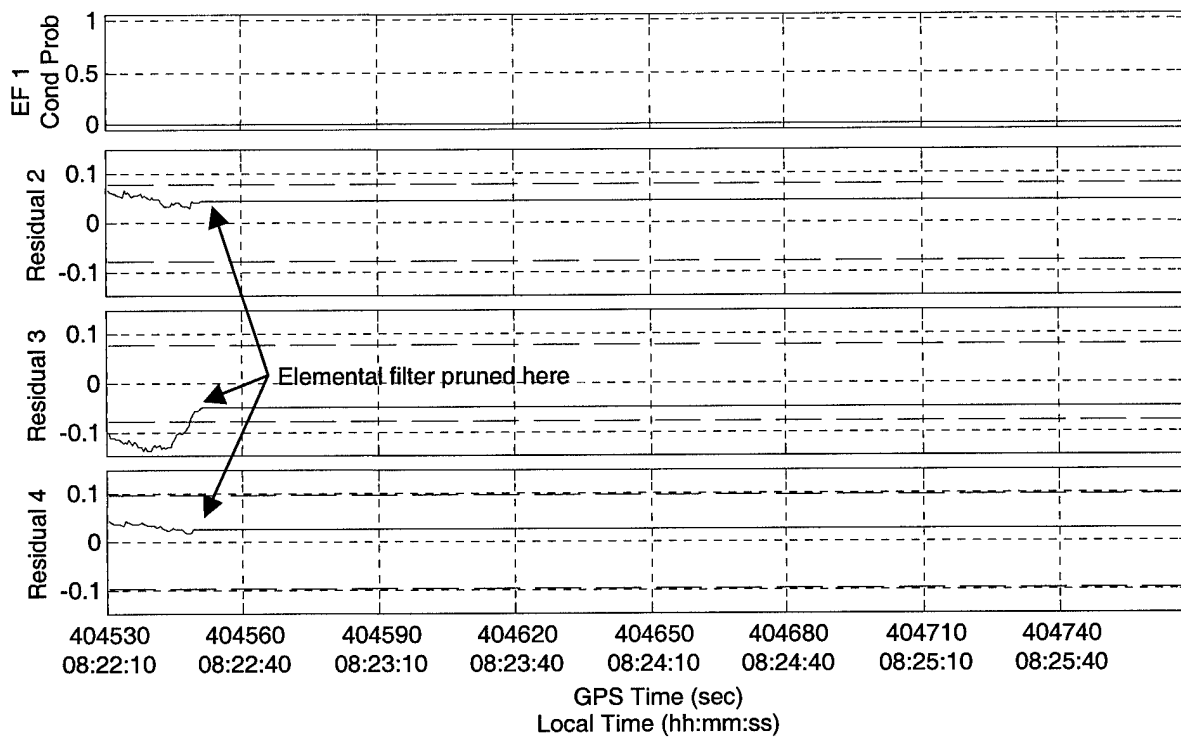


Figure 4-24. Case 6 - Elemental Filter 1 Probability and Residual Time Histories (Correct Ambiguities)

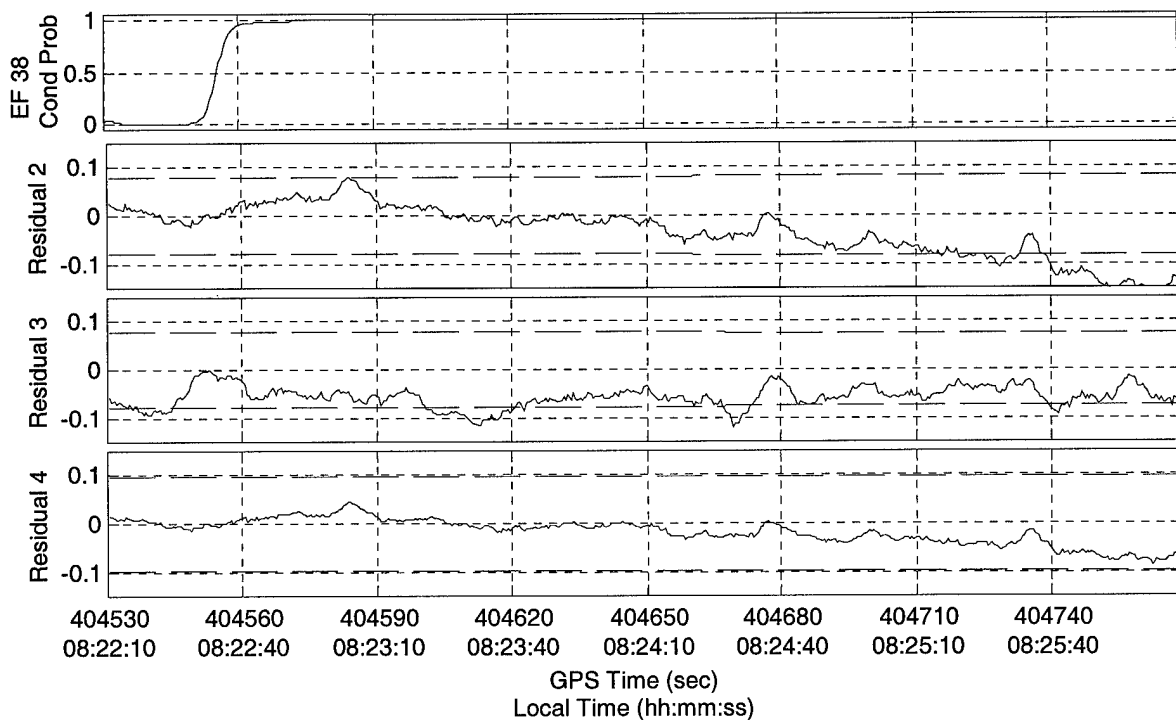


Figure 4-25. Case 6 - Elemental Filter 38 Probability and Residual Time Histories (Incorrect Ambiguities)

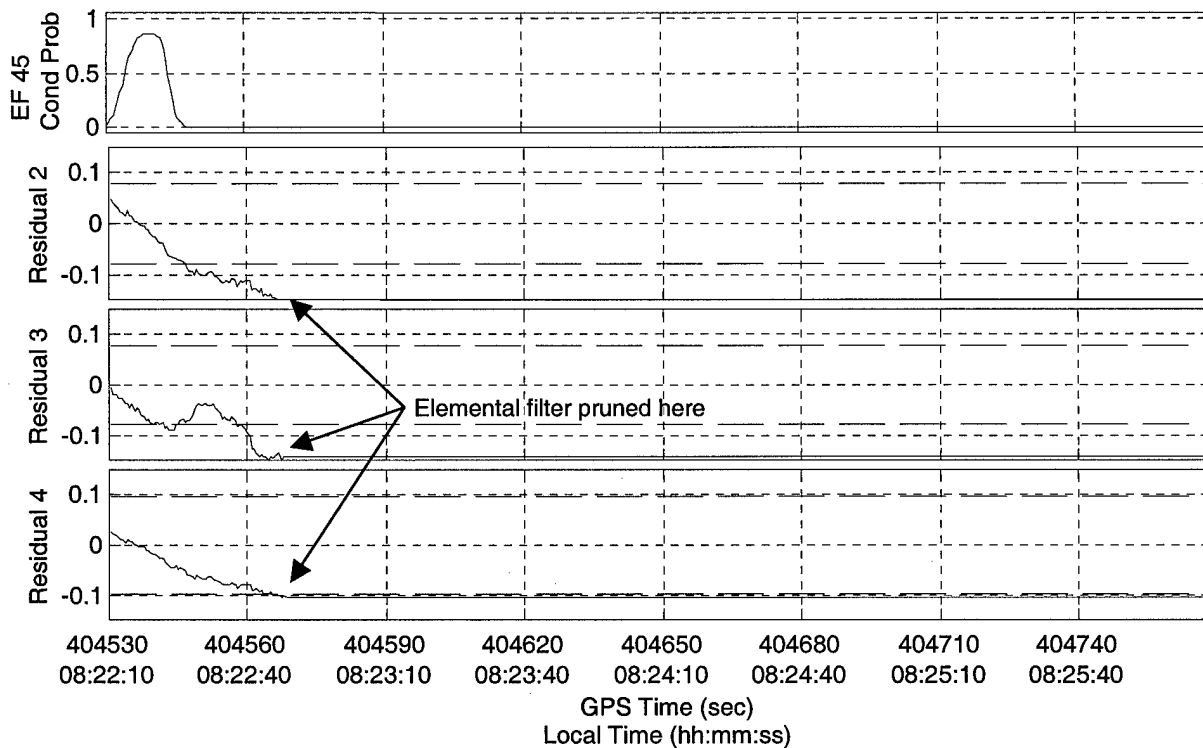


Figure 4-26. Case 6 - Elemental Filter 45 Probability and Residual Time Histories (Incorrect Ambiguities)

This is the first case where the MMAE converges to the wrong elemental filter (and ambiguity set), even though the correct ambiguity set is in one of the elemental filters. Because an incorrect filter's residuals are smaller than the correct filter's residuals for a period of time, the MMAE shifts the probability toward the wrong filter. The pruning logic then deletes the correct filter from the solution before the MMAE has a chance to shift the probability back to the correct elemental filter. Close to the end of the data run all of the elemental filter 38 measurement residuals are increasing. This would normally cause the MMAE to shift the probability toward another elemental filter, possibly the correct elemental filter. However, because the pruning logic removed all of the other

elemental filters, the MMAE must continue to use elemental filter 38 as the correct solution.

This case clearly shows the weakness in the current algorithm's pruning logic design. Once the pruning logic deletes the elemental filters from the MMAE there is no way to add additional elemental filters to check or recheck different ambiguity sets. An MMAE is a Multiple Model *Adaptive* Estimator. Removing elemental filters, in a desire to achieve the true fixed-integer solution, limits the ability of the MMAE to adapt or change its solution. When the MMAE is reduced to one elemental filter it can no longer adapt to any changes, as it is forced to use the one remaining hypothesis, even if it is the incorrect hypothesis. These problems point to many possible improvements in the current algorithm. A simple modification of not deleting the elemental filters from the MMAE would allow the MMAE to continually adapt to changes. The overall MMAE estimate can then be a blending of only those elemental filters with a high conditional probability of being the correct solution. Additional modifications might include deleting "bad" elemental filters, but then adding elemental filters to recheck ambiguity sets, or ambiguity sets close to the elemental filter that has the highest probability. Additional improvements to limit the chances of the MMAE converging the wrong solution might be to continuously cross check the MMAE solution with the floating-point solution. The two solutions should be closely related (within a few meters), and if they are not the MMAE could be reinitialized, or different ambiguity sets could be used.

4.3.4 Case 7: 32.2 km Baseline, 10,000 ft Altitude, Widelane Measurements

Case 7 is similar to Cases 5 and 6, except the baseline distance to the test aircraft was increased to 32.2 km. The time history position performance of the floating-point filter and the MMAE for the entire data run are shown in Figure 4-27 and Figure 4-28, respectively. As shown in Figure 4-28, the MMAE very quickly and smoothly converges to the correct elemental filter and the true fixed-integer solution.

The large “spike” in the floating-point filter solution at 7:47:30 is due to a bad pseudorange measurement. Again, because the MMAE only uses carrier phase measurements, the bad pseudorange measurement only affected the floating-point filter solution.

Once again the correct ambiguity set was placed in elemental filter 1, and an incorrect ambiguity set (one incorrect ambiguity) was placed in elemental filter 2. The true ambiguities and the ambiguities in the elemental filters are shown below in Table 4-10.

Table 4-10. Case 7 - True Ambiguities vs. Elemental Filter Ambiguities

True Ambiguity	1081928	-1205221	210188	-1885413	5587938
EF #1	1081928	-1205221	210188	-3181105	5587938
EF #2	1081928	-1205221	210188	-3181105	<u>5587939</u>

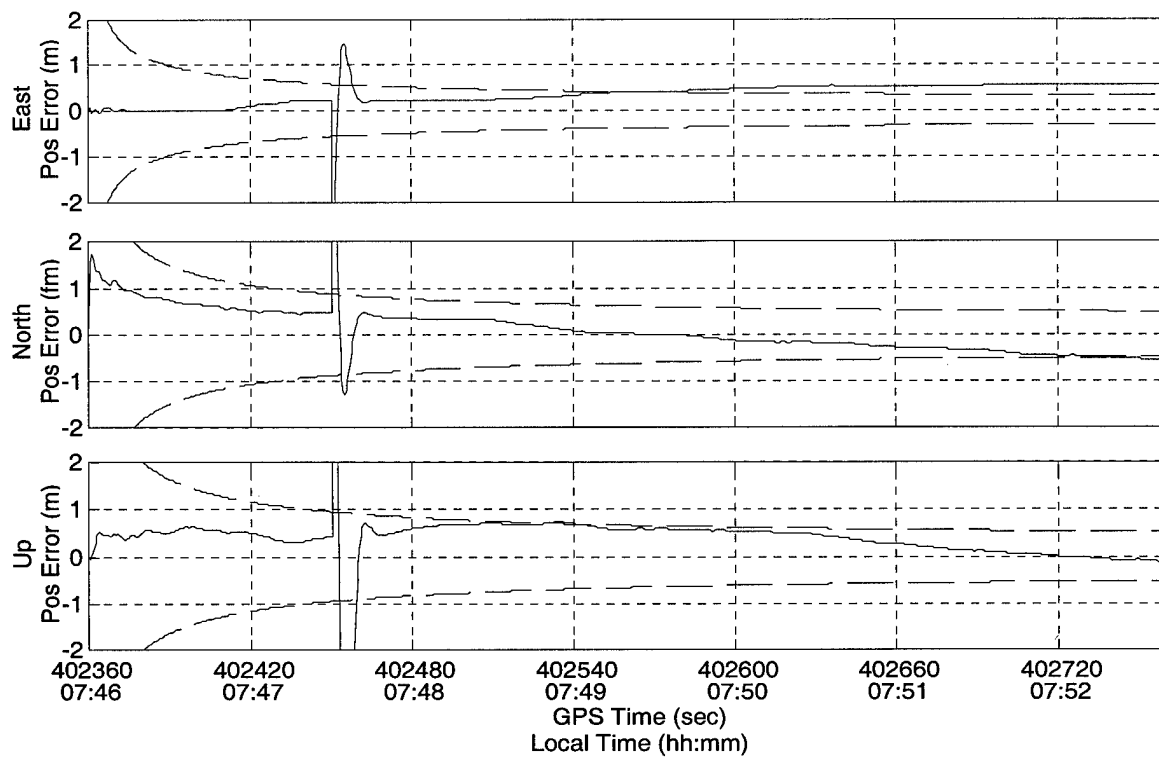


Figure 4-27. Case 7 – Floating-Point Filter Position Errors

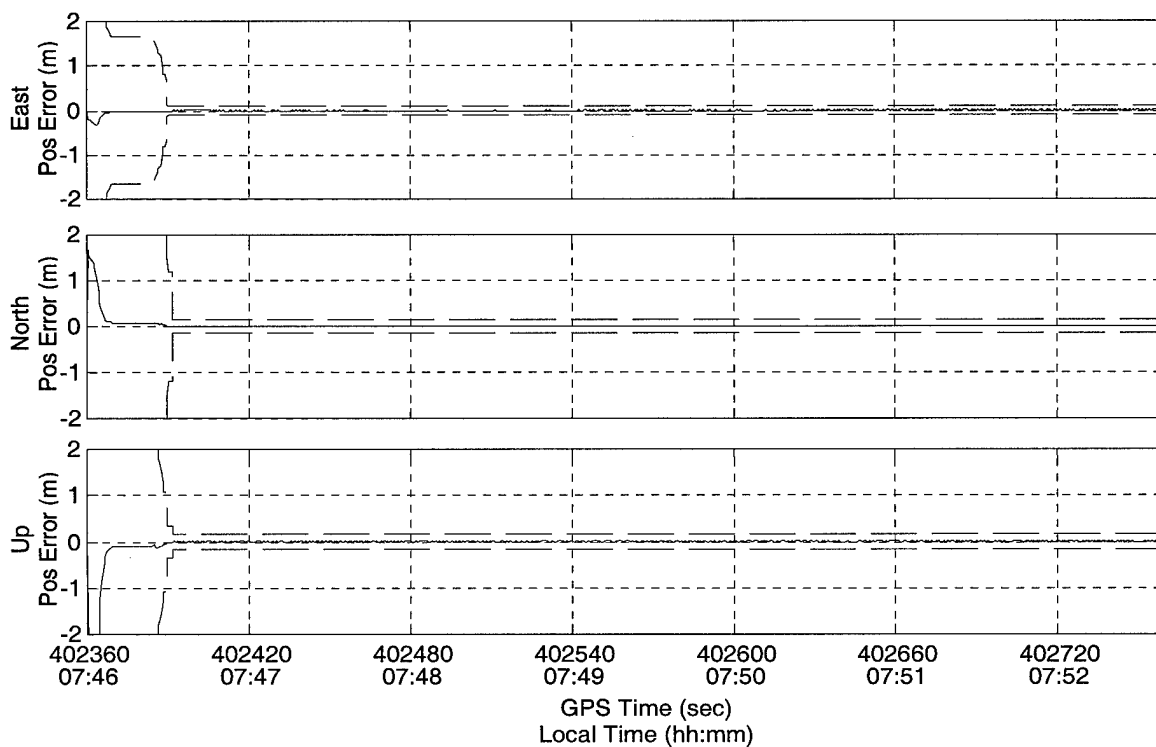


Figure 4-28. Case 7 - MMAE Position Errors

The conditional probability time histories and three of the measurement residual time histories for elemental filters 1 and 2 are shown in Figure 4-29 and Figure 4-30 respectively. Figure 4-30 shows the elemental filter 2 residuals for the entire data run, even though the elemental filter was deleted from the MMAE 21 seconds after the start of the data run.

As seen in Figure 4-29, the elemental filter 1 residuals were all very close to zero for the entire data run. This allowed elemental filter 1 to absorb over 90 percent of the conditional probability in the first 10 seconds. The MMAE converged to elemental filter 1 (the correct solution) 32 seconds after the start of the data run. In contrast, the elemental filter 2 residuals (Figure 4-30) either show a constant bias or an increase in magnitude over the 7 minutes of data.

The MMAE converged very quickly to the correct solution due to the almost ideal behavior of the elemental filter 1 residuals. The performance of this algorithm (and most other carrier-phase ambiguity resolution algorithms) is very dependent on the “quality” of the data set. A clean data set, or even a period of clean data within a data set, can dramatically improve the performance of an algorithm, and is a very typical problem with most carrier-phase ambiguity resolution routines.

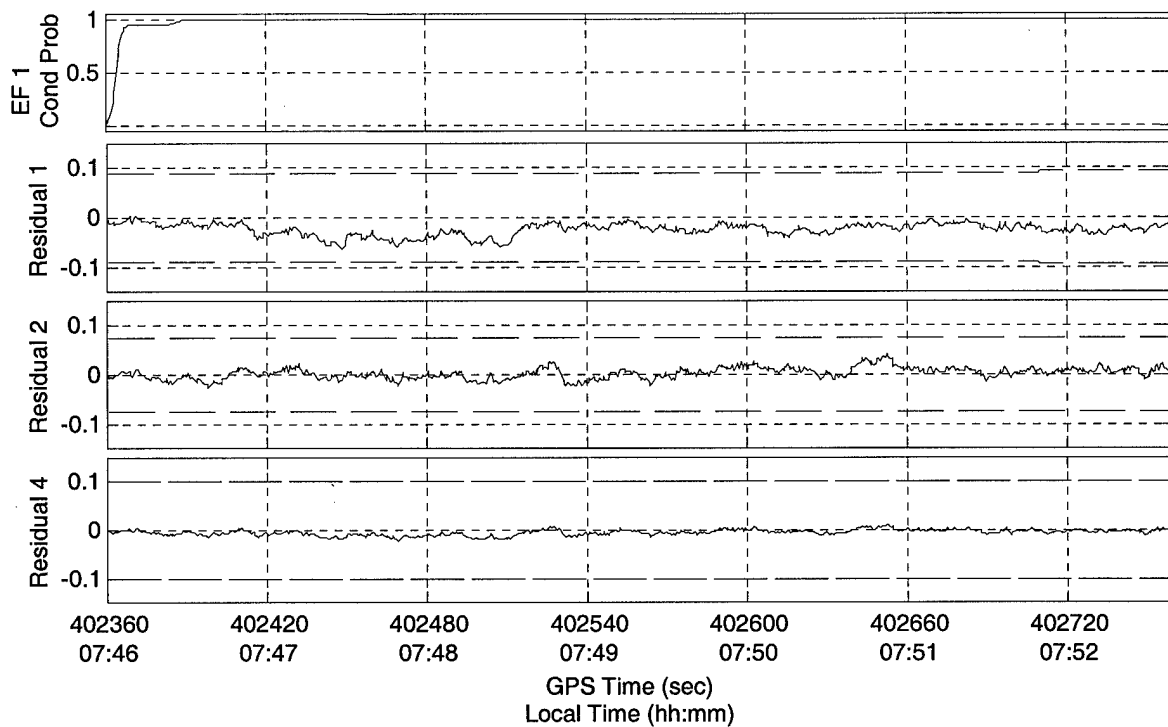


Figure 4-29. Case 7 - Elemental Filter 1 Probability and Residual Time Histories (Correct Ambiguities)

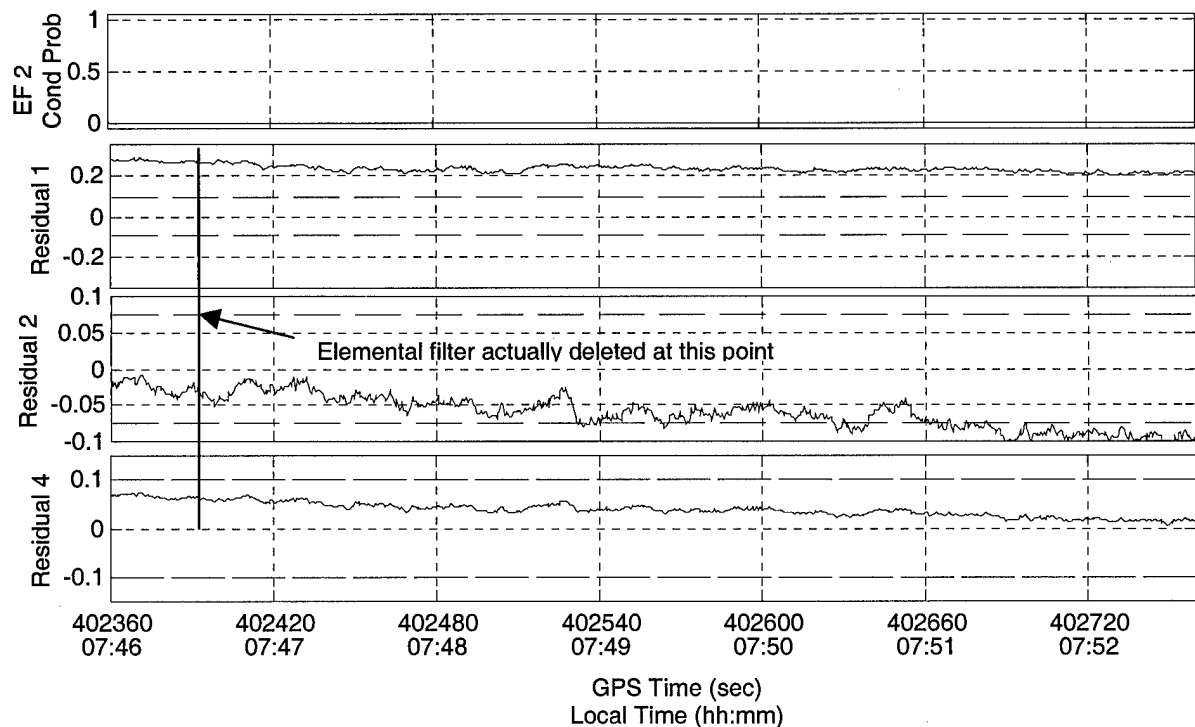


Figure 4-30. Case 7 - Elemental Filter 2 Probability and Residual Time Histories (Incorrect Ambiguities)

4.4 Summary

This chapter presented the performance results of an MMAE-based carrier-phase integer ambiguity resolution algorithm. The results were broken up into ground and flight test cases, with each case representing a difference distance, or distance and altitude from the reference receiver. Each case used real world data from Ashtech Z-surveyor receivers at both the reference and remote (or airborne) locations.

During ground tests, the MMAE was very efficient at determining the carrier-phase integer ambiguities at short baseline distances. As expected, the MMAE required more time to determine the correct integer ambiguity set as the baseline distances increased. In addition, even though the accuracy of the new algorithm degraded as baseline distances increased, the new algorithm provided a more accurate position solution than a floating-point DGPS solution. In most cases, the MMAE solution was as accurate, if not more accurate, than the floating-point solution as it converged to the true fixed-integer solution. In all cases, the MMAE solution was accurate to the centimeter level once it converged to the correct elemental filter. During the final ground test, the new algorithm demonstrated the ability of the MMAE to converge to the best possible ambiguity set in the elemental filters even if the correct ambiguity set is not available. Even though the MMAE converged to the best possible solution, improvements to algorithm to increase the probability of the correct solution being available within the MMAE were suggested.

During flight tests, the correct integer ambiguity set was not initially generated by the candidate ambiguity set generation subroutine, which suggests numerous improvements are required in the candidate ambiguity set generation subroutine. Therefore, the correct carrier-phase integer ambiguity set was artificially placed in one of the elemental filters.

Once the correct solution was available to the MMAE, the MMAE was generally able to determine the correct carrier-phase integer ambiguities, but the results were inconsistent. In two of the three flight test cases presented, the MMAE converged to the correct solution. In the remaining case, the MMAE converged to the wrong solution even though the correct solution was available. In this case, the correct filter was prematurely removed from the MMAE by the pruning logic before the MMAE was able to converge to it. This problem suggests improvements not in the MMAE, but in the pruning logic. By removing the elemental filters the MMAE cannot adapt to changes, and is forced to converge to whatever solution is available. Numerous simple changes may be made in the pruning logic to improve the overall performance of the algorithm.

The actual position solution accuracy of the new algorithm, under flight test conditions, was not always more accurate than the floating-point filter. Before the MMAE converged to the correct elemental filter, when the conditional probability shifted to an incorrect elemental filter, the MMAE solution was less accurate than the floating-point filter solution. These large initial errors were again due to the poor candidate ambiguity sets generated initially used in the elemental filters, again suggesting improvements in the floating-point filter and its role in the candidate ambiguity set generation subroutine. However, once the MMAE converged to the correct solution, it generated a navigation solution with centimeter level accuracy

In all ground test and flight test cases, even when the MMAE converged to the wrong solution, it very smoothly and quickly converged to a fixed-integer solution. There were no discontinuities or jumps in its solution typical of other carrier-phase ambiguity resolution routines.

5 Conclusions and Recommendations

5.1 Overview

This research presented the theory, modeling methodology, and results of a GPS carrier-phase integer ambiguity resolution algorithm based on a multiple model Kalman filter. Previous research in this area considered the use of MMAE algorithms for many purposes such as detection of failed actuators or sensors and GPS spoofing and jamming. Other research included extensive study into stand-alone integer ambiguity resolution algorithms, including both ambiguity set generation and ambiguity set determination. This research represents the first known use of an MMAE algorithm in the carrier-phase ambiguity resolution problem. The focus was not in the generation of ambiguity sets, but in the determination of the correct ambiguity set while using all available information to improve the GPS navigation solution.

Two different extended Kalman filter models were developed for this thesis: a floating-point DGPS filter and the elemental filters within the MMAE structure. Both of the filters incorporated a linear dynamics model with a nonlinear measurement model. The floating-point DGPS filter was used to initialize the MMAE, but more importantly, its outputs were used to generate the candidate ambiguity set used in the elemental filters in the MMAE. The elemental filters in the MMAE were each based on a different candidate ambiguity set in order to determine the correct integer ambiguity set, while using all available information to provide an accurate navigation solution. The standard MMAE structure was also modified to incorporate filter pruning and to use the latest

measurement, or “post-fit” residuals, in the MMAE conditional probability calculations, rather than conventional filter residuals. Both static ground tests and flight tests were conducted to verify the performance of the new algorithm.

5.2 *Conclusions*

The new algorithm developed in this thesis performed extremely well during the ground tests and flight tests analyzed throughout this research. The new algorithm was able to determine the correct carrier-phase ambiguities quickly and provided an accurate navigation solution. The new algorithm showed the additional benefit of transitioning rapidly and smoothly from a floating-point position solution to a fixed-integer position solution. In all cases, once the MMAE converged to the correct elemental filter, the solution was an order of magnitude more accurate than the floating-point filter solution, and provided a centimeter level accurate solution.

Of the ground test cases presented in Chapter 4, each shows the new algorithm will converge to the correct integer ambiguity set, and hence the correct fixed-integer solution, as long as the correct ambiguity set is in one of the elemental filters. The new algorithm essentially *instantaneously* resolved the correct carrier-phase ambiguities for short baseline distances. As expected, the algorithm’s performance degraded as the baseline distance from the reference receiver was increased. The MMAE also showed the ability to converge to the best possible solution, if the correct solution was not available as a hypothesis within the MMAE. In all cases, the MMAE smoothly approached the fixed-integer solution without the discontinuities typical of most carrier-phase ambiguity resolution algorithms. In addition, while transitioning to the fixed-

integer solution, the MMAE solution was generally more accurate than the floating-point solution.

For flight tests, the algorithm showed performance improvements over current algorithms even though the results were not as consistent as during the ground tests. For flight tests, the new algorithm was again able to determine the correct carrier-phase integer ambiguities (after the correct solution was artificially placed in an elemental filter), but the results were inconsistent due to problems in the pruning logic. In two of the three cases presented, the MMAE converged to the correct solution. Before the MMAE converged to the correct elemental filter, when the conditional probability shifted to an incorrect elemental filter, the MMAE solution was sometimes less accurate than the floating-point filter solution. However, these results were a direct function of the ambiguity sets generated by the floating-point filter and the ambiguity set generation subroutine, and not a function of the performance of the MMAE. Improving the performance of the floating-point filter and the ambiguity set generation subroutine will improve the performance of the overall algorithm. The MMAE solution smoothly and rapidly transitioned to a fixed-integer solution, and once the MMAE converged to the correct solution, its accuracy was at the cm-level -- an order of magnitude more accurate than the floating-point solution.

In the one remaining flight test case, the MMAE converged to the wrong solution, even though the correct solution was available in an elemental filter. The MMAE initially shifted the probability weight to an incorrect filter, and then the pruning logic deleted the correct filter before the conditional probability could be shifted back to the correct elemental filter. The MMAE converged to the wrong solution due to faulty

pruning logic and not as a result of the MMAE design. This case illustrated the need for careful engineering judgment in removing elemental filters from the MMAE. All of the tradeoffs must be considered before removing elemental filters and reducing or eliminating the ability of an MMAE to adapt to changes in the overall system. Numerous simple changes in the current pruning logic will greatly improve the performance of the algorithm.

Although not the focus of this research, the ability of the new algorithm to resolve the carrier-phase ambiguities correctly depends directly on the correct ambiguity set being hypothesized by one of the elemental filters. The current ambiguity set generation algorithm does not guarantee that the correct ambiguity set is available in one of the elemental filters. While this thesis focused on the ability of an MMAE to determine the correct carrier-phase ambiguity set, any future implementation of the algorithm created in this research must include advanced routines to improve the probability of the correct ambiguity being available as a solution in the MMAE.

The ground test and flight test profiles used in this research were adequate to test the performance of the algorithm and determine the effects of error sources in a DGPS application. This research has shown that under ground and flight test conditions, an MMAE can quickly and accurately resolve GPS carrier-phase ambiguities. For all but one case, the algorithm converged to the correct ambiguity set and provided a centimeter level accurate navigation solution. The limited results presented in this thesis are highly encouraging and warrant further research.

5.3 *Recommendations*

This initial attempt at using a multiple model adaptive filter to determine the correct carrier-phase integer ambiguities performed well enough to continue development. However, there are many modifications that may be made to the current algorithm to improve its performance.

The following recommendations are provided to extend this research and increase the usefulness of the current algorithm:

1. The performance of the MMAE directly depends on the correct ambiguity set being hypothesized by one of the elemental filters. To improve the performance of the algorithm it should be modified to:
 - Incorporate a larger number of elemental filters to improve the chance of the correct ambiguity set being hypothesized by one of the elemental filters. However, if the current Bayesian approach (weighted blending of the elemental filter solutions) is used to generate the overall MMAE state estimate, increasing the number of elemental filters will increase the effect of incorrect solutions on the final MMAE estimate. In addition, adding elemental filters increases the required computational power and memory.
 - Allow the floating-point filter more time to estimate the carrier-phase ambiguities before its estimate is used to generate candidate ambiguity sets. Currently, the candidate ambiguity sets are generated after only one

propagate and update cycle of the floating-point filter. Allowing the floating-point filter more than one cycle before using its solution to generate the candidate ambiguity sets would improve the likelihood of the correct ambiguity set being generated by the Z-transform and FASF routines.

- Reset some elemental filters with ambiguity sets “close to” (as determined by the appropriate search space) the “correct” elemental filter once the MMAE has converged to an elemental filter. If the “correct” elemental filter contains the true integer ambiguity set, the MMAE will again converge to it as the fixed-integer solution.
- Reset the elemental filters every M sample periods using the current candidate ambiguity set generation subroutine. This method is similar to the previous recommendation, but alleviates the need to determine what ambiguity sets are “close to” the “correct” elemental filter. It also allows the candidate ambiguity set generation subroutine to use the most recent ambiguity estimates from the floating-point filter.
- Perform some type of ‘likelihood test’ [25] on the elemental filters to provide insight into the “correctness” of the solution and the ambiguity sets in the elemental filters. If the solution has a low likelihood of being correct, the elemental filter(s) may be reset with different ambiguity sets.

2. The current algorithm design uses a Bayesian estimator (weighted blending of the elemental filter solutions) for the final MMAE state estimates. To achieve the true fixed-integer solution with the Bayesian estimator, the algorithm also uses pruning logic to delete “bad” elemental filters. To improve the performance of the algorithm, the final MMAE estimate, and avoid the problem of possibly pruning the correct elemental filter, the algorithm should be modified to:

- Not prune bad elemental filters, or not prune all but one elemental filter from the MMAE. This recommendation removes the problem of the MMAE losing its ability to adapt to system changes, and the possibility of removing the correct elemental filter from the MMAE. The overall MMAE solution would be a type of blending or weighted blending of the elemental filters remaining in the MMAE.
- Change the Bayesian estimator to a blended weighting scheme similar to the one described in reference [10], where the overall estimate is still a weighted average of elemental filter solutions. However, only those elemental filters with a conditional probability higher than some predetermined threshold are used in the final MMAE estimate. If the threshold is set high enough (but not restrictively high) this recommendation removes the need to eliminate elemental filters, and if the conditional probability of the “bad” elemental filters is below the threshold, then the final MMAE estimate will be the true fixed-integer solution.

3. The floating-point filter position solution is only used to initialize and reinitialize the MMAE. The two solutions should be closely related, generally within a few meters based on the accuracy of the floating-point filter. Therefore, the floating-point filter could be used to cross check the MMAE solution. If the solutions differ by a predetermined amount, the MMAE could be reinitialized, or different ambiguity sets could be generated and used in the MMAE
4. Modify the MMAE design to also include information from a "whiteness" test [15] [25] when trying to determine which elemental filter contains the correct carrier-phase ambiguity set. A whiteness test may not be an efficient way to initially determine the correct carrier-phase ambiguity, but after a few sample periods it may add enough additional information to stop the MMAE from incorrectly weighting an elemental filter whose residuals are momentarily small as they pass with a slope through zero.
5. Increase the order of the floating-point filter to include states for residual differential tropospheric errors and multipath errors to improve the performance of the floating-point filter. Improving the performance of the floating-point filter will improve the performance of the candidate ambiguity subroutine, and hence increase the likelihood that an elemental filter will contain the correct ambiguity set. In addition, a better floating-point filter solution will help the initialization and therefore the transient response of the MMAE.

6. Incorporate logic to handle the addition of new satellites to the GPS solution efficiently. Currently, when a satellite is added to the navigation solution, the MMAE is completely reinitialized to the floating-point filter, and new candidate ambiguity sets are generated. This removes any information or advantage already gained by the MMAE. The performance of the algorithm would be improved by using the previous MMAE solution to reinitialize all of the elemental filters and to generate new candidate ambiguity sets. The algorithm might also be changed to estimate the ambiguity of the new measurement accurately and incorporate it into the MMAE without reinitializing the entire MMAE.
7. Change the algorithm to a moving bank MMAE design. Instead of fixing the ambiguity sets hypothesized by the elemental filters, allow the MMAE to move throughout the search space to find the correct elemental filter.
8. Modify the current algorithm to estimate/resolve L1, L2 and widelane ambiguities independently and simultaneously. Widelane ambiguities are a linear combination of L1 and L2 ambiguities, and the additional ambiguity estimates could be used to validate the other ambiguity solutions, and/or increase the accuracy of the MMAE final solution.

Appendix A. Flight Test Profiles

INTRODUCTION

The flight tests described in this Appendix were flown as part of a combined Air Force Institute of Technology (AFIT) and USAF Test Pilot School (USAF/TPS) research and flight test program. Flight test points and maneuvers were divided into primary and secondary flight test points. The specific flight test points, maneuvers, and techniques flown during this thesis are described in the following sections. Due to funding limitations and time constraints not all test points detailed below were accomplished during the flight test phase of this research. Only the primary flight test points were accomplished.

PRIMARY FLIGHT TEST POINTS

The steady flight test points shown in Table A-1 were the primary data points. Figure A-1 gives a graphical illustration of the primary flight test point profiles. These flight test points started over the reference receiver location (Point A), flew out to the arc distance (Point B), flew the desired arc (Point C), then flew a straight line back to the reference receiver (Point A). The arc distance was defined as the horizontal distance from the GPS reference station to the test aircraft (Point A to B). The time listed for each test point combination of arc distance and altitude was the estimated total time required to fly the entire route - from the reference receiver to the arc, the arc, and then back to the reference receiver. The arc time was the estimated length of time data will be collected, at the

required arc distance and altitude, while flying each arc. The arc times listed in Table A-1 were based on a 0.6 Mach number. The number of runs listed in Table A-1 was the required number of data runs at each test point. Primary data point flight test tolerances are listed in Table A-2.

Table A-1. Primary Flight Test Data Points

Pressure Altitude	Arc Distance				
	10 nm	20 nm	30 nm	60 nm	100 nm
10,000 ft	7 min	15 min	22 min	X	X
20,000 ft	7 min	15 min	22 min	32 min	X
30,000 ft	7 min	15 min	22 min	32 min	60 min
Approx. Arc Time	4 min	8 min	12 min	12 min	26 min
Number of Runs	3	2	2	1	1

Table A-2. Primary Flight Test Data Point Tolerances

Parameter	Tolerance
Arc Distance	$\pm 10\%$ of Arc Distance or 5 nm whichever is less
Altitude	$\pm 1,000$ ft
Approx. Arc Time	± 1 min if Arc Distance < 30 nm, otherwise ± 2 min

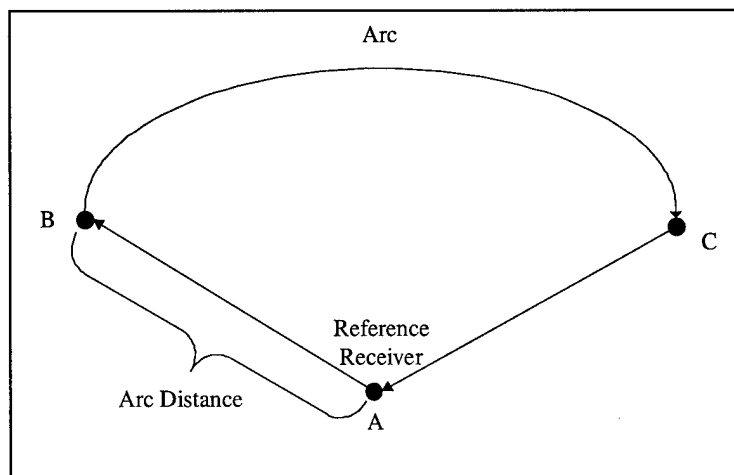


Figure A-1. Primary Flight Test Point Profile

SECONDARY FLIGHT TEST POINTS

Dynamic flight test points, or secondary data points, were started at the flight conditions shown in Table A-3. The letters in Table A-3 at each test point combination of arc distance and altitude refer to a specific flight test maneuver, described below. Secondary data point tolerances are listed in Table A-4.

Level Turns

A constant load factor level turn was accomplished to investigate angular acceleration effects on position and velocity accuracy. These turns were accomplished at load factors of 1.4G, 2G and 3G. Each maneuver was completed at an airspeed required to maintain the constant load factor.

Wind-Up Turn

A constant speed Wind Up Turn (WUT) was completed to investigate angular acceleration rate effects on position and velocity accuracy. The WUT maneuver varied load factor (G) from 1G to a maximum of 6G at an onset rate of 1G per 4 seconds.

Push Over / Pull Up

A Push Over / Pull Up was completed to investigate vertical acceleration effects on position and velocity accuracy. The Push Over / Pull Up varied load factor (G) from 0G to a maximum of 3G at an onset rate of 1G per 4 seconds.

Table A-3. Secondary Flight Test Data Points

Pressure Altitude	Arc Distance		
	10 nm	20 nm	30 nm
10,000 ft	A, B, C	A, B, C	A, B, C
20,000 ft	A, B, C	A, B, C	A, B, C

Table A-4. Secondary Flight Test Data Point Tolerances

Parameter	Tolerance
Arc Distance	Arc distances shown ($\pm 10\%$) are conditions for the start of the maneuver. The Arc Distance may vary as necessary to complete the maneuver.
Altitude	$\pm 2,000$ ft
Airspeed / Mach	± 10 KIAS / ± 0.05 Mach
Load Factor	± 0.2 G

Descending Turn

An additional secondary flight test point was a Descending Turn. This maneuver investigated altitude effects on position and velocity accuracy. The maneuver was flown at an arc distance of 5 (± 1) nm from the reference receiver, and a VVI of 4000 (± 200) fpm. The maneuver will start at 30,000 ft PA and end at 10,000 ft PA.

REFERENCE RECEIVER LOCATION

The reference receiver station for all flight test was located at the following WGS-84 coordinates

Latitude (Degrees:Minutes:Seconds)	Longitude (Degrees:Minutes:Seconds)	Altitude (m)
34 : 55 : 19.88982	-117 : 53 : 27.38584	679.8870

Bibliography

- [1] Ashtech Office Suite for Survey V.2. Copyright 1999 Magellan Corporation, Spectra Precision Terrasat GmbH.
- [2] Ashtech Z-Family Technical Reference Manual. Magellan Corporation, Spectra Precision Terrasat GmbH. May 1998.
- [3] Athans, M. et al. *The Stochastic Control of the F-8C Aircraft Using a Multiple Model Adaptive Control (MMAC) Method – Part 1: Equilibrium Flight*. IEEE Transactions on Automatic Control, AC-22(5):768-780, October 1977
- [4] Barum, Y. *Information, Consistent Estimation and Dynamic System Identification*, Rep. ESL-R-718. Electronic Systems Lab. Dept. of Elec Eng., MIT, Cambridge, Massachusetts, November 1976.
- [5] Chang, B. and M. Athans. *State Estimation for Discrete Systems with Switching Parameters*. IEEE Transactions on Aerospace and Electronic Systems, AES-14(4):418-424, May 1978.
- [6] Chen D. *Fast Ambiguity Search Filter (FASF): A Novel Concept for GPS Ambiguity Resolution*. Proceedings of the 6th International Technical Meeting of the Satellite Division of the Institute of Navigation (ION GPS-93). Salt Lake City, Utah, 1993.
- [7] Counselman, C. and Gourevitch, S. *Miniature Interferometer Terminals for Earth Surveying: Ambiguity and Multipath for the Global Positioning System*. IEEE Transactions on Geoscience and Remote Sensing, GE-19(4):244-252
- [8] Cox, D. and Brading, J. *Integration of LAMBDA Ambiguity Resolution with Kalman Filter for Relative Navigation of Spacecraft*. Proceedings of the ION National Technical Meeting, 28-30 Jun. 1999.
- [9] De Jonge, P. and Tiberius, C. *The LAMBDA Method for Integer Ambiguity Estimation: Implementation Aspects*. Delft Geodetic Computing Centre, LGR Series No. 12, Delft University of Technology, The Netherlands. August 1996
- [10] Eide, P. and Maybeck, P. *An MMAE Failure Detection System for the F-16*. IEEE Transactions of Aerospace and Electronic Systems, 32(3):1125-1136. July 1996
- [11] Erickson, C. *Investigations of C/A Code and Carrier Measurements and Techniques for Rapid Static GPS Surveys*. MS Thesis, UCGE Reports Number 20044, Department of Geomatics Engineering, University of Calgary, Calgary, Alberta, Canada, June 1992.

- [12] Fisher, K. *Multiple Model Adaptive Estimation Using Filter Spawning*. MS thesis, AFIT/GE/ENG/99M-09, School of Engineering, Air Force Institute of Technology (AU), Wright-Patterson AFB OH, March 1999 (AD-A361774).
- [13] GPS Aided Inertial Navigation Reference (GAINR) System, 412 TW/TSRE, Edwards AFB, California 1 August 1995.
- [14] GPS Aided Inertial Navigation Reference (GAINR) System Performance Summary, TSPI Department, Computer Sciences Corporation, Edwards AFB California. 30 September 1997.
- [15] Hanlon, P. and Maybeck, P. *Multiple-Model Adaptive Estimation Using Residual Correlation Kalman Filter Bank*. IEEE Transactions on Aerospace and Electronic Systems, Vol. 36, No. 2, pp 393-406, April 2000.
- [16] Hatch, R. *The Synergism of GPS Code and Carrier Measurements*. Proceedings of the Third International Geodetic Symposium on Satellite Doppler Positioning, DMS Las Cruces, New Mexico, 1982.
- [17] Hatch, R. *Instantaneous Ambiguity Resolution*, In Schwarz and Lapachelle, editors, Kinematic Systems in Geodesy, Surveying, and Remote Sensing. IAG Symposia, Springer Verlag, 1990.
- [18] Han, S. *Carrier-phase-Based Long-Range GPS Kinematic Positioning*. MS Thesis, UNISURV S-49, School of Geomatic Engineering, University of New South Wales, Sydney NSW 2052, Australia, August 1997.
- [19] Henderson, P. and Raquet, J. *Development and Testing of a Multiple Filter approach for Precise DGPS Positioning and Carrier-Phase Ambiguity Resolution*. Proceedings of the ION National Technical Meeting, Anaheim, CA. 26-28 January. 2000.
- [20] Kaplan, E. *Understanding GP: Principles and Applications*. Boston: Artech House Inc., 1996.
- [21] Li, Z and Gao, Y. *Construction of High Dimensional Ambiguity Transforms for the LAMBDA Method*. Pulsesearch Navigation Systems/Position Inc. Alberta Canada, 1996.
- [22] Magill, D. *Optimal Adaptive Estimation of Sample Stochastic Processes*. IEEE Conference on Decision and Control, AC-10(4):434-439, October 1965.
- [23] The MathWorks, Inc., 21 Elliot Street, Natick MA 01760. *MATLAB*®. October 1999. Version 5.3.1.
- [24] Maybeck, P. *Stochastic Models, Estimation and Control, I*. New York: Academic Press, Inc., 1979. Republished Arlington VA: Navtech, 1994.

- [25] Maybeck, P. *Stochastic Models, Estimation and Control, II*. New York: Academic Press, Inc., 1982. Republished Arlington VA: Navtech, 1994.
- [26] Maybeck, P. *Moving-Bank Multiple Model Adaptive Estimation and Control Algorithms: An Evaluation*. Control and Dynamic Systems: Advances in Theory and Applications, Vol. 31, Academic Press, Inc., pp 1-31, San Diego, 1989.
- [27] Maybeck, P. and Hentz, K. *Investigation of Moving-Bank Multiple Model Adaptive Algorithms*. Journal of Guidance and Control, 10(1):90-96 January-February 1987.
- [28] Maybeck, P. and Suizu, R. *Adaptive Tracker Field of View Variation via Multiple Model Filtering*. IEEE Transactions on Aerospace and Electronic Systems, 21(4):529-537, July 1985.
- [29] Maybeck, P., Herrera, T. and Evans, R. Target Tracking Using Infrared Measurements and Laser Illumination. IEEE Transactions on Aerospace and Electronic Systems, 30:758-768 July 1994.
- [30] Menke, T. *Multiple Model Adaptive Estimation Applied to the VISTA F-16 with Actuator and Sensor Failures*. MS Thesis, AFIT/GA/ENG/92J-01, School of Engineering, Air Force Institute of Technology (AU), Wright-Patterson AFB OH, June 1992
- [31] Miller, M. *Modified Multiple Model Adaptive Estimation (M3AE) for Simultaneous Parameter and State Estimation*. Ph.D. Dissertation, AFIT/DS/ENG/98-02, School of Engineering, Air Force Institute of Technology (AU), Wright-Patterson AFB OH, March 1998 (AD-A344312).
- [32] Multi-Sensor Optimal Smoother Estimating Software (MOSES), Version 6.0 412 TW/TSRE, Edwards AFB, California 1 August 1995.
- [33] Negast, W. *Incorporation of Differential Global Positioning System Measurements Using an Extended Kalman Filter for Improved Reference System Performance*. MS thesis, AFIT/GE/ENG/91D-41, School of Engineering, Air Force Institute of Technology (AU), Wright-Patterson AFB OH, December 1991 (AD-A243742).
- [34] Parkinson, B., Spilker, J. *Global Positioning System, Theory and Applications Volume I*. American Institute of Aeronautics and Astronautics, Inc. Washington D.C., 1996
- [35] Parkinson, B., Spilker, J. *Global Positioning System, Theory and Applications Volume II*. American Institute of Aeronautics and Astronautics, Inc. Washington D.C., 1996
- [36] Raquet, J. *Class Notes to EENG 633, Air Force Institute of Technology, Wright-Patterson AFB, Summer Quarter 1999*.

- [37] Raquet, J. *Development of a Method for Kinematic GPS Carrier-Phase Ambiguity Resolution Using Multiple Reference Receivers*. Ph.D. dissertation, UCGE Reports Number 20116, Department of Geomatics Engineering, University of Calgary, Calgary, Alberta, Canada, May 1998.
- [38] Rizos, C. and Han, S. *A New Method for Constructing Multi-Satellite Ambiguity Combinations for Improved Ambiguity Resolution*. Proceedings of ION GPS-95, Palm Springs, CA, September 12-15 1995.
- [39] Tellman, L. *Multiple Model-Based Robot Control: Development and Initial Evaluation*. MS thesis, AFIT/GE/ENG/88D-55, School of Engineering, Air Force Institute of Technology (AU), Wright-Patterson AFB OH, December 1988.
- [40] Teunissen, P. *The Least-Squares Ambiguity Decorrelation Adjustment: A Method for Fast GPS Integer Ambiguity Estimation*. Journal of Geodesy, Springer-Verlag, 1995.
- [41] Van Dierendonck, A. *Understanding GPS Receiver Terminology: A Tutorial on What Those Words Mean*. Proceedings of the International Symposium on Kinematic systems in Geodesy, Geomatics and Navigation. Banff, Canada. 30 August – 2 September 1994.
- [42] Vanek, B. *GPS Signal Offset Detection and Noise Strength Estimation in a Parallel Kalman Filter Algorithm*. MS thesis, AFIT/GE/ENG/99M-30, School of Engineering, Air Force Institute of Technology (AU), Wright-Patterson AFB OH, March 1999 (AD-A361773).
- [43] Vasquez, J. *Detection of Spoofing, Jamming, or Failure of a Global Positioning System (GPS)*. MS thesis, AFIT/GE/ENG/92D-37, School of Engineering, Air Force Institute of Technology (AU), Wright-Patterson AFB OH, December 1992 (AD-A259023).
- [44] Vasquez, J. *New Algorithms for Moving-Bank Multiple Model Adaptive Estimation*. Ph.D. Dissertation, AFIT/DS/ENG/98-10, School of Engineering, Air Force Institute of Technology (AU), Wright-Patterson AFB OH, May 1998 (AD-A347840).
- [45] Williamson, W. and Speyer, J. *A GPS/INS Multiple Model Adaptive Kalman Filter for Carrier Phase Integer Ambiguity Resolution and Cycle Slip Detection*. Proceedings of the ION National Technical Meeting, Anaheim, CA. 26-28 January. 2000.
- [46] Young, B. *An Integrated Synthetic Aperture Radar/Global Positioning System/Inertial Navigation System for Target Geolocation Improvement*. MS thesis, AFIT/GE/ENG/99M-32, School of Engineering, Air Force Institute of Technology (AU), Wright-Patterson AFB OH, March 1999 (AD-A361800).

Vita

Captain Paul E. Henderson grew up in Corry, Pennsylvania where he graduated from the Corry Area High School in 1988. He then attended Carnegie Mellon University in Pittsburgh, Pennsylvania where he earned his Bachelor of Science Degree in Electrical Engineering in 1992.

Having been appointed a Second Lieutenant in the United States Air Force in 1993, his first assignment was to the 963rd Airborne Warning and Control Squadron (AWACS) at Tinker AFB, OK. He spent three years working as a flightline maintenance officer, with numerous deployments to Operations Southern Watch and Northern Watch. In 1996, Captain Henderson was transferred to the Air Force Research Laboratory, Sensors Division, at Wright-Patterson AFB, OH as the lead reliability and maintainability engineer for developmental radars.

In 1998, he was selected to attend the joint Air Force Institute of Technology (AFIT) and USAF Test Pilot School (TPS) Program. Captain Henderson graduated from USAF/TPS as a Flight Test Engineer in December 2000, and will receive his Masters Degree in Electrical Engineering with a focus on GPS, Navigation, and Control in March 2001. His assignment, following AFIT/TPS, is to the 46th Munitions Test Squadron at Eglin AFB, FL where he will be flight-testing advanced GPS/INS guided munitions.

REPORT DOCUMENTATION PAGE				Form Approved OMB No. 0704-0188	
Public reporting burden for the collection of information is estimated to average 1 hour per response, including the time for reviewing instructions, searching existing data sources, gathering and maintaining the data needed, and completing and reviewing the collection of information. Send comments regarding this burden estimate or any other aspect of this collection of information, including suggestions for reducing this burden, to Washington Headquarters Services, Directorate for information Operations and Reports, 1215 Jefferson Davis Highway, Suite 1204, Arlington, VA 22202-4302, and to the Office of Management and Budget, Paperwork Reduction Project (0704-0188), Washington, DC 20503. PLEASE DO NOT RETURN YOUR FORM TO THE ABOVE ADDRESS.					
1. REPORT DATE (DD-MM-YYYY) 20-03-2001		2. REPORT TYPE Master's Thesis		3. DATES COVERED (From - To) Jun 1999 - Mar 2001	
4. TITLE AND SUBTITLE DEVELOPMENT AND TESTING OF A MULTIPLE FILTER APPROACH FOR PRECISE DGPS POSITIONING AND CARRIER-PHASE AMBIGUITY RESOLUTION				5a. CONTRACT NUMBER	
				5b. GRANT NUMBER	
				5c. PROGRAM ELEMENT NUMBER	
				5d. PROJECT NUMBER	
				5e. TASK NUMBER	
6. AUTHOR(S) Henderson, Paul E. Captain, USAF				5f. WORK UNIT NUMBER	
7. PERFORMING ORGANIZATION NAMES(S) AND ADDRESS(S) Air Force Institute of Technology Graduate School of Engineering and Management (AFIT/EN) 2950 P Street, Bldg 640 Wright-Patterson AFB OH 45433-7542				8. PERFORMING ORGANIZATION REPORT NUMBER AFIT/GE/ENG/01M-15	
9. SPONSORING/MONITORING AGENCY NAME(S) AND ADDRESS(ES) USAF Test Pilot School Attn: Lt Col Thomas A. Buter 220 S. Wolfe Ave Edwards AFB CA 93524-6485 DSN 527-3000				10. SPONSOR/MONITOR'S ACRONYM(S)	
				11. SPONSOR/MONITOR'S REPORT NUMBER(S) N/A	
12. DISTRIBUTION/AVAILABILITY STATEMENT APPROVED FOR PUBLIC RELEASE, DISTRIBUTION UNLIMITED.					
13. SUPPLEMENTARY NOTES					
14. ABSTRACT <p>The most precise relative positioning obtained using differential GPS depends on accurately determining carrier-phase integer ambiguities. To achieve high precision, many current static and kinematic algorithms use a floating-point solution until enough information becomes available to fix the carrier-phase ambiguities accurately.</p> <p>A new method is presented that uses a multiple model Kalman filter to resolve the carrier-phase integer ambiguities. This method starts with the floating-point results, yet smoothly and rapidly attains the precision of the correct fixed-integer solution, eliminating the need to decide when to switch from the floating to the fixed-integer solution. This method is based on a theoretically correct blending of solutions from multiple filters. This new technique is computationally efficient, providing a robust navigation solution useful in demanding applications such as precision landing and autonomous navigation.</p> <p>The new method was evaluated during static ground and flight tests. Initial results indicate that the new method is capable of quickly resolving the carrier-phase ambiguities and provides a highly accurate (centimeter-level) navigation solution. However, the performance of the new method depends on the correct carrier-phase ambiguity set being hypothesized by one of the multiple filters. Recommendations for further research are included.</p>					
15. SUBJECT TERMS Global Positioning System, GPS, Differential Global Positioning System, DGPS, Carrier Phase Ambiguity Resolution, Kalman filter, Multiple Model Kalman Filtering, Multiple Model Adaptive Estimation, MMAE					
16. SECURITY CLASSIFICATION OF:			17. LIMITATION OF ABSTRACT	18. NUMBER OF PAGES	19a. NAME OF RESPONSIBLE PERSON
a. REPORT	b. ABSTRACT	c. THIS PAGE			Raquet, John F. Major USAF
U	U	U	U	165	19b. TELEPHONE NUMBER (Include area code) 937-255-3636 x4580